General Disclaimer

One or more of the Following Statements may affect this Document

- This document has been reproduced from the best copy furnished by the organizational source. It is being released in the interest of making available as much information as possible.

- This document may contain data, which exceeds the sheet parameters. It was furnished in this condition by the organizational source and is the best copy available.

- This document may contain tone-on-tone or color graphs, charts and/or pictures, which have been reproduced in black and white.

- This document is paginated as submitted by the original source.

- Portions of this document are not fully legible due to the historical nature of some of the material. However, it is the best reproduction available from the original submission.

WANL-PR-(DD)-014
November 1, 1966

Westinghouse Astronuclear Laboratory

ANALYTICAL INVESTIGATION OF TURBINE EROSION PHENOMENA

Interim Technical Report Number I, Volume III

Contract NAS7-390

WANL-PR-(DD)-014
November 1, 1966

Westinghouse Astronuclear Laboratory

ANALYTICAL INVESTIGATION OF TURBINE EROSION PHENOMENA

Interim Technical Report Number I, Volume III
Contract NAS7-390

Astronuclear Laboratory

VOLUME III

EFFECT OF EXTERNAL VARIABLES ON THE EROSION PROPERTY OF MATERIALS

Authors: F. J. Heymann, F. R. Arcella

PREFACE

The literature on impingement erosion has been examined with a view to deducing empiric (or analytic) relationships for the relationships between erosion rate and external variables, in particular the velocity, angle of impingement, and size and shape of the impacting drops.

The difficulties inherent in the interpretation of erosion test data are discussed and a rationalized approach is described. The available data yield only very approximate generalizations, which should be subjected to further experimental trial.

One of the major difficulties in the correlation of test data is the variation of erosion rate during a test. An analytic model is proposed to explain this variation.

Except for a short discussion in Part C on dissolution of materials by liquid metals, this report is concerned with the effect of external conditions such as impact velocity, etc., on the erosion of metals by the impingement of liquid drops. It does not directly concern itself with the erosion resistance of specific materials, or - except in passing - with the relationship between erosion resistance and other material properties.

Part A constitutes a major revision of Section V of Reference 1. Much new material has been included, some of the old material has been deleted, and the conclusions have been revised. Some of the deleted material is still referred to by citing Reference 1, but in all important aspects this report is self-contained.

Part B, presenting an analytic model for the variations of erosion rate with exposure time is a development of Appendix B of Reference 2. A broader discussion of the time-dependence of the erosion rate (including this analytic model) is given in Reference 3.

Astronuclear Laboratory

TABLE OF CONTENTS

Astronuclear Laboratory

TABLE OF CONTENTS (Cont'd)

LIST OF ILLUSTRATIONS

LIST OF ILLUSTRATIONS (CONTINUED)

LIST OF ILLUSTRATIONS (CONTINUED)

LIST OF TABLES

Astronuclear Laboratory

PART A

SURVEY OF CLUES TO THE RELATIONSHIPS BETWEEN EROSION RATE AND IMPINGEMENT CONDITIONS

F. J. Heymann

1.0 GENERAL CONSIDERATIONS RELATING TO THE INTERPRETATION AND CORRELATION OF TEST DATA

1.1 Independent Variables

The objective in this part is to see whether the impingement erosion test data in the literature can be made to yield generalized relationships, by means of which the erosion to be expected under arbitrary operating conditions can be predicted. One would like to be able to express the erosion in terms of an empirical or semi-empirical equation, which would be a function of the operating variables and would contain constants which are properties of the materials of the target and of the impinging liquid.

The independent variables, or operating conditions, are as follows:

1) Area of target subjected to impingement,
2) Shape of target,
3) Size of impinging liquid drops or slugs,
4) Shape of impinging liquid drops or slugs,
5) Rate of impingement of liquid on target,
6) Impact velocity between liquid and target,
7) Angle of impact between liquid and target surface.
8) Physical properties of liquid such as:
   a. density,
   b. viscosity,
   c. compressibility, or acoustic velocity.

9) Physical properties of target. While the significant properties are still not known, these may be listed as possibilities:
   a. hardness, or other strength property,
   b. strain energy to rupture, or other energy property,
   c. elongation, or other ductility property,
   d. endurance limit, and fatigue S-N relationship,
   e. elasticity, or acoustic velocity.
10) Surface conditions of target, such as:
   a. roughness,
   b. work hardening or other surface effects due to previous preparation and/or erosion,
   c. presence of surface films of liquid.
11) Microstructure and orientation of surface layers.

In this part of the report primary emphasis will be given to the velocity and angle of impact, and the size and shape of impacting drops. Part B includes some discussions of the fatigue properties and surface conditions of the target.

1.2 Dependent Variables

One of the greatest difficulties in the interpretation and correlation of erosion test data lies not in the multiplicity of the independent variables but in the identification of the dependent variable or variables, which we have heretofore glibly referred to as "the erosion". All would be well if, under given conditions, erosion proceeded at a constant rate and could be unmistakably characterized by the uniform slope of the cumulative weight loss versus time curve. As is well known this is not what happens, and therefore some approach must be found to characterize "the erosion". Figure 1 (a) is intended to represent a typical weight loss versus time curve. (The axes are vaguely labeled "erosion" and "duration" quite deliberately, since these quantities will be discussed more fully later.) This curve is characteristic of much of the data found in the literature; the various "stages" of the curve and possible explanations for them are discussed at length in Part B of this report.

It can be shown that even a relatively well-behaved experimental plot is subject to a variety of interpretations. The circles in figure 1 (a) represent the hypothetical "raw data" points. A conservative method of drawing the "curve" is to join the experimental points by straight lines, as shown. Reference 4*, for instance, shows curves in this form. An erosion rate curve can then be constructed by plotting the slopes of these line segments versus the time corresponding to their mid-points. This is shown by the circles and solid lines in figure 1 (b). Reference 5 presents its data in this form. This approach requires no decisions, but obviously is not accurate unless the data points are very close together.

To draw in a "smoothed" curve, a conscious or unconscious decision must be made as to how this smooth curve should look. If it is believed that the erosion rate rises from zero during an incubation period to a constant maximum value, and subsequently declines to a secondary constant value, a curve will be drawn such as the dashed one in figure 1 (a), whose counterpart in figure 1 (b) is also shown dashed. If one believes the erosion rate reaches a rather steep peak value and then goes into a series of fluctuations, then the dash-dotted lines in figures 1 (a) and (b) may result. This does not by any means exhaust the possible variations, but will serve to show how this decision can have a considerable effect on the shape of the erosion curve presented, particularly so if data are presented in the form of erosion rate curves. (Graphical differentiation of empirical data with all its uncertainties is of course notoriously unreliable.)

This "prejudice" concerning what the erosion curves should look like is closely related to the question of just how these curves should be quantitatively characterized, i. e. just what the dependent variables are which should correlate with the operating conditions. The objective of this empirical approach is to predict the amount of erosion expected after a given time, or at least the time required to reach some "critical" degree of erosion.

---

*References cited are listed in a later section.

The parallel study reported in Part B concerns the possibility of predicting the form of the erosion versus time curve analytically, on the basis of assumed material removal mechanisms. This has not yet advanced to the stage where it can be of help in the present study. Therefore we adopt that view which is the most widely held and which is practical enough for present purposes. That is: The first stage in erosion shows little or no weight loss and represents plastic deformation of the surface and initiation of fatigue cracks. This stage merges into the second stage in which the rate of weight loss is at a maximum and approximately uniform over a period of time. This in turn merges into a later stage or stages in which the erosion rate diminishes and may or may not tend toward another uniform value. Whatever the precise cause or causes of this decrease in erosion rate may be, it is usually associated with rather general and severe damage to the surface, which through geometrical effects alone may result in an effective alteration of the impingement conditions. Thus the best parameters to describe the progress of erosion in a relatively simple and yet significant manner are:

1) A quantity representative of the duration of the initial (incubation) stage, denoted by T_o in figure 2.
2) A quantity representative of the rate of erosion during the second stage, denoted by R in figure 2. This is the most significant quantity, and most of the following sections deal with it.
3) Of additional interest would be some quantity representative of the degree of damage at the "end" of the second stage. This would help to establish whether this transition is really a geometric effect, and also whether the first two stages do really cover the "permissible" degree of erosion in a practical application. However, very little information on this is available.

There are test data to which the foregoing generalizations and conclusions do not seem to apply, but for most of the usable data they do seem valid, and our correlation attempts are based on this type of curve. Eventually, however, the deviations from this type of curve must also be understood and accounted for. It is important to remember that more than one mechanism of material removal may be active: the above-described behavior applies to those conditions under which a fatigue mechanism predominates. This is valid for most of the

material and impact velocity combinations for which test data are available, and probably to most turbine operating conditions. If, however, impact velocities are increased, then material removal due to individual impacts will also occur, and at sufficiently high speeds the rate of material removal by this process may be sufficiently high so that there is not enough time for fatigue failures to occur at all. The shape of the erosion-time curve, the significant dependent quantities, and their functional relationships to such independent variables as drop size and impact velocity, can all be expected to change during this transition from one predominant mechanism to another. Test data at relatively high velocities (around 2000 ft/sec) are being generated but are not yet available. Steam turbine blades will soon be operating in this velocity range also.

1.3 Correlation Problems

Returning now to our assumed characteristic curve, another difficulty will be demonstrated. Figure 3 shows three hypothetical but typical erosion-time curves from a given test series. Curves A, B and C might have been obtained for three different materials under the same operating conditions, or for the same material at three different impact velocities or with three different "drop" or "jet" sizes. One may then seek to "compare" these curves, or determine from each a number which represents the erosion, to be correlated with material properties or with operating parameters. With insufficient thought given to the problem, the temptation might be to select a convenient point in time (say T = 3 on figure 3) and compare either the cumulative erosion, or, with more sophistication, the slope of the erosion-time curve at that point. This, indeed, has been done by a number of authors. It should be evident from the earlier discussions, however, that this procedure is entirely invalid. It can result in spurious "comparisons" between erosion rates corresponding to completely different stages of the erosion process. Thus, in figure 3 at time T = 3, Curve B is in the probably significant second stage; Curve A has already "broken" and is into the third stage; Curve C may well still be in the incubation period.

For a valid comparison there are two desiderata, of which at least one or preferably both should be fulfilled. These are:

1) The measured slopes, or erosion rates, should be as nearly as possible average or effective values representative of the second stages of the erosion-time curves.
2) The measured slopes should be as nearly as possible the averages or effective values over the same range of cumulative erosion, i.e. associated with the same degree of damage done to the surface.

The first desideratum can be fulfilled only if the "end" of the second stage is clearly seen; if the test duration is not long enough for this to occur, then the second rule must suffice, and one must endeavor to choose the erosion interval over which the slope is measured in such a way that the first stage, or incubation period, is excluded. In figure 3, this is simply not possible for Curve C; and when one examines the available test data the choice is often reduced to one between spurious comparisons or no comparisons at all.

1.4 Rationalized Parameters

It was pointed out earlier that the axes in figure 1 have been labeled rather vaguely as "erosion" and "duration". Direct comparison between different test data is often complicated by the fact that the "erosion" may be given in terms of weight loss, or volume loss, and the "duration" in terms of time, or number of impacts (for wheel-and-jet apparatus), or in other ways. The target areas involved, and the quantity of water impinging on it, will differ not merely between different test series, but may also vary within a given test series as a consequence of varying one of the other independent parameters. Thus, for instance, if in a wheel-and-jet apparatus the jet diameter is changed, this effectively alters the area of the target subjected to impact and also the quantity of water involved in each impact, and if the impact velocity is changed by changing the speed of rotation, this also alters the weight of water impacting per unit time.

In order to permit valid comparisons and correlations, it is therefore essential to express the erosion and the duration in a rationalized form which will compensate for these test variations.

Since the undesirable aspect of erosion is the loss of volume and the change of geometry--and this change of geometry in turn affects the rate of erosion--volume loss rather than weight loss should be considered. There can be little argument that the obvious rationalized erosion parameter is volume loss per unit area, also sometimes referred to in the literature as mean depth of penetration (MDP).

The appropriate rationalized duration parameter is not quite so obvious. One could make a case for selecting the number of impacts per unit area. At present, however, preference is given to the volume of liquid impinged per unit area. This is attractive because results expressed in this way will show directly the effect of subdividing a given quantity of impinging liquid into particles of different sizes or shapes, and because it makes the "rationalized erosion rate" (E)a non-dimensional quantity, as follows:

$$E = \frac{\text{Volume of material lost per unit area per unit time}}{\text{Volume of liquid impinged per unit area per unit time}}$$

The rationalized incubation time parameter corresponding to the above is, of course, the cumulative volume of liquid impinged per unit area at time T_o as defined by figure 2.

For some correlations, where neither the target material nor the impinging liquid is changed, the rationalized erosion rate can be satisfactorily represented in terms of weight of material lost and weight of water impinged.

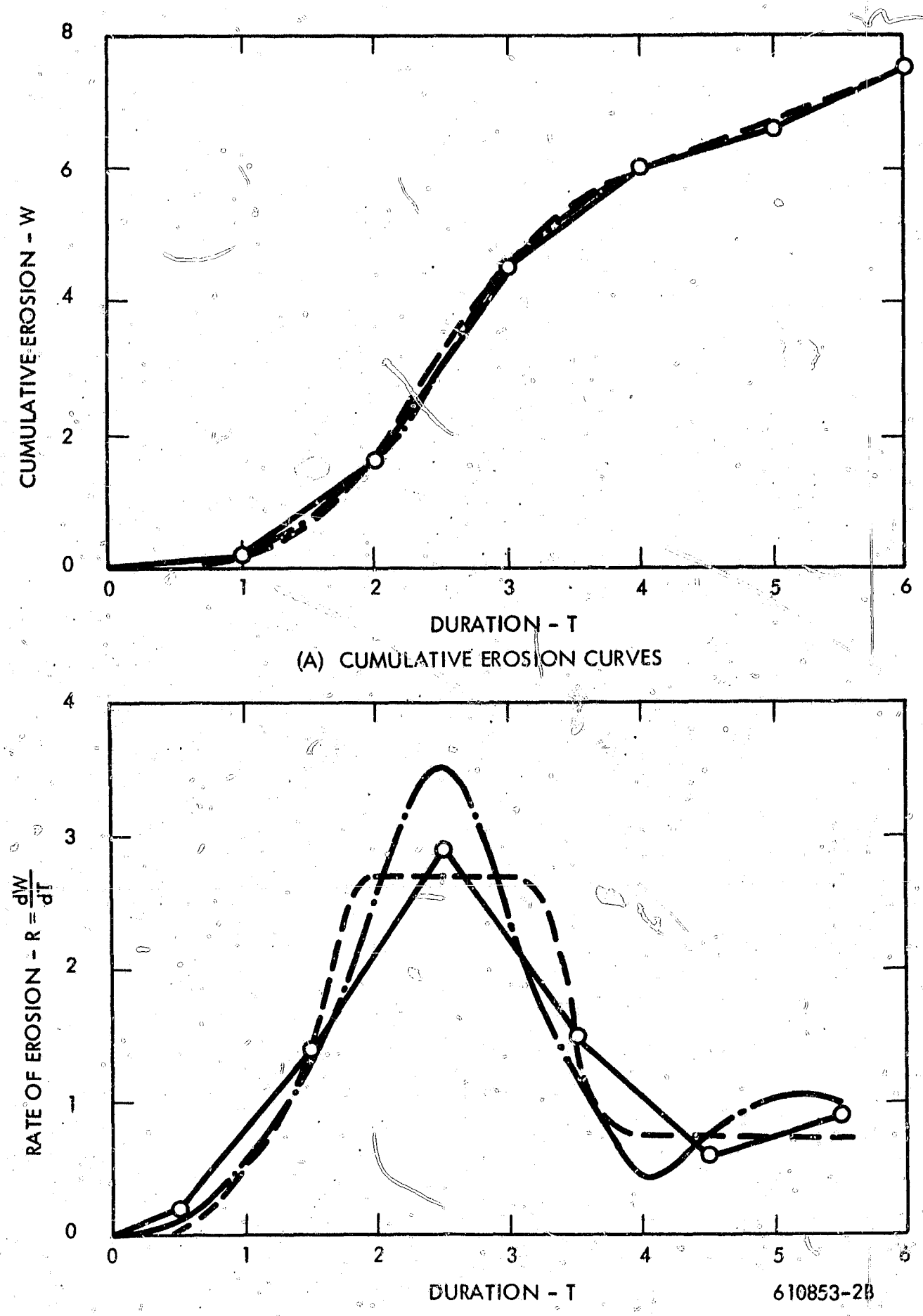

(A) CUMULATIVE EROSION CURVES

(B) EROSION RATE CURVES

Figure 1. Various Interpretations of Same Hypothetical Erosion Data Points

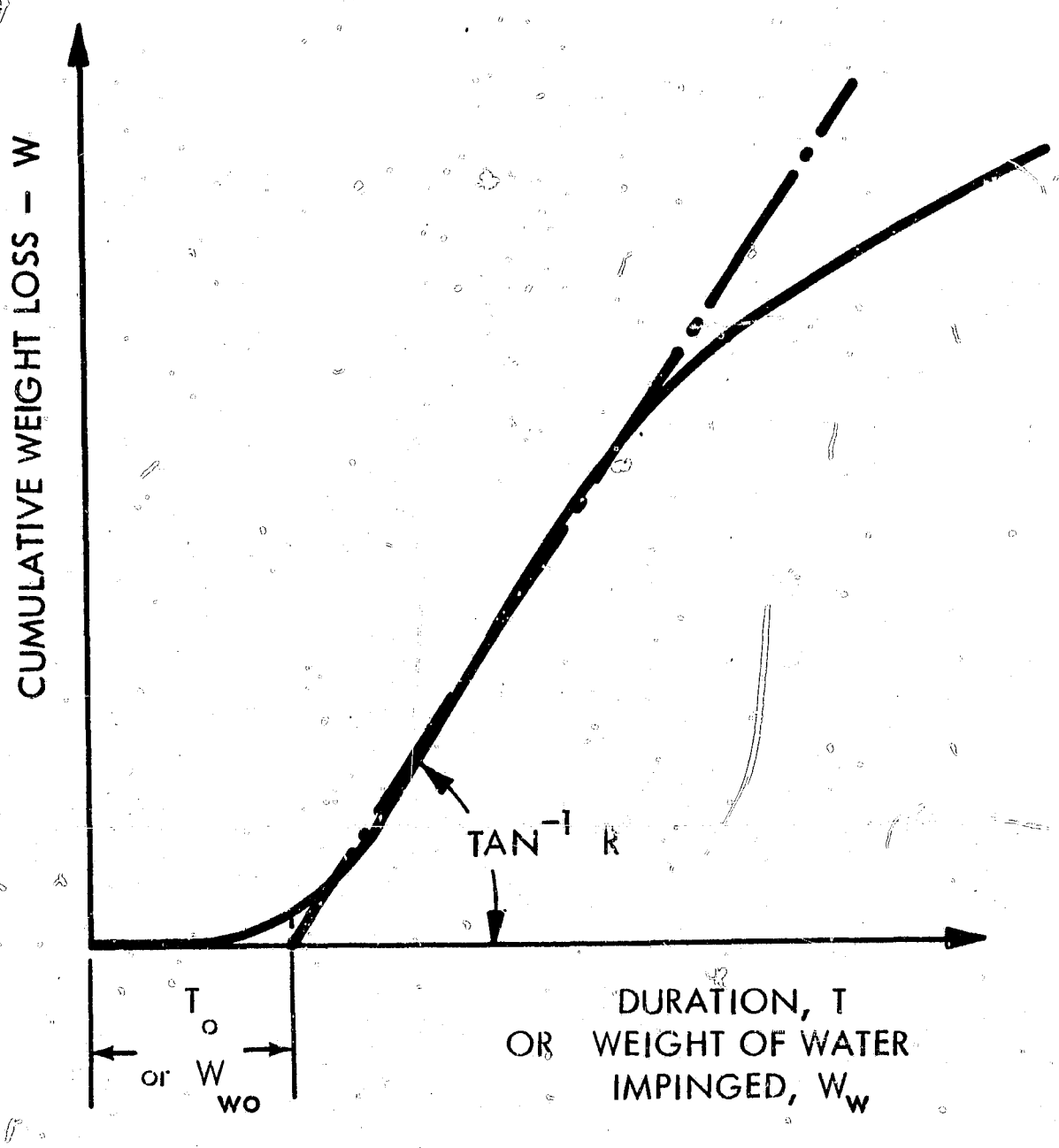

Figure 2. Definition of Incubation Period, T_o, and "Steady-State" Erosion Rate, R

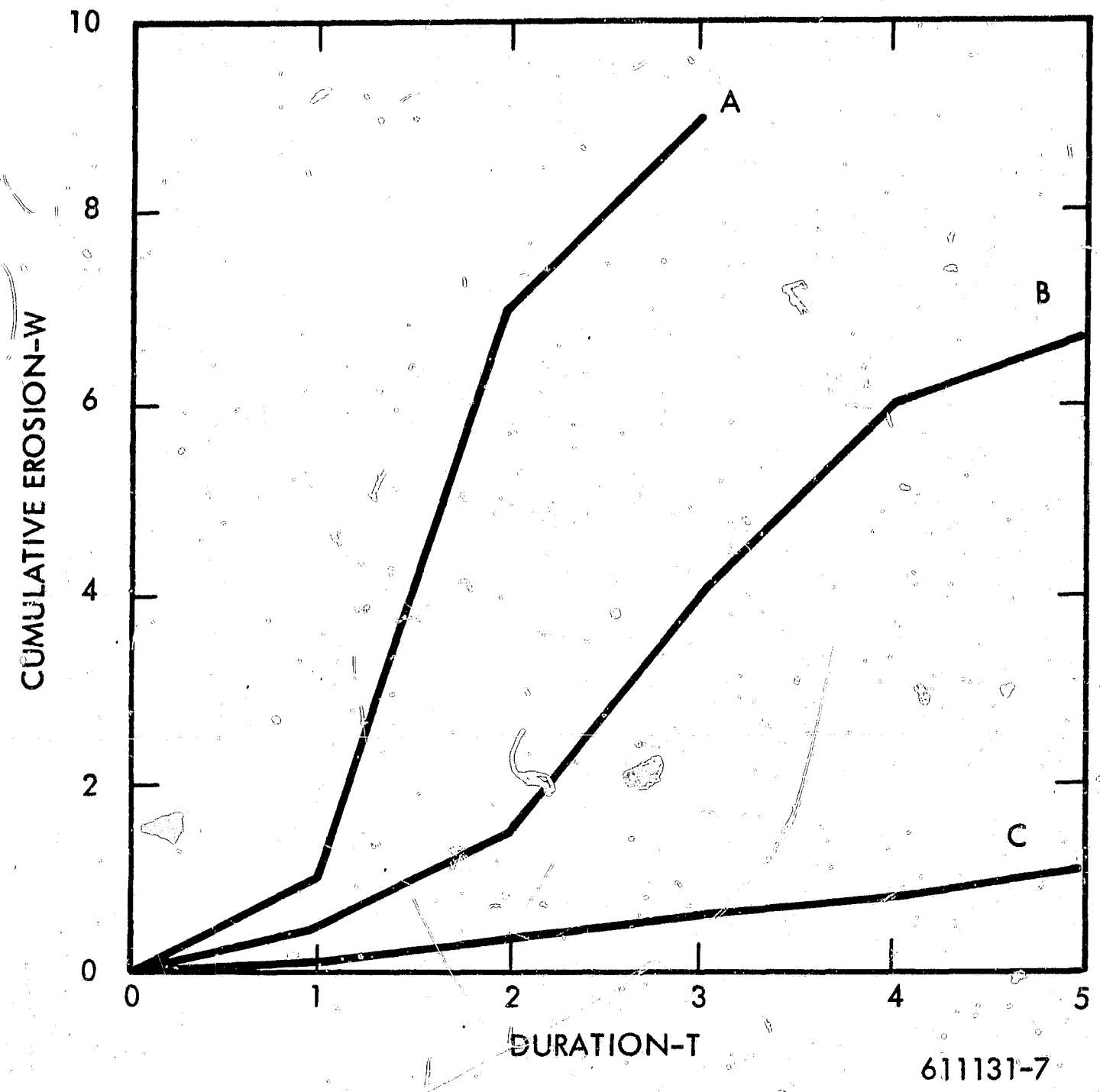

Figure 3. Hypothetical Erosion Curves

2.0 DEPENDENCE ON IMPINGEMENT ANGLE

Only recently have investigators shown serious concern with the impingement angle. The consensus appears to be that the normal component of the impingement velocity is that primarily responsible for the damage, with the tangential component playing a secondary role.

Thus, according to Fyall and King,[6] [7] for initially smooth surfaces the normal impact velocity can be used successfully for correlations valid during the initiation and earlier stages of erosion, but that when the surface has been roughened by erosion, the tangential component also becomes significant because the true local impact angles can become more normal to the absolute velocity. No quantitative estimate is made for the latter effect.

Langbein and Hoff[8] [9] state that the normal component governs the erosion; they show loci of equal average erosion rates plotted on a field of absolute velocity versus inclination angle and state that these correspond to loci of constant normal velocity component ($V_n = V \cos \theta$).

Pearson[10] [11] has proposed the following correlation equation to represent the erosion rate E in terms of the impingement velocity V and inclination angle θ measured from the normal direction (expressed in our terminology):

$$E = K (V \cos \theta - V_c)^n / \cos \theta \qquad (1)$$

in which K, V_c, and n are to be regarded as constants of the target material. (Actually, at least some of these constants must also be functions of the impinging liquid properties, drop sizes etc.)

Pearson justifies introducing the $1/\cos \theta$ term by presenting the data reproduced here as figures 4 and 5. (These are direct copies of Pearson's figures except that our terminology has been substituted and the curves drawn through the points have been omitted.) It appears that E cos θ correlates somewhat better with V cos θ (figure 5) than does simply E with V cos θ (figure 4). This improvement is hardly dramatic, however, and the $1/\cos \theta$ correction should, in our opinion, be regarded as tentative and subject to analytic or further experimental verification.

For 12 percent chromium stainless steel, Pearson obtained values of approximately 400 and 2.6 for V_c and n respectively, for use in equation 1. Ratios of erosion rate at angle θ to that at normal incidence (E_θ/E_o), based on this relationship, have been plotted in figure 6 for three different velocities. Some independent support for this formulation may be provided by data points also shown in figure 6, which have been deduced from erosion-time curves given by Busch and Hoff[12]; these were obtained in their supersonic rain erosion facility, with target cones of different angles, but same base diameter. The material was pure aluminum; the absolute impact velocity was Mach 1.2, or approximately 1320 ft/sec.

In this situation, the area exposed to erosion changes with the angle, but the total amount of impinging water remains the same. Thus, no area correction is necessary if the slopes of the erosion-time curves are compared; it is necessary, on the other hand, for a rational comparison of incubation times.

Note that the erosion rate at $\theta = 10^\circ$ is actually somewhat higher than that at $\theta = 0^\circ$; if this is actually so, it would support an observation by Brunton[70] that the damage in single-impact tests could be greater at slight angles of inclination than with normal impact. (Note that at 1300 ft/sec on aluminum, single-impact damage is certainly occurring.) On the other hand, this may be an apparent effect only and due to scatter or some other experimental variable. The curves in Reference 12 do not show actual data points.

The critical velocity V_c for aluminum would certainly be far lower than that for 13 percent chrome steel-perhaps on the order of 100 ft/sec. If one computes E_θ/E_o from Pearson's equation with $V = 1300$ and $V_c = 100$, n remaining 2.6, one obtains Curve E, which fits the data points reasonably well. Is this a confirmation of Pearson's equation, or is it merely fortuitous? The former can be true only if the assumptions of $V_c = 100$ and $n = 2.6$ are indeed correct.* (Differences in the values of K cancel out, of course.)

In a previous progress report (Reference 7) it had been suggested that the data of Reference 12 could also be represented by the simple relationship $E_\theta/E_o = \cos^2\theta$, which is shown as Curve A in figure 6. This simple angle-dependence does not fit any of Pearson's results presented in figures 4 and 5, and therefore should be rejected.

*In Section 4 of this report it is concluded that the exponents n in equations of this type generally fall between 2.3 and 2.6.

The physical meaning of Pearson's equation is that erosion is in the first instance a function of the normal component of the impact velocity, and that the additional erosion due to a tangential component is accounted for by the $1/\cos\theta$ multiplier. Such a relation could not have been deduced from the data of Reference 12 alone, since in those tests the absolute velocity was held constant, and the normal velocity component varied. Thus there was no way of telling whether the change in erosion with the angle was to be attributed to a function of the angle alone, or to a combination of the changes in the angle and the normal velocity. A reliable formulation for the angle effect can be obtained only if a reliable formulation for the velocity effect is simultaneously determined, i.e. from test programs in which velocities and angles are varied independently. This is what Pearson has attempted to do, and therefore, pending further testing of the generality of his equation, it is the best information available.

One set of data somewhat at variance with the foregoing was reported by Brandenberger and DeHaller.[4] They tested one material in a relatively low-speed wheel-and-jet apparatus at various combinations of specimen velocity (u) and jet velocity (v). The "jet velocity" in a wheel-and-jet apparatus is of course in a direction perpendicular to the specimen velocity, and the absolute impact velocity is given by $w = \sqrt{u^2 + v^2}$. If the specimen were of round cross-section, as in a number of similar investigations, then w would also be the effective normal impact velocity. In this case, however, the specimens were of rectangular shape, and thus the velocity w is inclined at an angle, $\theta = \tan^{-1}(v/u)$, from the normal to the specimen surface. For a given value of u, considerably different results were obtained for different values of v. The authors claimed that these differences were far too great to be accounted for by the resulting differences in the absolute velocity w.

They speculated that cavitation may have been induced by the flow geometry but rejected this as a likely explanation because the location of the maximum damage was not consistent with this. They finally concluded that the tangential velocity v had some pronounced independent effect, not presently explainable, on the erosion measured. This conclusion has been introduced at some length because it has been quoted by subsequent authors, and because examination of the actual data simply does not bear it out, as will be shown below.

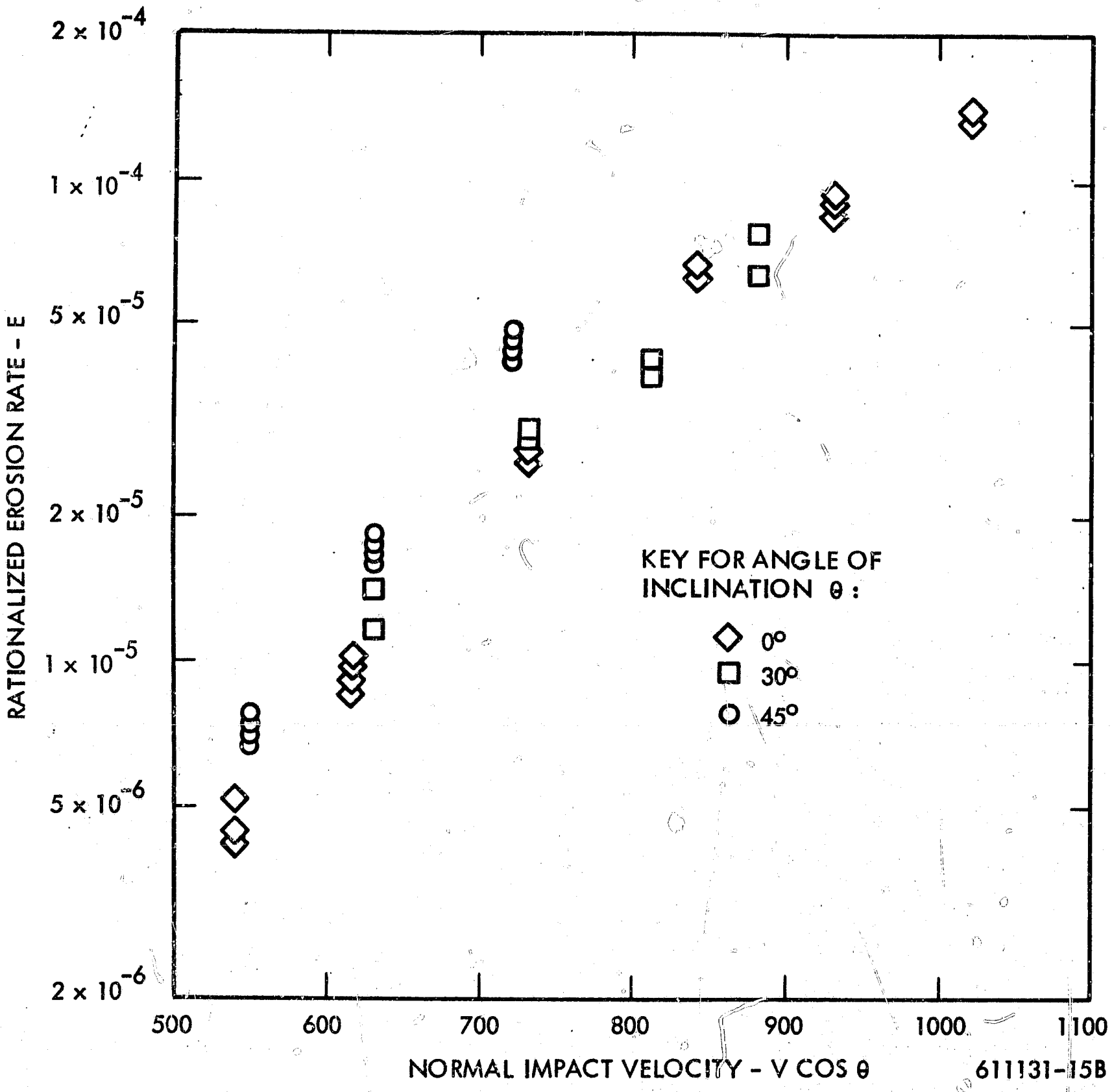

Figure 4. Rationalized Erosion Rate Versus Normal Impact Velocity
(From Figure 4 of Reference 11)

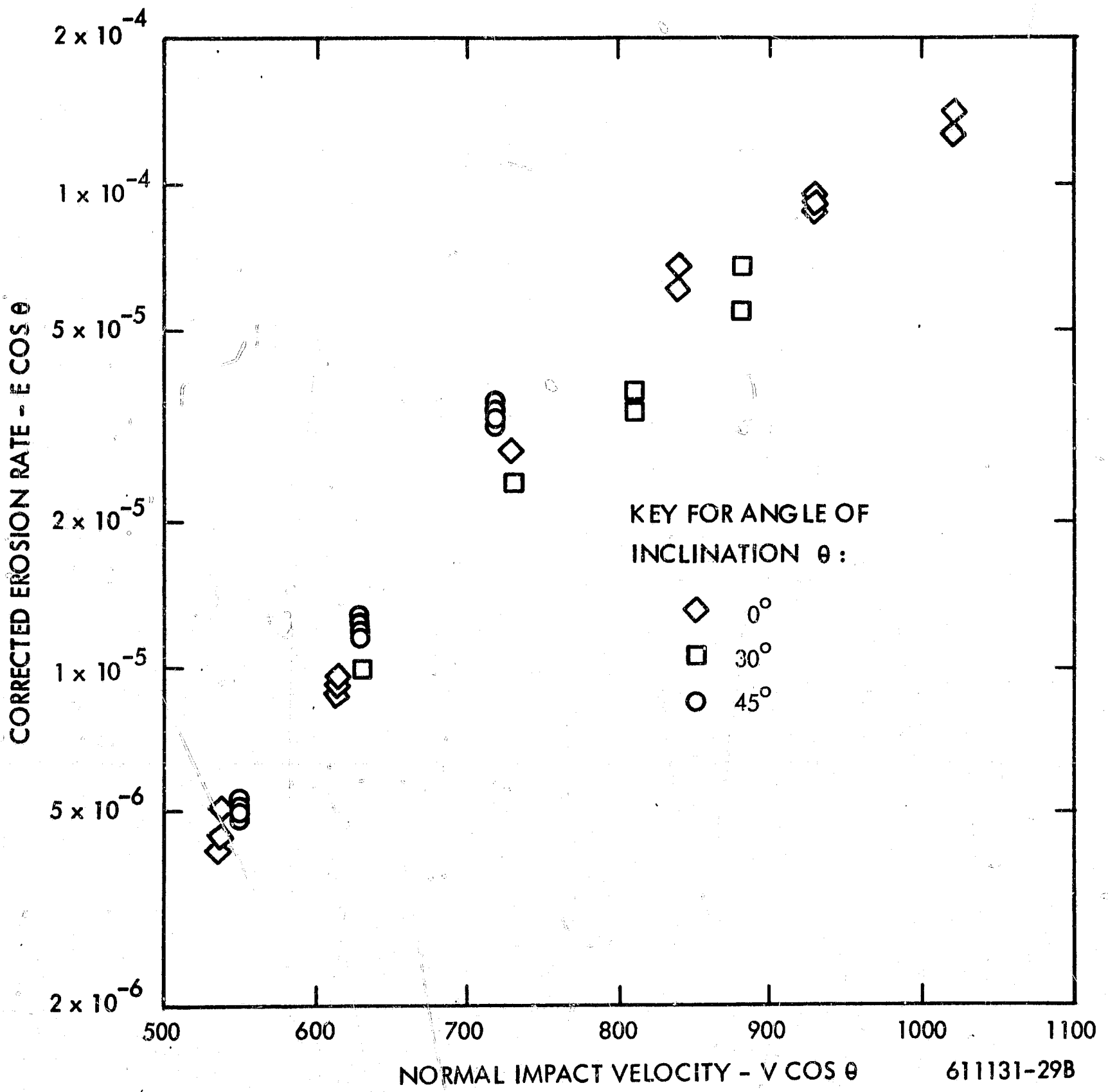

Figure 5. Corrected Erosion Rate (E cos θ) Versus Normal Impact Velocity (From Figure 5 of Reference 11)

TABLE 1

EROSION RATE E FOR DIFFERENT SPECIMEN VELOCITIES u AND JET VELOCITIES v
(FROM BRANDENBERGER AND DEHALLER 1927, REFERENCE (4))

v	u	w	θ	E	E'
m/sec	m/sec	m/sec	deg	gm/10^6 impacts	E cos θ - gm/10^6 impacts
52	20	55.7	21	1.05	0.98
52	15	54.2	16	0.86	0.83
52	10	53.0	11	0.67	0.66
52	5	52.3	6	0.64	0.64
42	20	46.5	25	0.32	0.29
42	15	44.5	20	0.26	0.245
31	20	36.9	33	0.122	0.102
31	15	34.4	26	0.075	0.067

(Note: The jet diameter was 6 mm, and the target material low carbon steel.)

Table 1 lists best estimates of the mean erosion rates, for the weight loss interval of 0.05 to 0.5 gm, from figures 4 and 6 of Reference 4. The normal, tangential, and absolute velocities are also listed, as well as the angles and the "corrected" erosion rates based on Pearson's hypothesis for angle effect discussed above. Figure 7 (a) shows the data points plotted versus the normal impact velocity u, with the "1/cos θ" angle correction. Figure 7 (b) shows the same data (without angle correction) plotted versus the absolute velocity w. The following observations can be made:

1) When plotted against u, there is a different curve for each value of v. A correction based on Pearson's assumption ($E_{v,\theta} = E_{v,o}/\cos\theta$) did not suffice to bring them into line.
2) When the data are plotted against the absolute velocity w, they fall quite well into one curve.

These observations not only contradict the conclusion reached by the authors of Reference 4, but also seem to provide evidence contradicting the angle effect theory proposed by Pearson (equation 1). A possible conclusion to be drawn from all of the observations taken together is, however, that in this case there is no angle effect– or none of the commonly expected nature–as a result of the jet velocity. This is conceivable when it is considered that the direction of the tangential component of the impact velocity is also the direction in which the impacting mass of liquid is of infinite length.

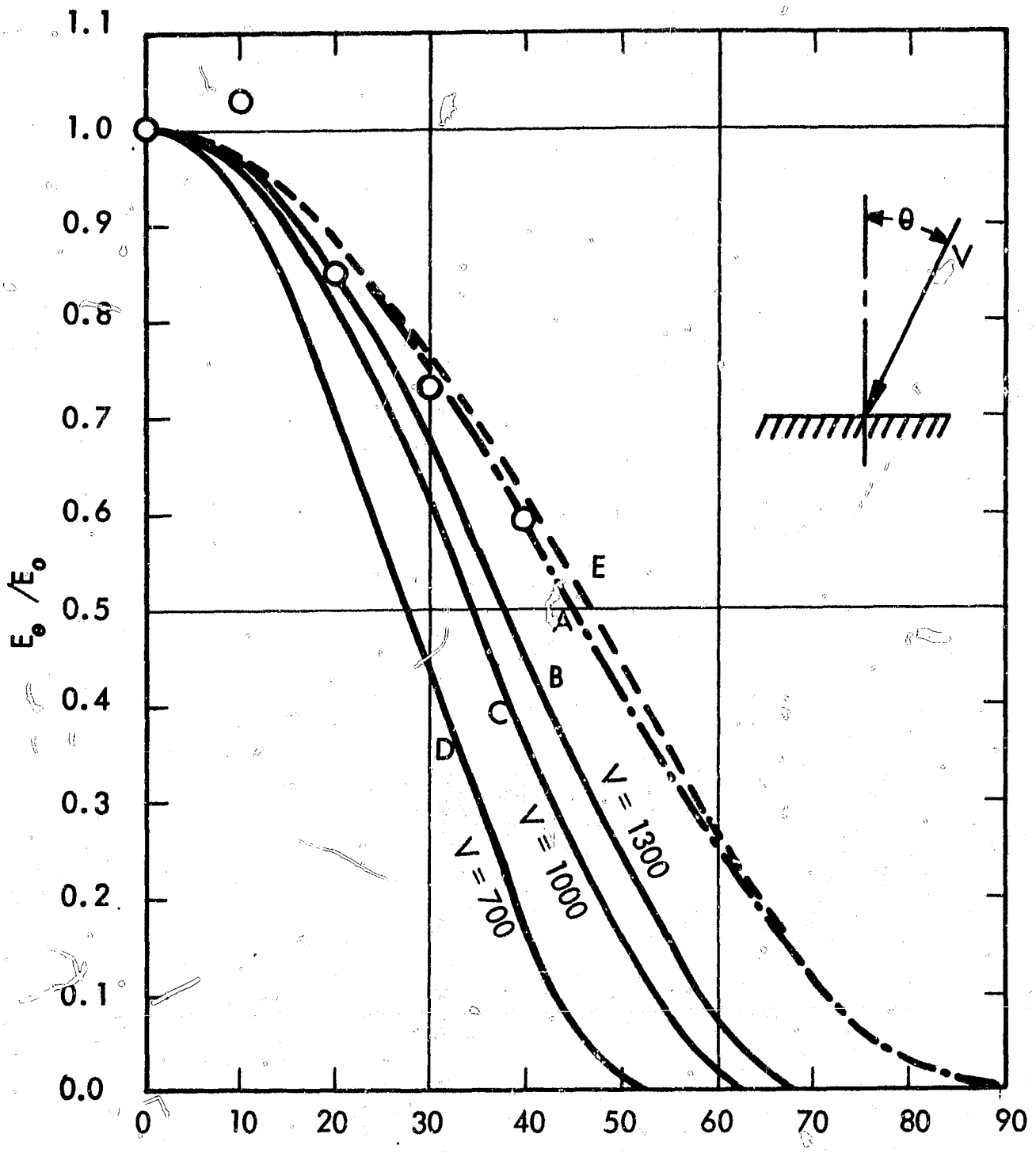

O DATA POINTS COMPUTED FROM BUSCH & HOFF (REFERENCE 12)

A: $E_\theta / E_o = \cos^2 \theta$

B, C, D: COMPUTED FROM PEARSON'S EQ.:

$E = K(V \cos\theta - 400)^{2.6} / \cos\theta$

E: $E = K(1300 \cos\theta - 100)^{2.6} / \cos\theta$

B: V = 1300 fps
C: V = 1000 fps
D: V = 700 fps

Figure 6. Comparison of Erosion Versus Angle Curves

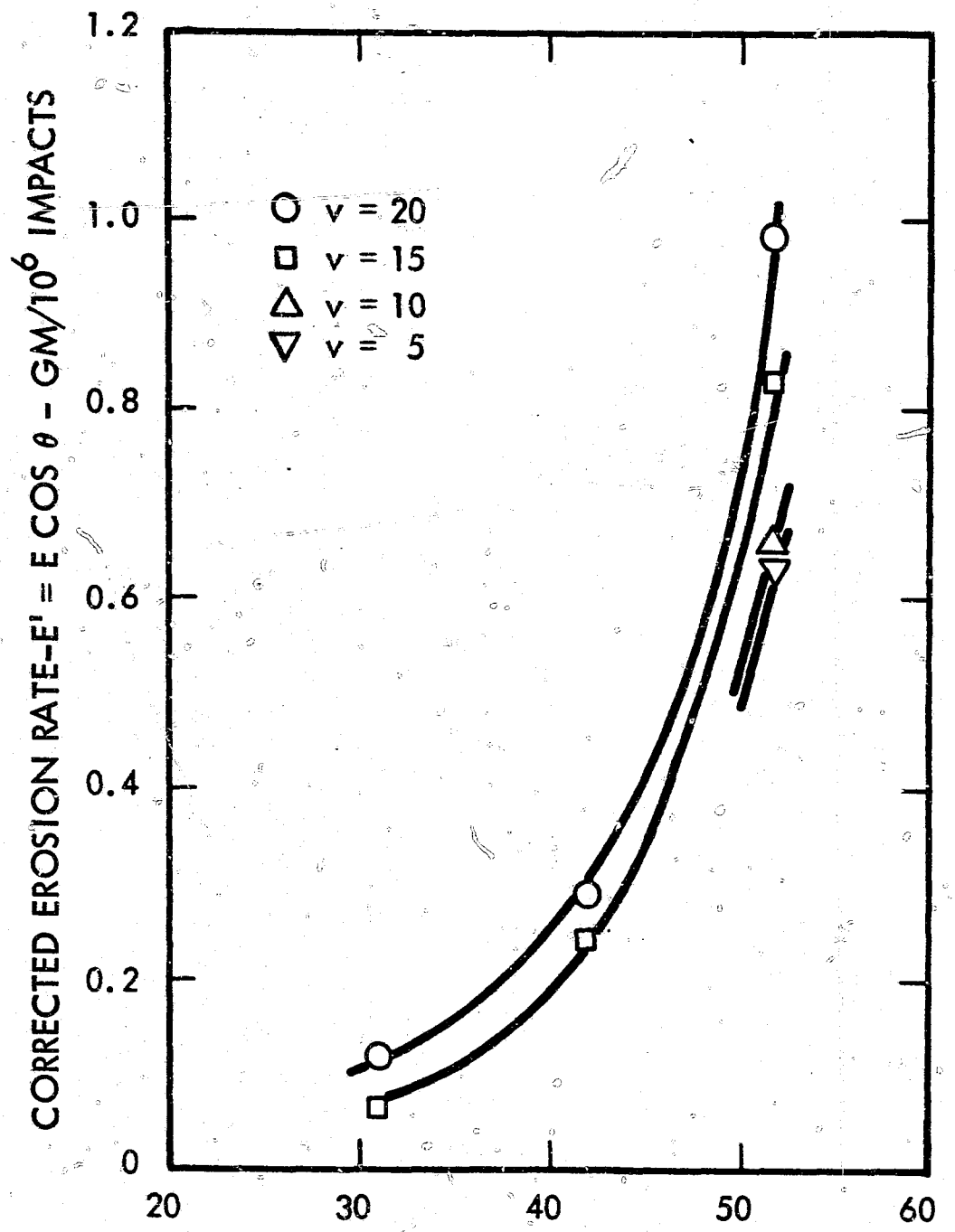

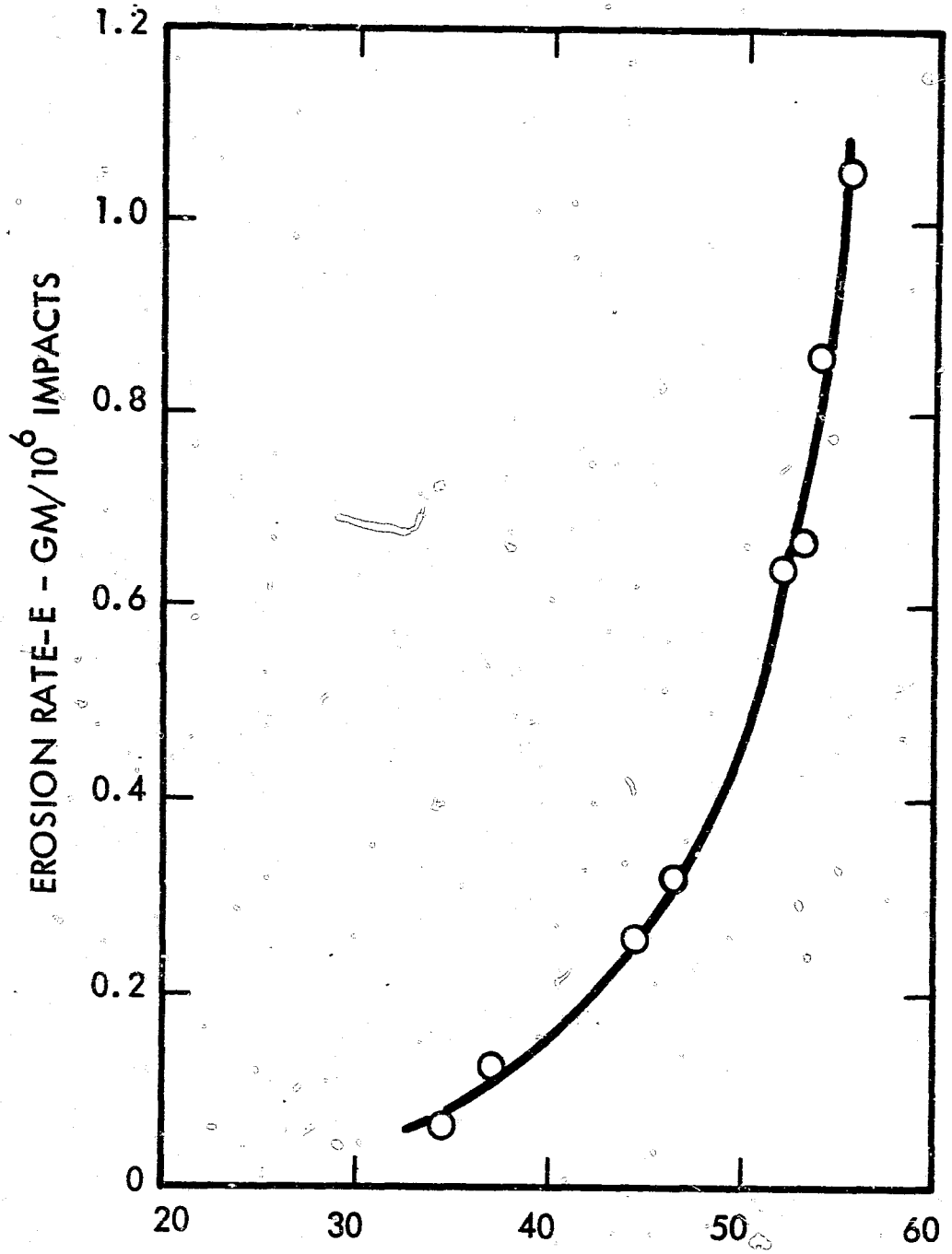

Figure 7. Erosion Versus Velocities
(Computed from Data of Reference 4)

3.0 DEPENDENCE ON DROP SIZE AND SHAPE

3.1 Review of Available Data

Despite the fact that the maximum impact stress is generally a function of the material properties and the impact velocity, and should be independent of the size of the impacting drops, there is ample evidence that both the size and the shape of the impacting liquid masses do affect the erosion measured. Here again, the quantitative data in the literature from which generalized relationships could be deduced is very scant.

A frequently cited test is that of Honegger,[5] in which he compared the erosion produced in a wheel-and-jet type apparatus by impact with one 1.5 mm water jet, with that produced by nine 0.5 mm jets, arranged as shown in figure 8. The results are described as follows: "The splitting up of the jet is accompanied by a considerable reduction of the erosion, the numerical value of the reduction largely depends upon the speed, and for tests under consideration it varies from 1 to 5 for high speeds and 1 to 10 for low speeds." It will be noted that the test was so contrived as to fulfill the requirements of a rationalized erosion measurement: both the target area subjected to erosion and the volume of impinged water were the same for both configurations. Yet, upon reflection, one must conclude that this was not a valid test of the drop size effect, at least not if figure 8 accurately portrays the nine-jet arrangement. This is because only the first three jets would impact on a dry surface; a liquid layer from these would almost certainly still be present to cushion the effect of the next three impacts, and similarly so for the last three. Thus no quantitative conclusions should be drawn from these results, but the qualitative findings are of interest.

Some systematic tests with differing jet diameters were reported by Brandenberger and DeHaller.[4] The weight-loss versus time curves are reproduced in figure 9a. The jet diameters varied from 4 mm to 12 mm, and attention should be given to the seeming anomaly presented by the 6 mm and 8 mm curves, which gives rise to the suspicion that these curves may have been accidentally mis-labeled, and should in reality be switched. This possibility will be further considered below.

The first step in evaluating these data must be to express them in rationalized form (as discussed in Section 1.0 of this report). Figure 9b is a replot of the data in terms of rationalized coordinates. The solid lines represent the original curves as labeled, and again there seems to be a seeming anomaly between the 6 mm and 8 mm curves. If the labeling on the original curves had indeed been switched, then the true rationalized 6 mm and 8 mm curves would appear as shown by the dotted lines in figure 9b. In that case, the 6 mm through 12 mm curves would all come very nearly on top of one another, with the 4 mm curve the only discrepancy.

Relative values of the slopes of these erosion-time curves have been measured for the damage interval of 0.15 to 0.4 in figure 9b, and these have been plotted in figure 10. Figure 10a represents the data with the original curves as labeled, and figure 10b with the 6 mm and 8 mm curves reversed. In neither case can any curve be established through these points with any degree of confidence. In figure 10a, as shown, a proportionality between erosion rate and diameter could be supported, provided the 6 mm data point is rejected. In figure 10b a straight-line relationship, not passing through the origin, has been shown, but the most that can be said, on the basis of the data points alone, is that they would support some relatively weak function of jet diameter.

Recently Pearson [11] [13] has conducted systematic tests with different drop sizes in his wheel-and-spray type of apparatus. Figure 11 is a reproduction of figure 1 of Reference 13, with our terminology. As in all of Pearson's results, the erosion rate given is an "angle-corrected" rationalized value of the maximum slope measured on the weight-loss versus time curve. It represents mass loss per unit area divided by mass of water impacting per unit area. The impingement angle correction used by Pearson was described in Section 2.0 above. While figure 11 shows an anomaly in the crossing of the 920μ and 1050μ lines, it seems to confirm that the relative effect of drop size diminishes at high drop sizes and high velocities-i.e., as one gets away from what may be considered the "threshold" conditions.

A cross-plot of the data on figure 11 is shown in figure 12; here as in figure 10 it is difficult to justify a purely empirical curve other than a straight line to represent the E versus drop diameter relationship, in the absence of any rational basis for some other type of curve. The extrapolation of the solid straight lines to their intercepts on the coordinate axes is, however, questionable. The dotted lines are based on a correlation to be developed below. (Reference 13 does not attempt to present any analytical or empirical equation for the drop size effect.)

In Section V-5 of Reference 1 a hypothesis was introduced which resulted in the drop size effect as being represented by a factor of the form

$$\left[1-G/V^2D\right]$$

where G represents a "critical" or "threshold" combination of velocity and drop diameter, such that for $V^2D \leq G$ no significant erosion occurs. Even if the hypothesis is not accepted in toto, the attempt to use the above factor to correlate data on drop-size effect may be justifiable. The data of Reference 13 is for the same material as that of Reference 11, in which a critical velocity V_c of 390 ft/sec was found when testing with a drop size D of 660μ. Thus $G = 390^2 \times 660 \approx 1.0 \times 10^8$, and the above mentioned factor, which we shall denote as the "critical factor" or "K_c", takes on the value

$$K_c = \left(1 - 10^8/V^2D\right) \qquad (2)$$

for this set of data.

Table 2 lists K_c for a number of combinations of V and D, and also the values of the erosion rate E taken from the curves (not the original data points) drawn in figure 11. These values are the same ones plotted in figure 12.

If K_c were a simple correction factor to be added to an equation such as equation 1, then one would expect that E/K_c would become a function of velocity only. This is not the case, as can be seen in the fifth column of table 2; although the spread of the E/K_c values for different drop sizes, at a given velocity, is much smaller than the spread of the E values.

TABLE 2

DROP-SIZE CORRELATION ATTEMPTS FOR DATA OF FIGURE 11

V (ft/sec)	D (μ)	$K_c \equiv 1 - \frac{10^8}{V^2 D}$	E x 10^6 (From Figure 11)	$\frac{E \times 10^6}{K_c}$	$K_c V$
	350	0.205	2.0	9.75	123
	450	0.383	3.8	9.90	230
600	660	0.578	10.0	17.3	347
	920	0.694	17.0	24.5	416
	1050	0.735	19.0	25.9	441
	350	0.419	7.0	16.7	293
	450	0.547	10.7	19.6	383
700	660	0.690	24.0	34.8	483
	920	0.778	38.0	48.9	545
	1050	0.801	41.0	51.1	561
	350	0.554	20.5	37.0	443
	450	0.642	30	46.7	513
800	660	0.763	47	61.6	610
	920	0.830	78	94.0	664
	1050	0.851	78	91.6	680
	350	0.646	49	75.8	581
	450	0.725	64	88.3	652
900	660	0.813	88	108.0	732
	920	0.886	148	171.0	780
	1050	0.882	138	157.0	793
	350	0.714	100	140.0	714
	450	0.778	116	149.0	778
1000	660	0.848	140	155.0	848
	920	0.891	250	280.0	891
	1050	0.905	220	243.0	905

Another and really more rational way of regarding K_c - since it is a criterion of the deviation both of drop size and velocity from a threshold or critical value - is to argue that the erosion rate E should be a function of $K_c V$, rather than of $(V - V_c)$ as proposed by equation (1). Here V is understood to mean the normal component of impact velocity. The values of $K_c V$ are listed in the last column of table 2, and figure 13 shows that when E is plotted versus $K_c V$, an almost surprisingly good correlation results.

Another valid approach would be to retain the form of equation 1, and accept from the factor $\left[1 - G/V^2 D\right]$ merely the consequence that for a given drop diameter D the critical velocity is given by $V_{cd} = \sqrt{G/D}$. That, in fact, was the reasoning which led to taking the value of $G = 10^8$. This suggests plotting E versus $(V - V_{cd})$ with V_{cd} in this instance being given by $V_c = \sqrt{10^8/D}$. The values of V_{cd} are listed in table 3, and the points corresponding to those of table 2 are plotted in figure 14. Again the correlation seems quite good, though careful examination of the points suggests that the "scatter" is more systematic with drop size than that in figure 13. No formal attempt at curve-fitting has been made for either figure 13 or figure 14, and therefore no statistical data can be given to substantiate or disprove the feeling that the former provides the better correlation. A hand-fitted curve from figure 13, together with values of D_c from table 3, have been used to generate the dotted lines shown in figure 12.

TABLE 3

CRITICAL VALUES OF V_{cd} AND D_c BASED ON $(V^2 D)_c = 10^8$

D (μ):	350	450	660	920	1050
V_{cd}(ft/sec):	535	471	396	330	308
V(ft/sec):	600	700	800	900	1000
D_c(μ):	276	204	156	123	100

The results discussed above should be regarded with caution until similar approaches can be tested against other sets of data. Some validating evidence is afforded by curves of

the dependence of the critical velocity V_c (below which no erosion takes place) on the jet diameter D (in a wheel-and-jet apparatus) presented by Vater.[14] He presented two curves, valid for materials of corrosion fatigue endurance limit of 2000 and 2200 kg/cm^2, which have been approximately averaged and reproduced here as the solid line in figure 15. According to the above hypothesis, this relationship should be represented by $V_c^2 D = G$ = constant if the jet diameter can be regarded as analogous to drop diameter. The dotted line in figure 15 shows such a relationship and follows very closely the experimental curve.

3.2 Physical Reasons for Drop Size Effect

Consider the question as to why there should be a drop size effect at all. The maximum pressure developed under the impinging drop is generally held to be on the order of the water hammer pressure, ρCV, where V is the impact velocity, ρ is the density of the liquid and C is the pressure wave velocity. This magnitude may be modified by factors which depend on the drop shape (e.g. Engel[15]); although Bowden and Field,[16] hold that the maximum value of ρCV holds for spherical drops as well as flat-ended drops), and on the relative acoustic impedance of the target and drop materials (e.g. Vater[14]). None of these is explicitly a function of drop size.

It is not really known, however, what the true criterion of erosion damage is. While some general correlations have been made between the ρCV value corresponding to the critical velocity, and the endurance limit, it has also been shown[17] that surface deformation can occur at ρCV values far below the yield point.

When erosion does take place, there is no certainty that the rate of erosion is strictly a function of impact pressure levels. Thiruvengadam[18] has proposed that in cavitation damage the energy available from the collapsing bubbles is a criterion of the volume rate of material removal, so that the impact energy of impinging drops might be of interest.

The question to be asked is: What properties of the impacts, or of their effect on the target surface, vary when one reduces the size of droplets into which a given amount of water, impinging on a given target area in unit time, is subdivided?

The total impact area (as distinguished from target area) actually increases, since the number of drops increases as D^{-3} and the impact area per drop decreases as D^2 when the drop diameter D is reduced.

In other words, each target area element will be subjected to a greater number of stress pulses per unit time, if one can assume that the contact area of the impact bears a fixed relationship to the projected area of the drop. If this were a significant criterion, then the erosion would be expected to increase with decreasing drop size, which contradicts all experience.

However, another consequence of the increased impact area is that the total kinetic energy (which remains constant) of the impinging water is spread out over a greater area, and therefore the energy flux per unit area is reduced. A hypothesis based on this fact, referred to earlier, led to the suggestion that the factor K_c (See equation 2) represents the drop size effect.

Another factor which is very likely of significance is the duration of the pressure pulse on impact. Whatever precise reasoning is used to predict this duration (e.g. as in Reference 16), it is clear that for geometrically similar drops it must be proportional to drop diameter. Thus the impulse per unit area is smaller in the impact of a smaller drop, and perhaps this is of consequence. Certainly the duration of the impact pressures (on the order of microseconds) are short enough so that strain rate effects, in those materials that exhibit them, may become significant. The smaller the drop, the higher the effective strain rate, and therefore the higher the effective yield point and the smaller the strain induced by the given applied stress which is determined by the impact pressure.

Finally, the impact areas may well be small enough where a size effect of the material itself becomes important. Particularly in the impact of a spherical drop (or sideways against a cylindrical jet), the impact area at the moment of peak pressure will be a small fraction of the projected area of the drop or jet. Size effects have been found in the values of endurance limits of notched specimens, and this has been explained by Peterson[19] by the argument that for fatigue failure to occur, the endurance limit must be exceeded not merely at a "point" or "line" but across a dimension which is on the order of 0.002 to 0.003 inch, and may

bear some relation to the grain size of the material. Since erosion damage, in the velocity domain now under consideration, is primarily a fatigue process and failure has been shown to occur initially by intergranular cracking (e.g. Marriott and Rowden[20], a similar size effect is very possible.

A physical or phenomenological picture of this kind of effect may be formed with reference to a fatigue model proposed by Weibull[21]. He points out that the fatigue process consists of two stages: crack initiation, and crack propagation. A crack will initiate at a point in the material with a high "damage factor" k, which can be regarded roughly as the ratio of the nominal applied stress magnified locally by stress raisers such as scratches or inclusions, to the idealized strength of the material diminished locally by dislocations or other imperfections. The higher the local value of k, the smaller is the number of stress cycles N_o which are required to initiate a fracture at that point. Since the k values are dependent on local aberrations they vary statistically, and hence "N_o is a random variable with large scatter". Once a crack has been initiated, it "raises" the k-field in the vicinity so that adjacent points are brought more rapidly to the crack-initiation stage, and the crack thereby propagates.

As the drop size increases so does the surface area over which the impact pressure (assumed independent of drop size) extends, and so does (by elastic analysis) the depth to which a given stress level extends below the surface. Thus the stress gradient into the material is reduced and the "k" field under the surface is increased. Thus, not only is there a greater chance of initiating a sub-surface crack by virtue of the fact that a greater volume is highly stressed, but the higher value of the "k" field will result in more rapid and deeper crack propagation. In fact, if the depth of the stress field is less than some value characteristic of the grain size, it is unlikely that the cracks would ever propagate around the grain and no erosion may take place. This would establish the "threshold drop size".

It is noteworthy that size effects have been found in other material removal processes: Backer et al [22] discovered a large increase in the shear energy required to remove a unit volume of material, as the chip size (or depth of cut) decreases in turning, micro-milling and grinding operations; the depth of cut in these tests ranged from about

0.010 inch down to 2×10^{-5} inch. It is thought that, as the affected depth of material is reduced, the "theoretical strength" of the material is approached. These findings have been considered by Finnie[23] to be of relevance to erosion by solid particle impingement.

3.3 Effect of Drop Shape

The effect of the shape may be divided into two questions, of which one is difficult to answer at the present, and the other is relatively easy, at least qualitatively.

The first is the effect of the shape of the "front" of the drop, that surface which contacts the target. As previously mentioned, some authors have stated that this shape affects the maximum contact pressure, whereas others hold that it does not. In either case, however, the time rate of the pressure rise and fall, and the variation in time of the actual contact area, will definitely be affected, and both of these (and the interaction between them) will certainly affect the damage produced, if the strain rate effect and material size effect previously mentioned are indeed significant. In addition, the shape of the front of the drop will affect the radial outflow velocity over the target surface after impact (see e.g. Bowden and Brunton[24] and Engel[15], and this in turn is of importance at impact velocities high enough to cause single-impact damage. Complete theories or experimental data relating this geometry to the damage are, however, lacking.

The second question is that of the "tail" of the drop, or its length perpendicular to the contact plane. Bowden's group and also DeCorso[25] have shown in single-impact tests that the length of the impinging mass of water is of little significance. The duration of the high (water hammer) pressure is governed essentially by the time it takes pressure-release waves to move inward from the boundaries of the contact area and meet (or, in the case of an extremely "short" mass of liquid, for the pressure wave to be reflected from its back end as a release wave and return to the contact face). Thereafter, the contact pressure is only the stagnation pressure $\rho V^2/2$, and the mass of liquid arriving then is relatively harmless.

Thus the "effective mass" of an impinging drop or mass of liquid may perhaps be hypothesized to be approximately that mass through which the pressure release waves must travel before the water-hammer pressure is completely relieved at the contact face.

A test result with some bearing on this was given by Brandenberger and de Haller.[4] An elongated jet cross-section was used in a wheel-and-jet apparatus and when impacted by the specimens on its broad side, resulted in far more rapid erosion than when impacted on its narrow side. Unfortunately no quantitative conclusions can be drawn, because in the latter case the "second stage" of erosion was not reached, so that a reliable comparison of erosion rates is not possible, and further because the actual dimensions of the jet cross-section are not given, (although the proportions are suggested by a sketch), so that the size effect and the shape effect cannot well be distinguished. Additional experiments of this type would seem to be of value in helping to establish the significant criteria of a drop's damage potential, even though drop shapes met with in actuality may be of fairly uniform shape.

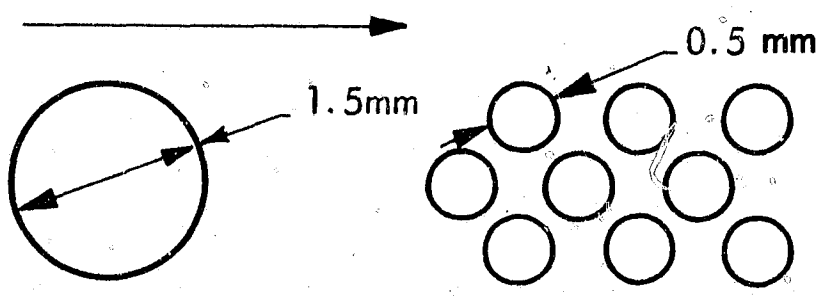

THE ARROW SHOWS THE DIRECTION OF MOTION OF THE SPECIMEN.
LEFT: A SINGLE NOZZLE, RIGHT: NINE NOZZLES

610853-8B

Figure 8. Arrangement of Nozzles for Water-Jet Tests (Taken from Reference 5)

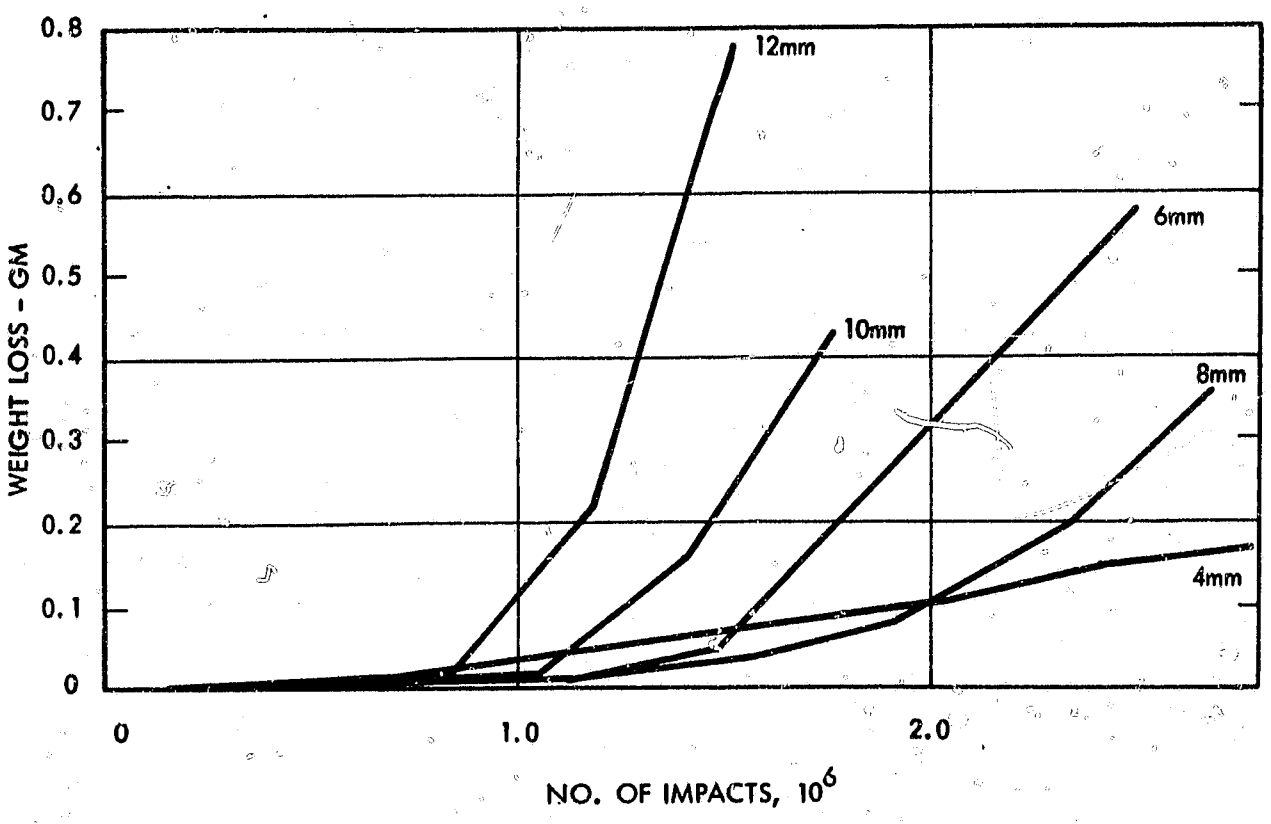

(A) DATA AS PRESENTED IN REFERENCE 4

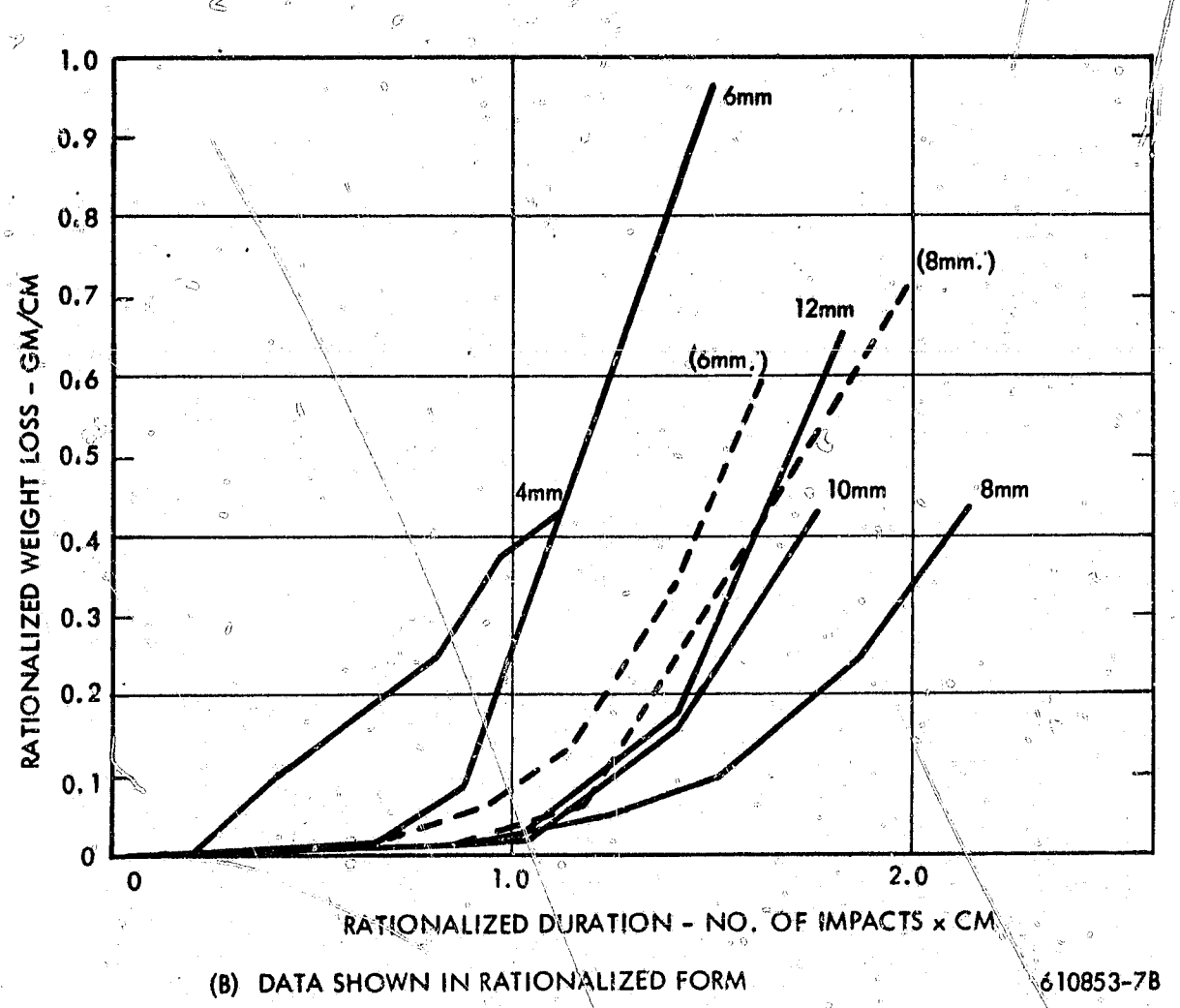

(B) DATA SHOWN IN RATIONALIZED FORM

610853-7B

Figure 9. Erosion Versus Jet Size (Adapted from Reference 4)

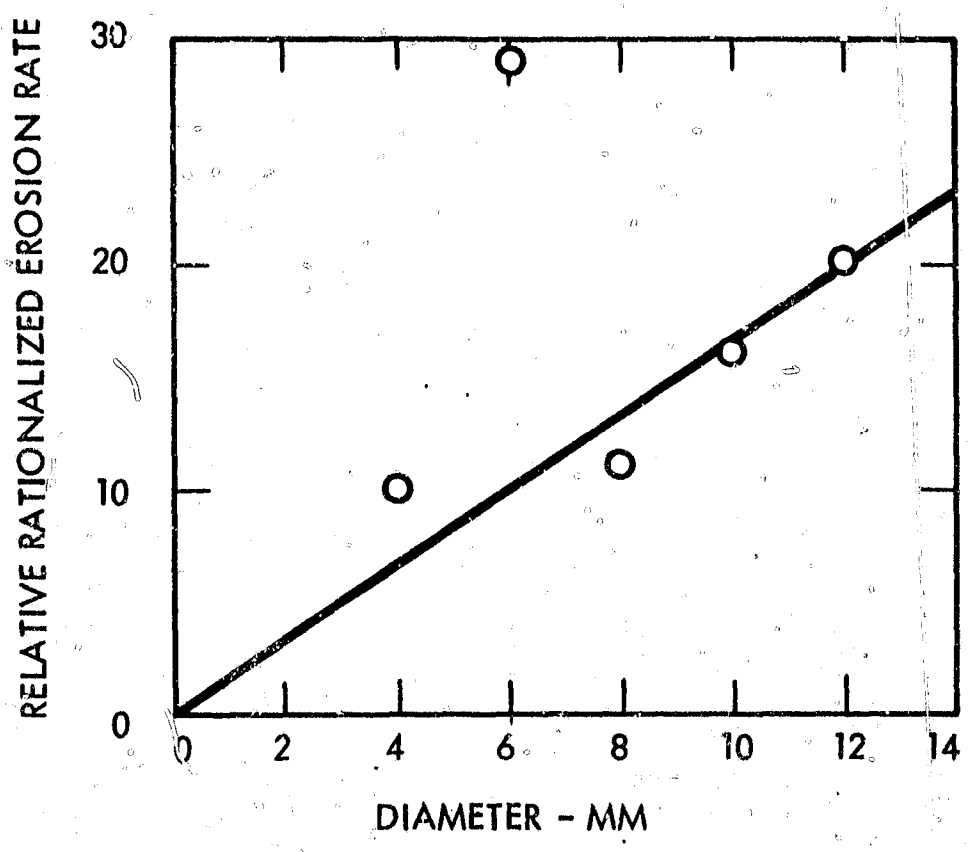

(A) DATA WITH 6mm & 8mm AS LABELED

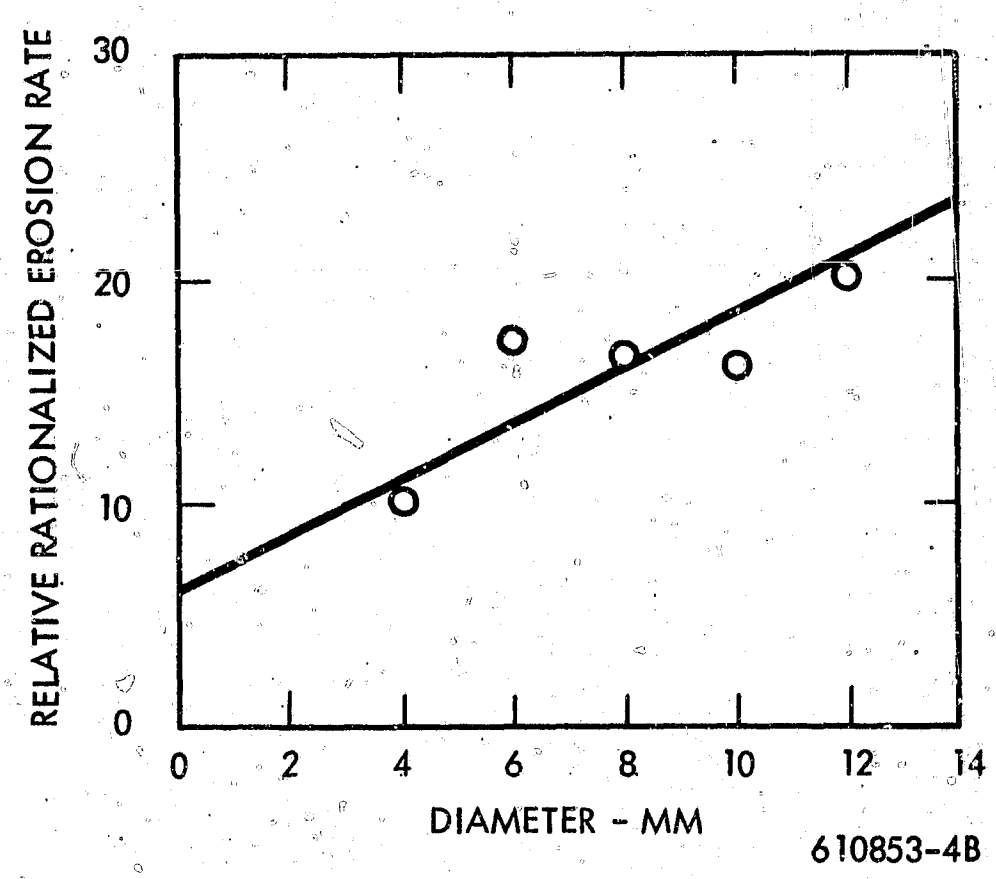

(B) DATA WITH 6mm & 8mm REVERSED

Figure 10. Erosion Rate Versus Jet Diameter (From Data of Figure 9)

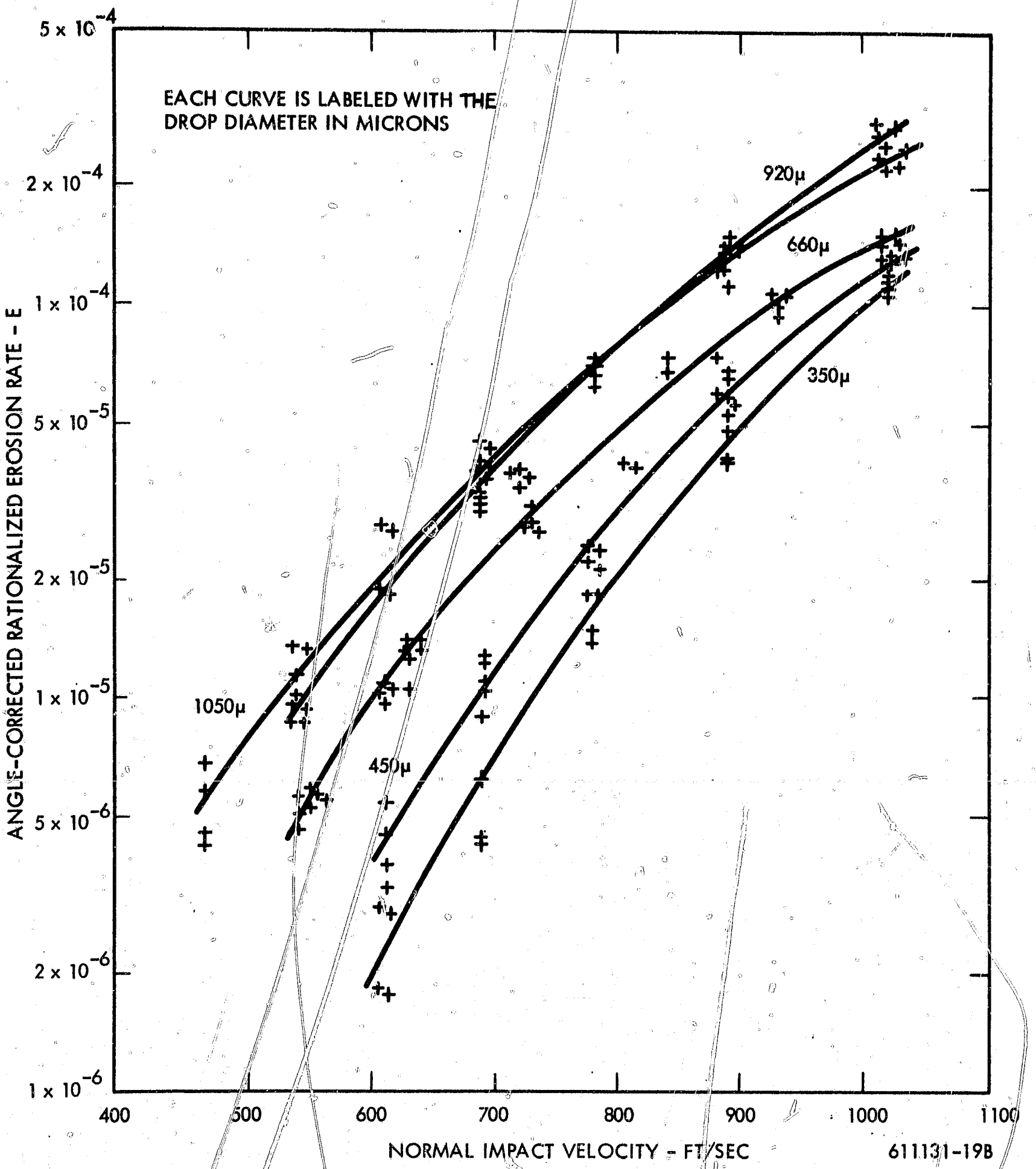

Figure 11. Effect of Drop Size on Erosion Rate (From Reference 13)

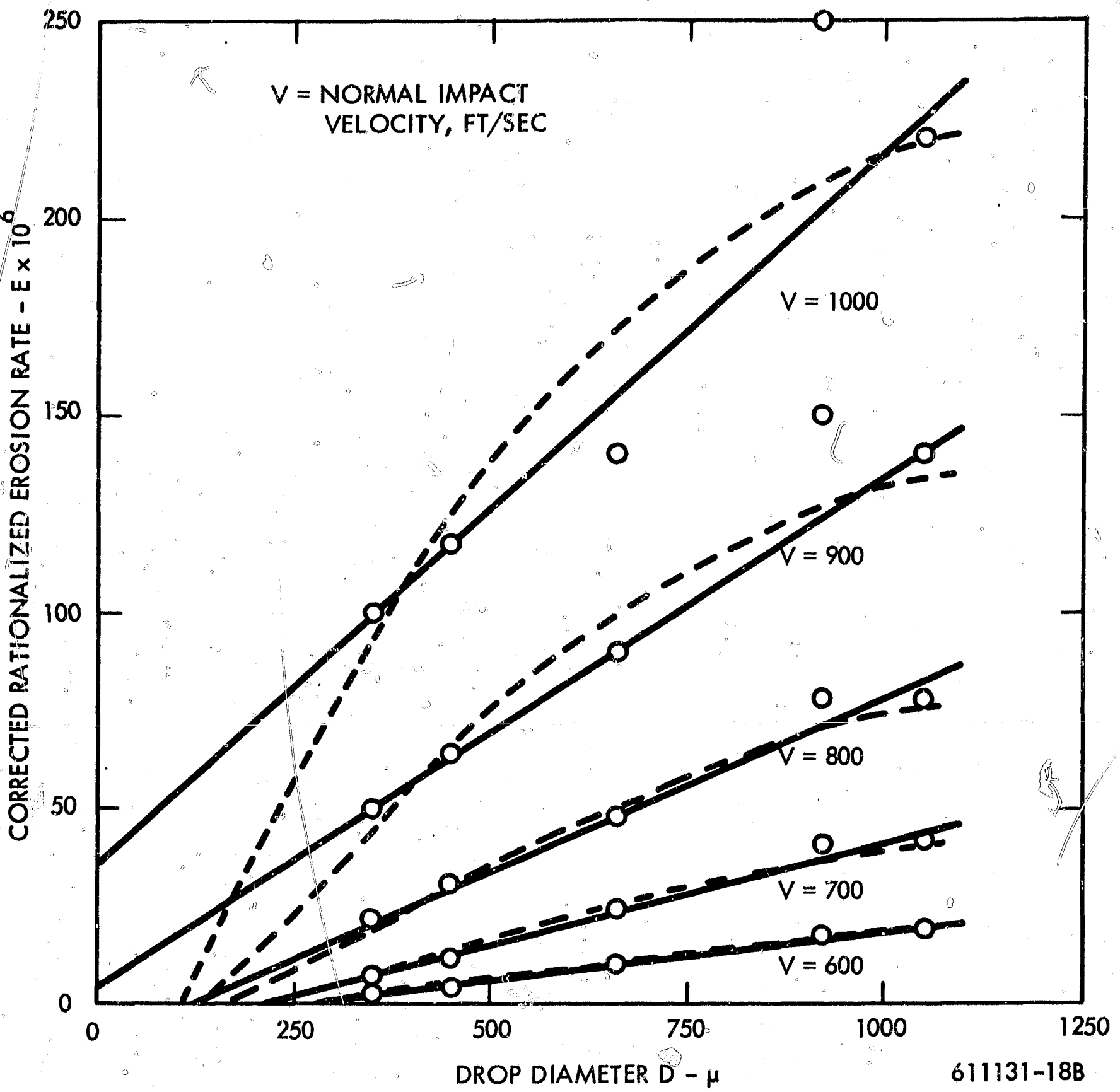

Figure 12. Effect of Drop Size on Erosion Rate (Data Cross-Plotted from Figure 11). Dotted Lines are Based on Correlation of Figure 13.

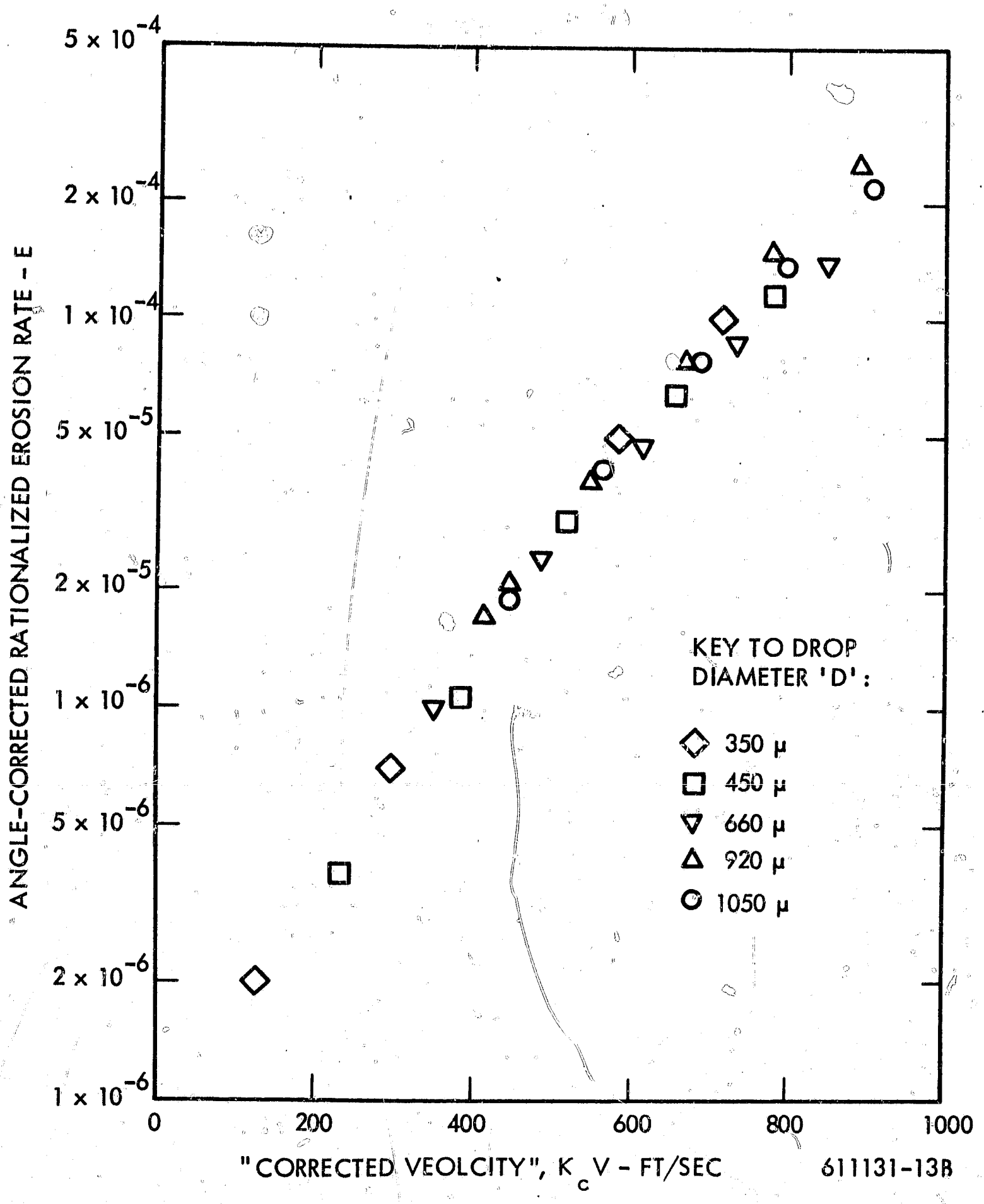

Figure 13. Correlation of Data of Figure 11 by Use of "Critical Factor"

$$K_c \equiv \left[1 - 10^8/V^2D\right]$$

Astronuclear Laboratory

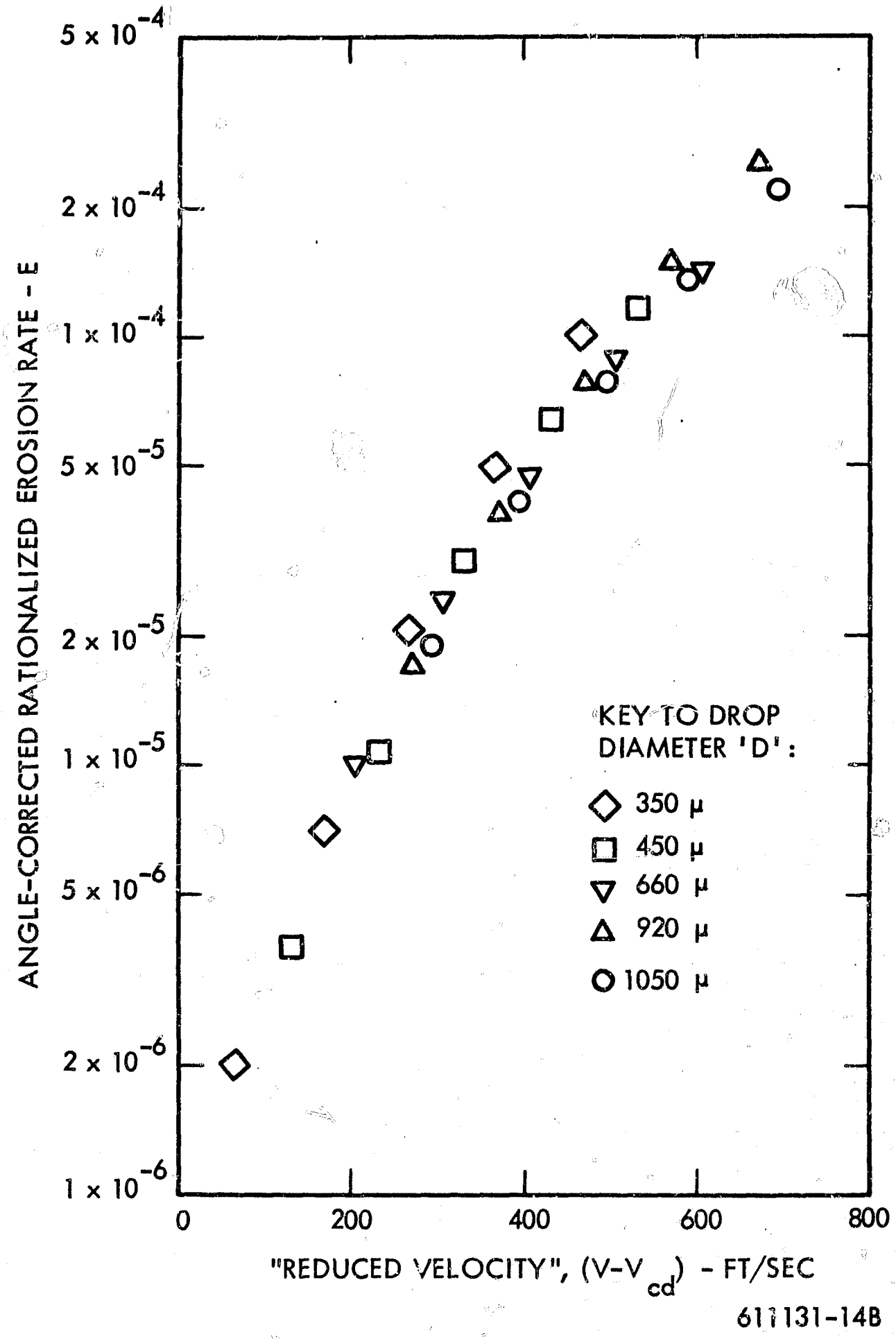

Figure 14. Correlation of Data of Figure 11 by Use of "Critical Velocity"

$$V_{cd} \equiv \sqrt{10^8/D}$$

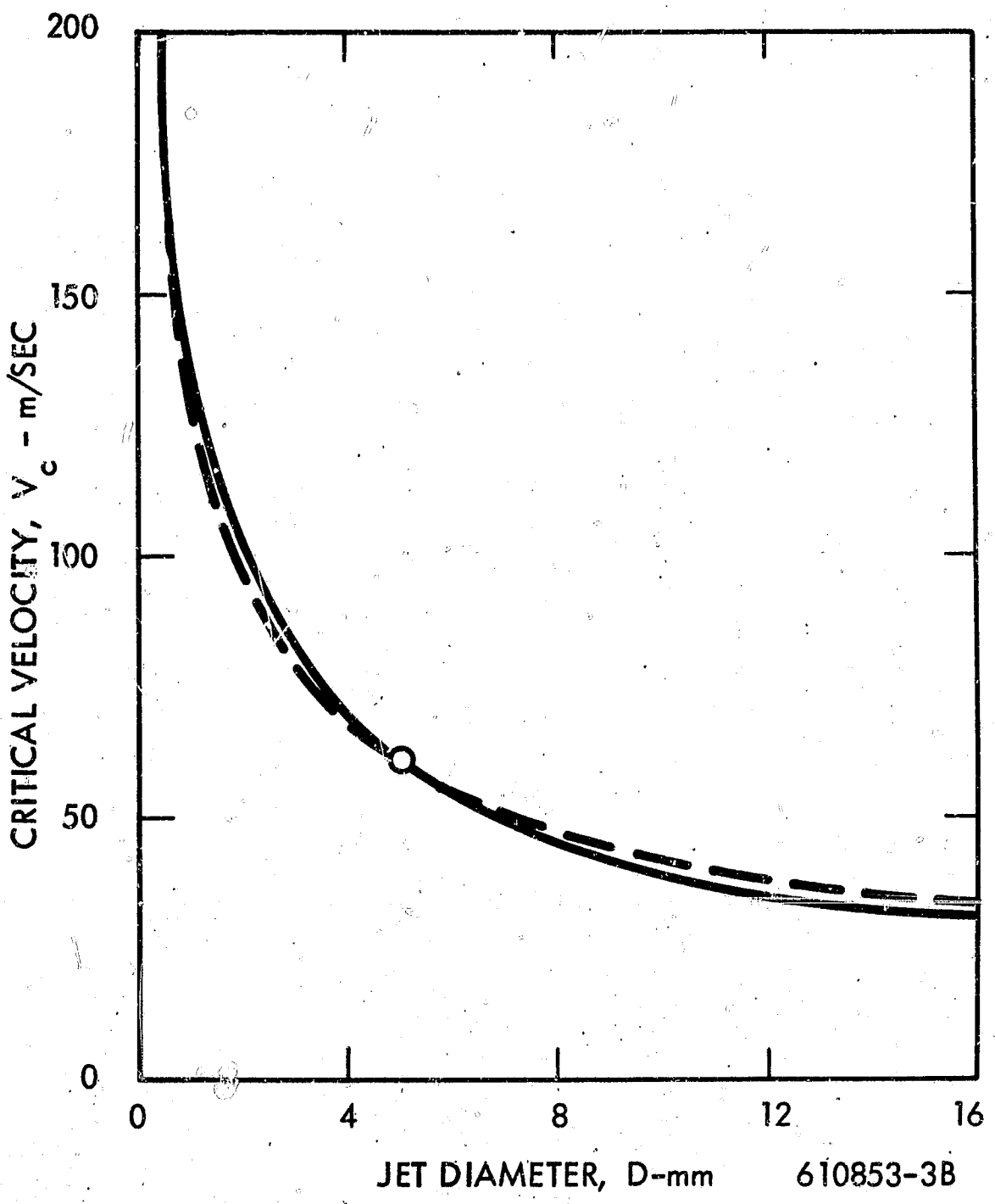

SOLID LINE: CURVE FROM REF. (14)

DOTTED LINE: $V_c^2 D$ = CONSTANT (NORMALIZED TO PASS THROUGH POINT 5, 60)

Figure 15. Critical Velocity Versus Jet Diameter

4.0 DEPENDENCE ON IMPACT VELOCITY

4.1 Some Simple Empirical Equations for Velocity Dependence

The literature contains a considerable body of data relating erosion to velocity, but the usefulness of much of these data is limited by the considerations discussed in Section 1.0.

There are various functional forms to which one can attempt to fit such data; the most obvious ones are briefly discussed below. Here E = erosion rate and V = velocity.

$$E = a\, V^n \tag{3}$$

This represents a simple power relationship, and implies that some erosion will take place no matter how low the velocity is. Usually, however, it is thought that there is a critical or threshold velocity V_c below which erosion is absent for all practical purposes. An obvious type of relationship to reflect this is

$$E = a\,(V - V_c)^n \tag{4}$$

$$= a_1 \left(\frac{V}{V_c} - 1\right)^n \tag{4a}$$

This implies that erosion is proportional to a power of the velocity in excess of the critical or threshold velocity V_c. Pearson's equation, previously quoted in Section 2 of this report, is of that type, and, as will be seen later, it has been used by a number of other authors to express their results.

Another type of relationship involving a critical velocity is

$$E = a\, V^n - b \tag{5}$$

which implies $V_c = (b/a)^{1/n}$

and can be rewritten

$$E = a_1 \left[\left(\frac{V}{V_c} \right)^n - 1 \right] \qquad (5a)$$

Clearly both (4) and (5) have the property that

when $\left(V/V_c\right)^n >> 1$, $E \rightarrow a_1 \left(\frac{V}{V_c} \right)^n$ (6)

and when $V/V_c \rightarrow 1$, $E \rightarrow 0$.

4.2 Some Physical Considerations Relating to Velocity Effect

4.2.1 Analogy with Fatigue S-N Data

Which among equations (3), (4) and (5) is a more logical choice depends to some extent on what physical reasoning--if any-- is used to account for the influence of velocity. One physical argument can lead to yet another type of relationship: Vater [14] [16] has noted that since erosion is a fatigue phenomenon, and the applied stress is proportional to (or at least a function of) velocity, the relation between velocity and erosion lends itself to a treatment analogous to the relation between stress and cycles to failure in fatigue. He has presented curves in which velocity is plotted versus the number of impacts to obtain a given weight loss (Figure 16a), or versus the reciprocal of the weight loss obtained after a given number of impacts (Figure 16b). (The latter is, however, once more an example of spurious comparisons, since after a given number of impacts, different stages of the erosion-time curve may have been reached.)

Some caution must be exercised in making direct analogies between S-N fatigue curves and velocity versus erosion curves. If one assumes that erosion is taking place as a steady-state process, and that the mean size of erosion fragments is independent of V, then the volume rate of erosion E would indeed be proportional to 1/N, where N is the mean number of impacts required to generate a loose erosion fragment. In turn, N could be assumed to be related to the impact

stress and hence to the velocity V in a manner similar to the relation between cycles to failure and stress in conventional fatigue tests.

If these assumptions are correct, a V - (1/E) curve should exhibit similar characteristics to a S-N fatigue curve. Even if erosion cannot be conceived of as a steady-state process, then the number of impacts to obtain a given cumulative volume loss (as plotted in figure 16a) should be a valid analogy, provided that there are no variations in the initial target surface conditions which could affect the life-times of the original surface layer elements. (It might be pointed out that one implication of the erosion-rate-time model proposed in Part B is that the erosion process during the period of maximum erosion rate is generally not a steady-state process; rather this peak in the rate-time curve can occur as a result of a "deluge" of erosion fragments being loosened at about "the most probable value" of the number of impacts to failure, as measured from the time the impingement attack was initiated. It is only because of scatter in the sizes and the impacts-to-failure of the erosion fragments, that there is a tendency toward a steady-state value.)

Fatigue S-N data are often depicted as an approximately straight line on a semi-log plot for intermediate values of N, as follows:

$$S = S_o - b \log N$$

with a leveling off to $S = S_y$ at low values of N, and a transition to $S = S_E$ at high values of N. where

S = stress corresponding to N cycles

S_o = intercept of straight line on stress axis ($S_o > S_y$)

S_y = yield stress

S_E = endurance limit.

Consequently, one might expect some analogous relationship such as

$$V = a - b \log \left(\frac{1}{E}\right)$$

or, in a form which is equivalent but more consistent with the previous types of equation listed,

$$E = a\, e^{nV} \tag{7}$$

where e is the base of logarithm chosen. This equation of course does not predict a critical velocity and must be combined with the separate condition that there is a transition to $E \rightarrow 0$ at some value $V = V_c$.

As pointed out before, this relation, even for conventional fatigue data, is valid only within a limited range. A number of more complicated equations have been proposed for representing S-N data over the full range of values; these are surveyed on pages 174-178 of Reference 27. Such equations would predict a critical velocity. It does not seem profitable to attempt to use these, however, partly becuase of the computational difficulty involved and partly because one of the previously mentioned assumptions inherent in this direct analogy is almost certainly unjustified; that is the assumption that the mean erosion fragment size is independent of impact velocity. Since a higher velocity generates a greater impact pressure which in turn produces a larger stress-field in the target, i.e. a greater volume of material is highly stressed, it seems very likely that the mean fragment size increases with velocity. A velocity relationship could be postulated from this fact alone, as will be shown below.

4.2.2 Approach Based on Size of Stress-Field under Impact

The approach will be demonstrated with reference to a two-dimensional model, which would apply to the wheel-and-jet type of apparatus: It is assumed that the contact pressure between the "jet" whose side impinges against the target (or vice versa), and the target surface, can be reasonably represented by a belt of uniform pressure over the surface of a semi-infinite solid, and furthermore that the effective width "2a" of this belt is a function of "jet" size and shape and is independent of impact velocity. (This assumption seems more reasonable than a Hertzian contact stress distribution which would imply that the liquid behaves as an elastic solid on impact.) This corresponds to Case No. 11 on page 322 of Roark [28] where formulae are given for the compressive and shear stresses anywhere within the solid. Since the shear stress is surely a better criterion for failure than the compressive stress,

consider the locus of a constant value of shear stress, S, as a function of the contact pressure p and the semi-width of the pressure belt, a. The formula given by Roark is

$$S = 0.318\, p \sin\alpha \qquad (8)$$

$$= (1/\pi)\, p \sin\alpha$$

where α is the angle subtended, at the point in question, by the boundaries of the pressure belt on the surface. It can easily be shown that the locus defined by equation (8) consists of two circular arcs of radius r, where

$$\frac{r}{a} = \frac{1}{\pi}\,\frac{p}{S} \quad ,$$

whose centers lie a distance d respectively below and above the solid surface, where

$$\frac{d}{a} = \sqrt{\left(\frac{r}{a}\right)^2 - 1}$$

This is shown in figure 17. The region stressed to values greater than S lies between the two arcs. Figure 18 shows these loci for a number of values of p/S; the highest value of the shear stress is of course $S = p/\pi$, and its "region" reduces to a semi-circular locus of radius r = a.

Figure 18 can be regarded in two ways. It can represent the loci of various shear stresses in a given stress field, if we assume the contact pressure p to be a fixed quantity. On the other hand, assuming the shear stress S to be the independent fixed quantity, then the lines on figure 18 represent the "spreading" of the boundaries of the region bounded by that stress, as the contact pressure p is increased. It is the latter point of view which we adopt for our argument.

For the purpose of this argument we assume that if a "reference stress" S is selected exceeding an appropriate critical value or endurance limit, then the "reference time" (or number of impacts) required for fracture to have occurred all around the locus of S is independent

of the length of that locus, since a greater length presents a proportionately greater number of crack initiation points. At this fixed "reference time", all the material between the original surface and the lower locus will have been lost. Therefore, a lower limit to the change in the erosion rate with contact pressure (and hence with velocity) is provided by the change in the area A_S which lies between the original surface and the lower locus of a given value of S, as p is increased.

The non-dimensionalized area A_S/a^2 has been computed as a function of p/S and is plotted on log-log scales in figure 19, which therefore should represent an approach to a velocity-erosion rate relationship. Note that the slope begins at a high value and gradually approaches the value of 2.

One should not, of course, take this model so literally as to infer from it that fracture actually occurs by cracks following along these loci. Moreover, it clearly gives a lower limit to the erosion rate because it ignores the fact that earlier fractures will occur above the reference stress locus because of the higher stresses there, thus altering the geometry and causing the locus of S to progress further down into the solid. In particular, this model predicts that when the pressure reaches $p = \pi S$, the erosion jumps from zero to a value corresponding to an area $A_S/a^2 = \pi/2 = 1.57$. In actuality, if the "reference stress" S is chosen to be above the endurance limit S_e so that the "reference time" is not infinite, then for all values of p such that $p > \pi S_e$ there will still exist stresses high enough to cause material loss, though not within the same reference time. The model does show, however, that some quantitative conclusions may be drawn from a fatigue point of view, without any reference to specific S-N relationships. It also serves to emphasize that the extent of the stress field under the impact must be taken into account in any analytical approach to predicting the erosion-velocity relationship, whether that approach is based on stress or energy concepts.

4.2.3 Energy Considerations

An energy approach was described in pages 167-174 of Reference 1, which sought to predict effects both of velocity and drop size on the erosion. It was based on the assumption that the volume of material removed per unit area per impact, is proportional to (or a function of) the impact energy per unit area in excess of some energy threshold per unit area character-

istic of the material surface. This resulted in the following relationship, expressed in non-dimensional terms:

$$E = f\left\{ k_2 \left[\frac{\frac{1}{2} \rho_L V^2}{S_o} \right] \left[1 - \frac{e_o}{k_3 \frac{1}{2} \rho_L V^2 D} \right] \right\} \qquad (9)$$

where

E = rationalized erosion rate

$= \left(\frac{\text{volume of eroded material}}{\text{volume of impinged liquid}} \right)$

V = impact velocity

D = characteristic dimension of droplet

ρ_L = density of liquid

k_2 = ratio of "effective" volume to total volume of drop

k_3 = ratio of "effective volume" to "effective impact area" times drop dimension

s_o = characteristic strength (or elastic modulus) of material

e_o = "threshold energy" per unit area of material surface

f = functional relationship or factor of proportionality

In a simplified form, and to bring out the "threshold conditions" implicit in it, equation 9 can be rewritten as:

$$E = f_1 \left[V^2 \left(1 - \frac{G}{V^2 D} \right) \right] \qquad (9a)$$

where G represents a "critical value" such that if $V^2 D < G$ no erosion takes place. (The relationship is of the type of equation 5.) This critical value has proved quite successful, in one or two instances, of correlating drop-size effect data, as was shown in the previous section.

In particular, it was shown that the data of Pearson in Reference 13 correlated well in the form

$$E = f_2 \left[V \left(1 - \frac{G}{V^2 D} \right) \right] \qquad (10)$$

However, the difference between equations 9a and 10 indicates that the energy threshold concept – at least in its present form – is still deficient.

While a number of authors recently have sought to predict both erosion strength and erosion attack severity in terms of energy concepts (e.g. Thiruvengadam[18, 29, 30 and 31]; Hoff et al[9]; Shalnev et al[32]), there are considerable difficulties to be faced. The energy balance involved in a droplet impact is very complex and has not yet really been examined in sufficient depth. Part of the kinetic energy of the impinging drop will remain as the kinetic energy of the radial outflow velocities; part will be dissipated in the shock or pressure waves passing through the drop and part in the shearing associated with the change of direction of the liquid flow; part will be dissipated in the target material, and here too, the energy dissipation associated with stress waves should be examined considered as well as the quasi-static plastic strain hysteresis energy associated with each impact stress cycle. The picture is further complicated by the rather large amount of energy which will temporarily be stored as elastic strain energy in the target and which will reappear in one of the previously-mentioned forms.

The energy dissipated in the target material is that associated with fracture and therefore with erosion. But it is by no means true to assume that the volume of material removed is proportional to that energy. Two reasons account for this: One is that (at least in the case of larger drops at moderate velocities) erosion fragments produced by the random linking-up of fatigue-like cracks (See Reference 20) are not likely to be deformed to the fracture point throughout their volume, and therefore the accumulated plastic strain energy may be more related to the surface area of the fragment than to its volume, or, at the least, be non-uniformly distributed within the volume. The other is that in fracture due to the repeated stressing, the total energy input increases greatly with the number of cycles to failure. This is evident in McAdams' results for impact fatigue tests,[33] and has recently been documented for a large collection of fatigue data

by Halford.[34] Even if one postulates that the damaging energy is the same in all cases and the excess hysteresis energy is dissipated through non-damaging processes, the fact remains that all of the dissipated energy is supplied by the impinging droplets and even if the energy absorption by the target material is known, that in itself will not establish the erosion rate. The crudest broad conclusion one can draw from the above is that the erosion is likely to vary with the velocity to a power higher than 2, since the "impinging energy" is proportional to velocity squared, and the total energy to failure decreases with increasing velocity (i.e., with increasing stress and decreasing number of impacts to failure).

4. Relation Between Impact Pressure and Velocity

A final note of relevance to this subject concerns the relationship between the impact velocity and the contact pressure generated. This relationship is often presented as the water-hammer equation,

$$p = \rho CV \tag{11}$$

although with a relatively elastic target material, its characteristics must also be considered and hence, the elaborated form:

$$p = \frac{V}{\left(\frac{1}{\rho C} + \frac{1}{\rho_T C_T}\right)} = \frac{\rho CV}{\left(1 + \frac{\rho C}{\rho_T C_T}\right)} \tag{12}$$

where

p = impact pressure

V = impact velocity

ρ = liquid density

ρ_T = target density

C = pressure wave velocity in liquid

C_T = stress wave velocity in target

The question of whether these equations are to be modified by virtue of the drop geometry has been touched on in Section 3.2. The point to be made here is that for the conditions of a high-speed impact, in which V is a substantial fraction of the acoustic velocity C_o in the liquid, or may even exceed it, it is quite incorrect to approximate C by C_o (and, ultimately, to approximate C_T by C_{oT}, the acoustic velocity in the target material).

To clarify this conceptually, one may imagine a long cylinder of liquid impinging end-on upon a rigid surface: a compression front, which forms the boundary between the liquid brought to rest and that still moving, then leaves the plane of impact and propagates upstream through the liquid cylinder at a velocity C relative to the approaching liquid. From simple momentum considerations one can then deduce the relationship $p = \rho CV$, but it is also obvious that C must always exceed V no matter how great the latter, since otherwise the compression front could not move away from the impact surface and no "storage space" would be created for the liquid brought to rest. The exact determination of C as a function of V depends on the compressibility properties of the liquid and is not obtainable in any simple analytical form. Pearson [35] has made this determination for water up to $V = 1600$ ft/sec, and has compared his results with earlier ones of Kirkwood and Montroll [36] which extended to a somewhat higher velocity. His data are shown in figure 20. Pearson stated that the results can be approximated by

$$p \propto V^{1.3} \qquad (14)$$

This, however, is true only for a limited range of the data, and one could show easily that the relationship $C \propto V^n$, implicit in equation 14, is not a proper form even for an empirical C-V relationship. Unfortunately, even a simple empirical form seems to be elusive.

At any rate, the numerical results of Pearson show that at $V = 1500$ ft/sec, the actual impact pressure is 60 percent greater than that based on $C = C_o$, and in general, since p increases

more than linearly with V, the rate of change of erosion rate with respect to velocity will be greater than that of erosion rate with respect to stress or impact pressure (such as deduced in Section 4.2.2 above).

4.3 Empirical Data from the Literature Search

4.3.1 Preliminary Remarks

In attempting to fit a simple equation to experimental data, equations like (3), (4), (5) or (7) would be selected. Equation (4) would form a straight line on log-log paper if plotted versus $(V - V_c)$, but one does not know V_c ahead of time. Equation (7) would form a straight line on semi-log paper, with V along the linear scale.

Figure 21 shows examples of these various relationships on a log-log plot. The upper portion represents equations of types (4) and (5) with V/V_c plotted against E, and the lower portion equations of types (3) and (7) with V plotted against E. For consistency, the constants "a" have been chosen so that all curves pass through the point E = 1, V or $V/V_c = 2$. A plot of this kind may be of help in deciding what type of relationship to try to fit to experimental data points when these are plotted on a log-log graph. A corresponding plot of these families of curves could be constructed on semi-log paper, with E as the log coordinate; in that case the equations of type (7) would, of course, plot as straight lines.

A number of problems arise when attempting to establish an equation of one of these types for experimental data, either by plotting the data points on log or semi-log paper, or directly by numerical methods.

One of the problems is that much of the data are obtained at velocities not very much greater than the critical velocity (seldom at more than $V/V_c = 2$). Therefore one is probably examining that portion of the curve in which a "transition" is taking place or in which, even in a log-log plot, the curvature is greatest. This has the consequence that small errors in the data points, or small differences in the manner in which a smooth curve is "fitted" to them, will have a large effect on the values of the exponent n and the critical velocity deduced therefrom.

This difficulty is compounded by the facts that the scatter in erosion data is inevitably fairly great, that in many of the test series no more than three velocities have been investigated,

and that the ratio of the highest to the lowest of these is often quite small - about 1.5 . This covers a very short span of the velocity axis on log-log paper. In short, a problem exists in which:

1) In the velocity range investigated the "true" relationship will not appear as a straight line.
2) There are too few data points and these cover too short a velocity range to allow a curved line to be fitted with the necessary accuracy.

If testing could be done at much higher velocities, then in theory the influence of V_c on the "apparent exponent" - i.e. the slope of the curve on a log-log plot - would be reduced and a more accurate determination could be made of n. In practice, however, at velocities much above $V/V_c = 2$ one gets into the region of single-impact damage, whose velocity dependence may not be the same as that for fatigue damage, and so one may well be in another transition region.

4.3.2 Examination of the Better Test Data

One of the earliest comprehensive sets of test data at various velocities was given by Honegger.[5] His often quoted conclusion was that while the behavior of the various materials differs considerably, the rate of erosion "may be generally expressed as":

$$E \propto (V-125)^2 \qquad (15)$$

where V is the impact velocity in m/sec. The above relationship was evidently deduced from his figure 7, on which was plotted the "specific loss in weight" (weight loss per impact, hence a measure of erosion rate E) after 215,000 impacts, versus velocity. This type of comparison, as pointed out before, is not valid. Also, the equation fits a "mean curve" drawn through the band of experimental curves; but some individual curves suggest exponents that are much higher. Thus, the curve for Specimen No. 26 is well described by $E \propto (V-110)^{3.3}$.

For a more valid basis of comparison, the rate-time curves presented for various materials and for the speeds of 175, 200 and 225 m/sec should be reviewed. From these, one can, with some effort, deduce characteristic erosion rates which fulfill the criteria

specified in Section 1 of this report. This has been done in a very approximate manner, and the results are plotted on log-log coordinates in figure 22. Their shape is not unlike what is predicted by figure 19, at velocities close to the threshold value, but it would be bold indeed to attempt to fit any empirical equation to these data.

An interesting set of results on one material was reported by Brandenberger & DeHaller,[4] which was discussed earlier in Section 2, with reference to the angle-effect. The " rationalized erosion rates" deduced from Reference 4 were plotted in figure 7, and the data points of figure 7b have been re-plotted on semi-log coordinates on figure 23. They fall remarkably well into a straight line, giving some support to the simple fatigue model of velocity dependence represented by equations of type (7). It should be pointed out, however, that the determination of the "best" values of E, from the irregular slopes of the very small graphs shown in Reference 4, involved a certain amount of judgment and some extrapolation for the u = 31 m/sec data. In preliminary attempts, with fewer pretensions to accuracy, the results were such as to fit equations of types (4) or (5) better than type (7). The following equations have been fitted to the data of Reference 4 during these several attempts:

$$E \propto (V-20)^{3.5}$$

$$E \propto (V-25)^{2.6}$$

$$E \propto \left(\frac{V}{31}\right)^{4} - 1.0 \qquad (16)$$

$$E \propto e^{0.126\,V}$$

$$E \propto V^{6}$$

And yet these data are among the better in the literature, in that the velocity range covered was almost 2:1 and there were 8 data points in that range. This, again, demonstrates the (near)

futility of applying a purely empirical approach and hoping to deduce therefrom some useful generalizations.

Another set of data covering an even larger velocity range was given by Hobbs in his discussion to a paper by Leith and Thompson,[37] although no information was given on the material tested. The data were plotted on linear coordinates, labeled "rate of weight loss, mg/sec" and "impact velocity, ft/sec" respectively. From the units in which the erosion rate is given, one must infer that these data are not "rationalized", and that, therefore, the erosion rates should be divided by a factor proportional to the corresponding velocities to put them on a rationalized basis, i.e., on the basis of equal rates of impinging water. The actual data points from Hobbs' graph, and the values of E computed therefrom, are given in Table 4:

TABLE 4

DATA OF HOBBS IN REFERENCE 37

V ft/sec	Erosion Rate, R gm/sec	Rationalized Rate, E (2×10^3 R/V)	"Reduced Vel." (V-270) ft/sec
270	0	0	0
330	0.02	0.122	60
385	0.03	0.156	115
440	0.06	0.272	170
495	0.11	0.444	225
570	0.32	1.12	300
620	0.40	1.29	350
680	0.85	2.50	410
735	1.01	2.75	465
775	1.28	3.30	505
825	1.58	3.83	555

The values of E have been plotted on log-log scales in figure 24, both against actual velocity V (Curve "a"), and also against $(V-V_c)$ with V_c taken as 270 ft/sec (Curve "b"). Smoothly

fitted curves are drawn as solid lines, and straight-line approximations as broken lines. These latter suggest that the results can be represented, over a certain range, by

$$E \propto V^{4.4} \quad , \text{ or by}$$

$$E \propto (V-270)^{2.4} \tag{17}$$

The latter may result in somewhat less scatter, but is valid over a more restricted range. The same data are shown plotted on semi-log coordinates in figure 25. A straight line fits the data well in the lower velocity range, but a distinct breakaway from it occurs at about 700 ft/sec. Thus, these results, too, provide no evidence pointing toward any particular simple type of empirical formulation.

The most comprehensive body of test data recently made available is that of Pearson.[11] [13] These data have already been discussed in relation to angle effects in Section 2 and drop size effects in Section 3, and in the latter section there was success in "collapsing" the data for different drop sizes into a single curve, by two different methods, as shown in figures 13 and 14. No actual curves were drawn in those figures so as not to obscure the data points themselves. Curves fitted by hand to these points are shown in figure 26. Curve (a) represents figure 13 and Curve (b) figure 14. The same curves, transposed onto log-log coordinates, are shown in figure 27, and straight lines (dot-dashed) are shown which coincide with the curves themselves at the values $E = 10^{-5}$ and $E = 10^{-4}$, and are reasonably valid approximations for the range from $E = 5 \times 10^{-6}$ to $E = 2 \times 10^{-4}$. These lines represent relationships as follows:

$$\text{Curve (a):} \qquad E \propto (K_c V)^{3.05}$$

$$\text{Curve (b):} \qquad E \propto (V-V_{cd})^{2.5} \tag{18}$$

where K_c and V_{cd} have been defined in Section 3 and in figures 13 and 14.

Note that the latter has an exponent fairly close to the expression deduced by Pearson[11] for a single drop size:

$$E \propto (V-390)^{2.6} \qquad (19)$$

Note also that the general appearance of the curves of figure 27 is similar to those of figure 24 (except for the curvature at the highest velocities), and that the general appearance of those in figure 26 is not unlike that of figure 25: In particular curve 26a could reasonably well be approximated by a straight line below about 600 ft/sec with a breakaway above that. (It must be remembered, however, that in figure 25 the horizontal scale is actual velocity, whereas in figure 26a it is a "corrected velocity" which is not a linear function of the actual velocity.)

4.3.3 Conclusions

About the only conclusion which seems justifiable, at this stage, is that even the best available erosion-versus-velocity data do not follow exactly any law such as represented by equations of types (3) through (7), but can, over limited ranges, be approximated by any of them. Equations of type (4) have seemed intuitively as most rational and have been adopted by many authors, including Honegger (See equation 15 above), Pearson (equation 19 above), and Fyall et al[6] who present the following equation for the erosion rate of "perspex":

$$\text{Weight loss rate} \propto (V-208)^{3.37}$$

This, however, refers to the velocity of a target within a given "rainfall": thus the rate of water impingement increases linearly with velocity and the "rationalized erosion rate" would be given by

$$E \propto (V-208)^{2.37} \qquad (20)$$

Comparison of the various equations of type (4) which have been listed above suggests that when data can be represented in this manner, the value of the exponent will be not too far from 2.5.

Comparison of figures 23 - 27 suggests that equations of type (7) tend to fit better in the lower velocity region (although there must also be transition to the critical velocity), whereas equations of type (4) fit best in the intermediate velocity region.

If a direct power law of type (3) is used to represent the results, the exponents tend to range from 4 to 6, though for brittle materials such as glass exponents as high as 13 have been quoted by Langbein. (8)

In no case does it appear justifiable to use any of these curve-fitting equations for the purpose of extrapolating out of the test range.

Astronuclear Laboratory

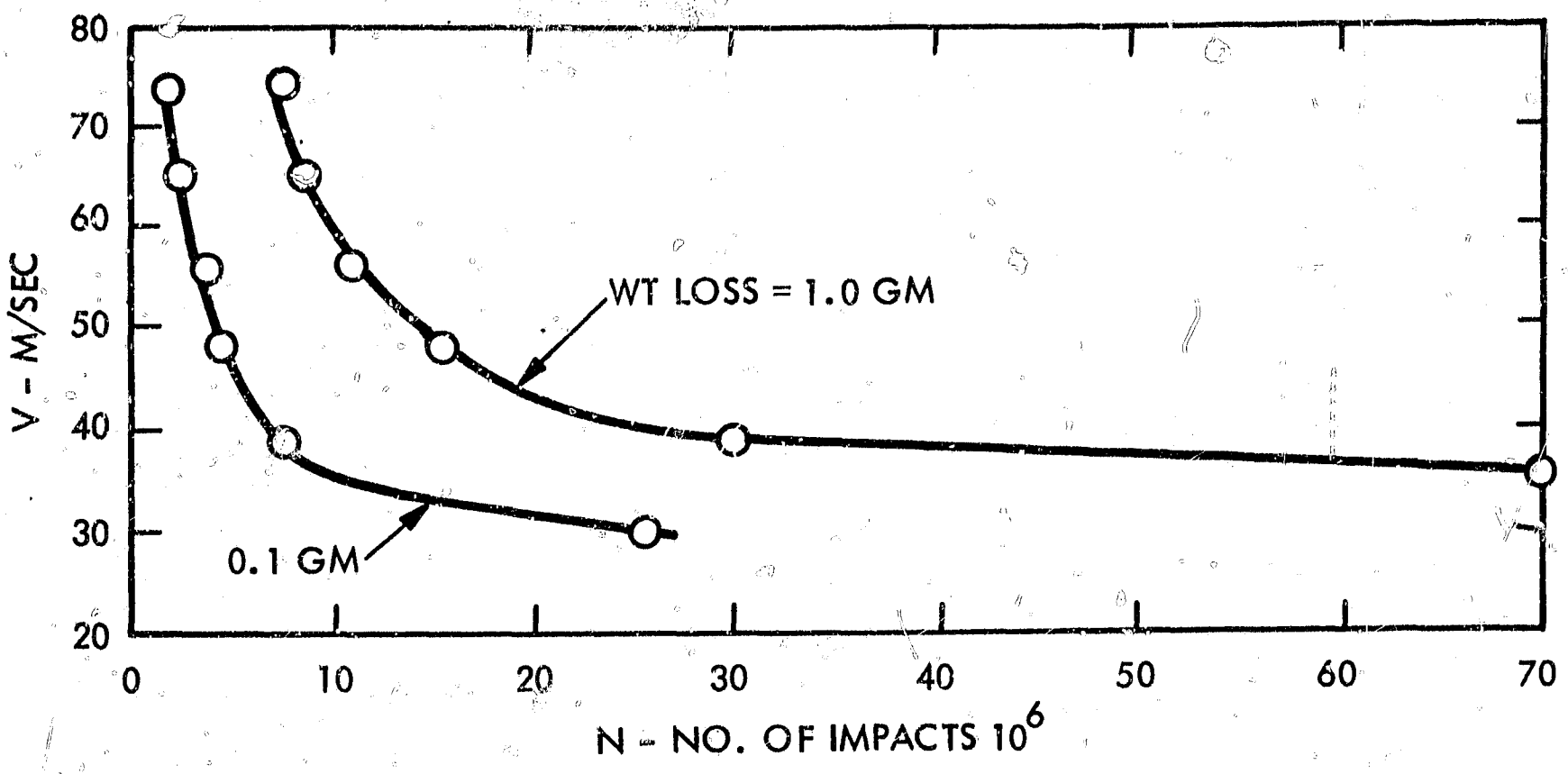

Figure 16a. Example of V-N Curve (Adapted from Figure 15 of Reference 14)

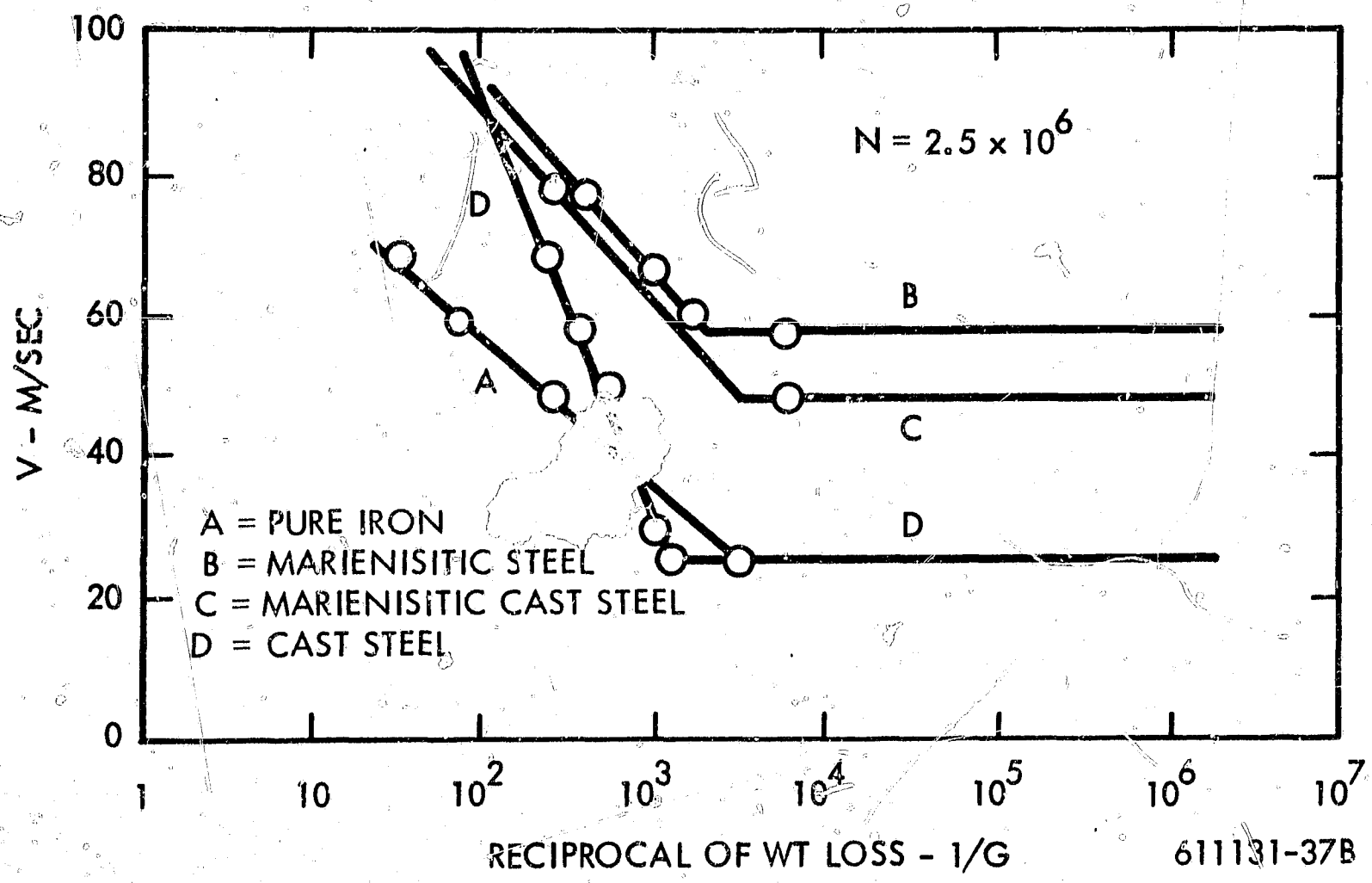

Figure 16b. Example of V-(1/G) Curve (Figure 5 in Reference 14 and Figure 8 in Reference 26)

Figure 16. Erosion-Velocity Relationships Plotted in the Manner of Fatigue Data

Astronuclear Laboratory

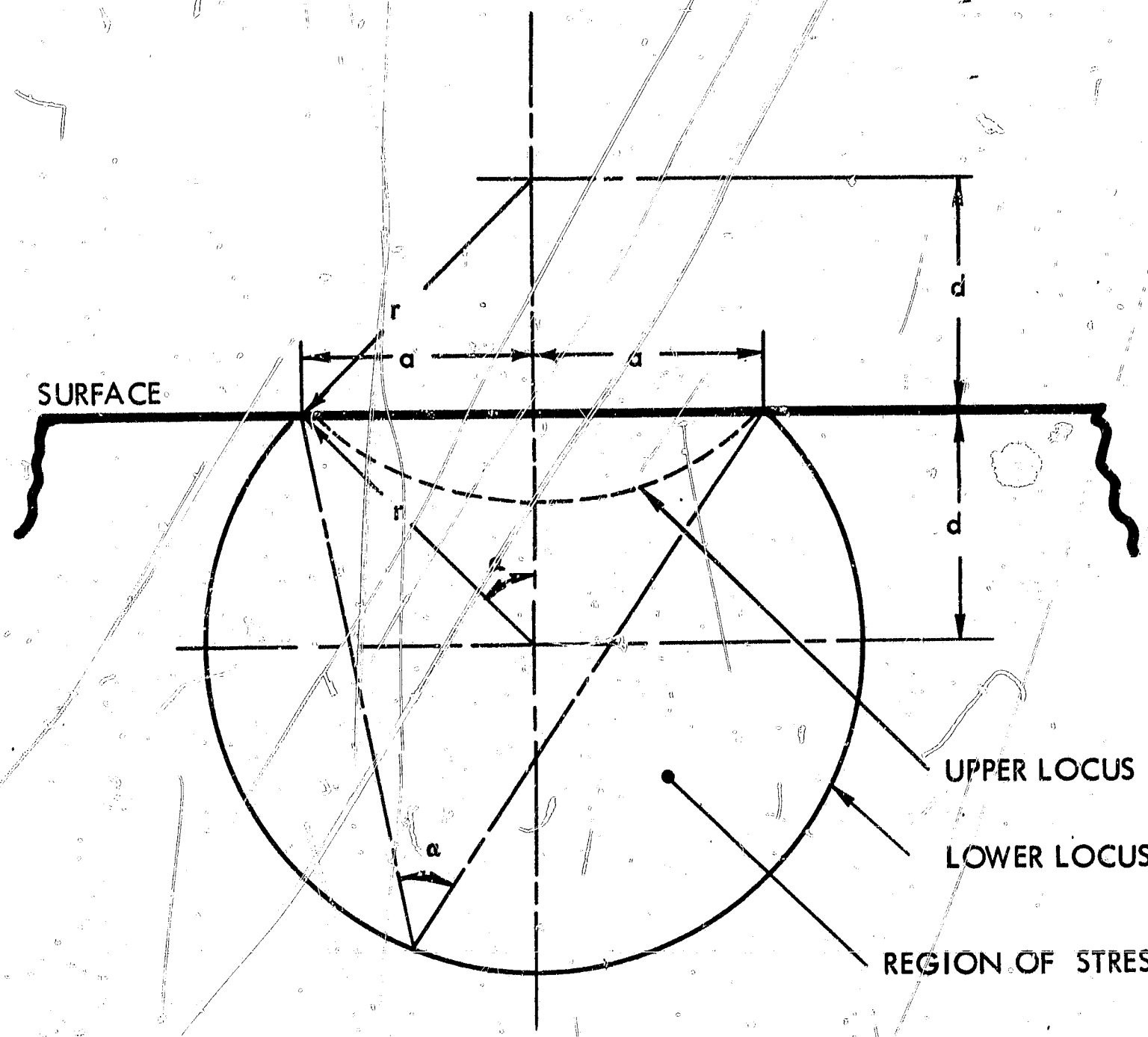

LOCI OF SHEAR STRESS $S = p \sin \alpha/\pi$
BY ANALYTIC GEOMETRY, $\sin \alpha = a/r$
THEREFORE, LOCI ARE CIRCLES OF $r = ap/\pi S$

611131-34B

Figure 17. Loci of Constant Shear Stress S in Semi-Infinite Solid with Belt of Uniform Pressure p

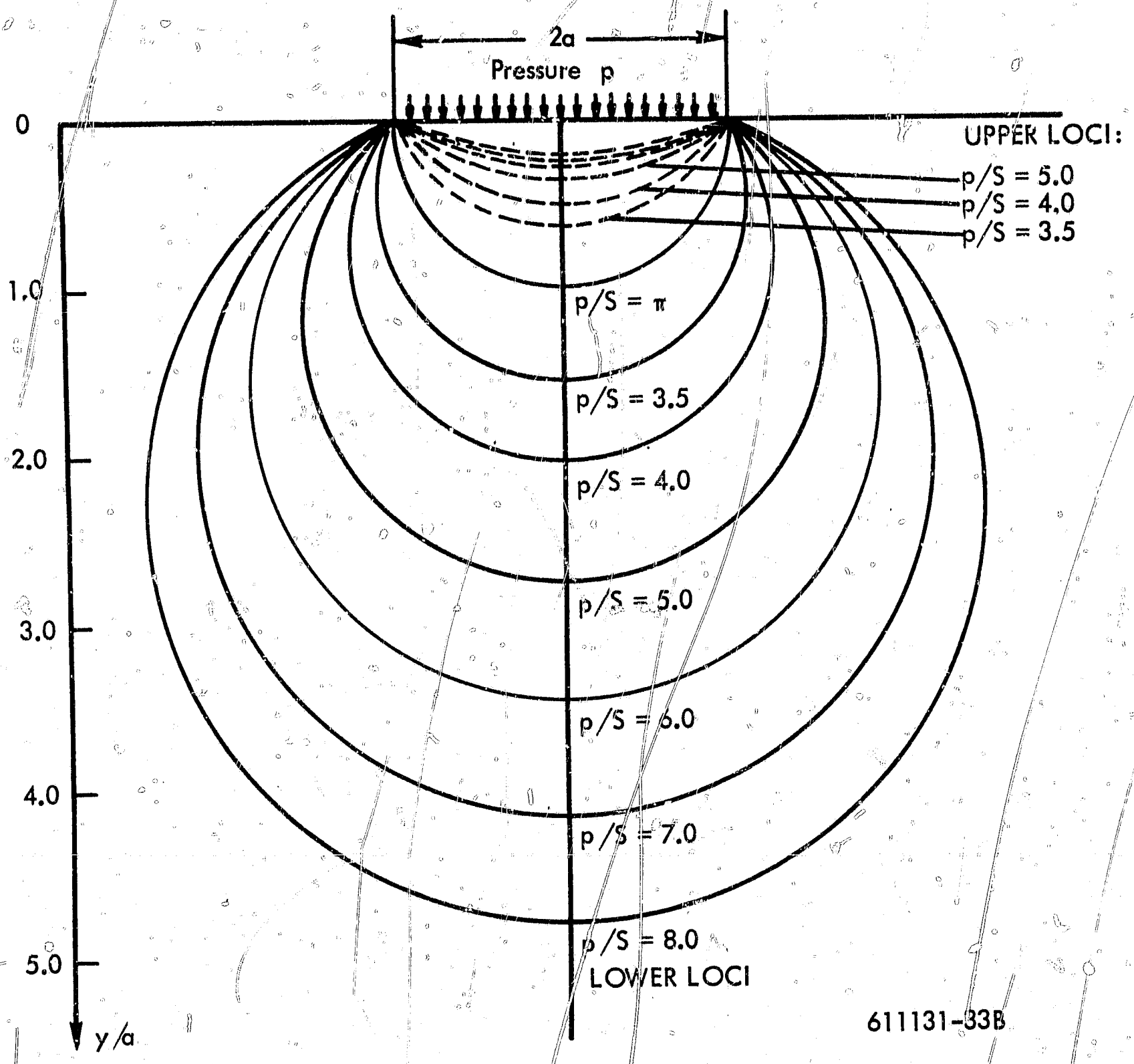

Figure 18. Upper and Lower Loci for Various Values of Pressure/Shear Stress Ratios

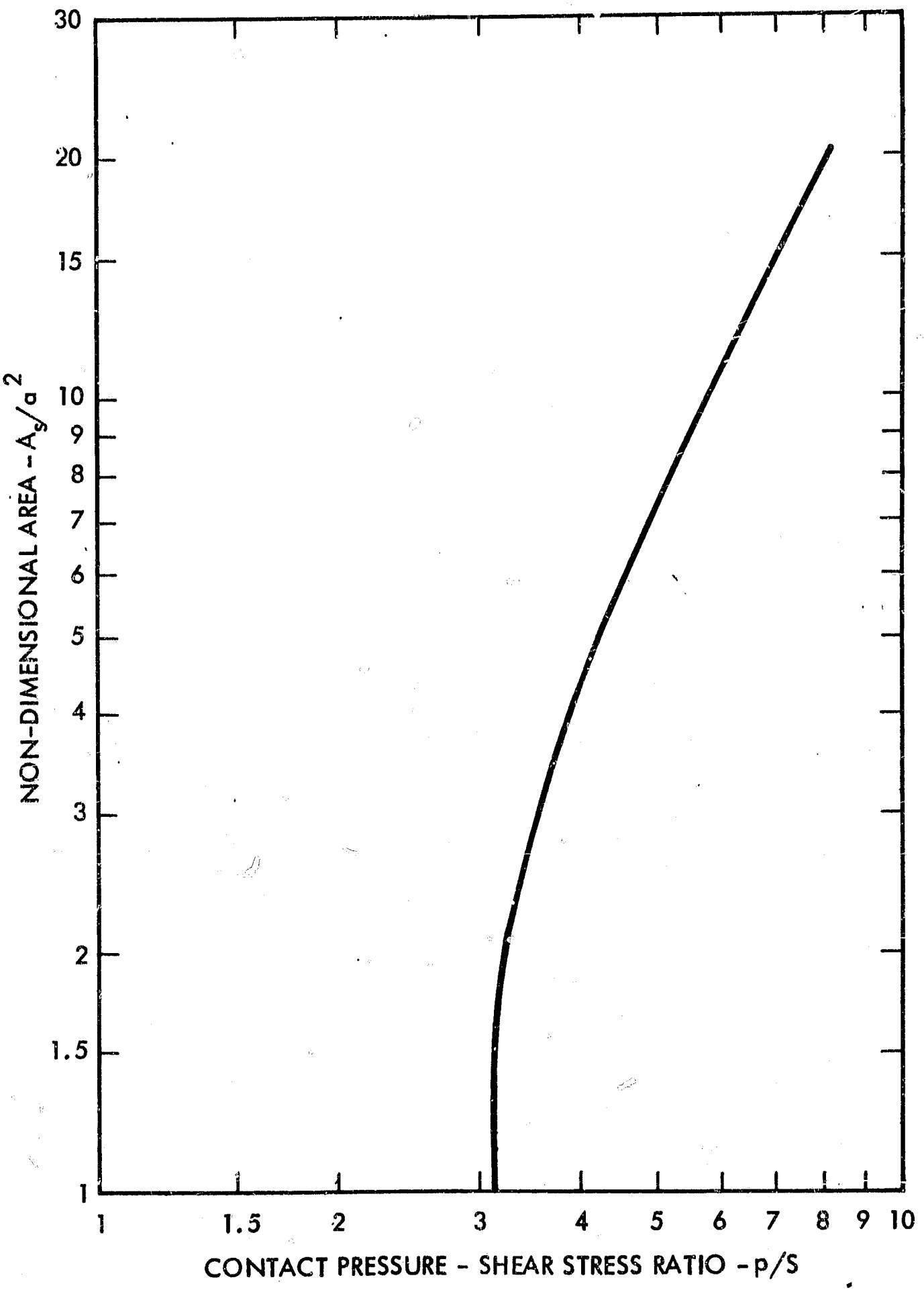

611131-31B

Figure 19. Area Between Surface and Lower Stress Locus (See Figure 18)

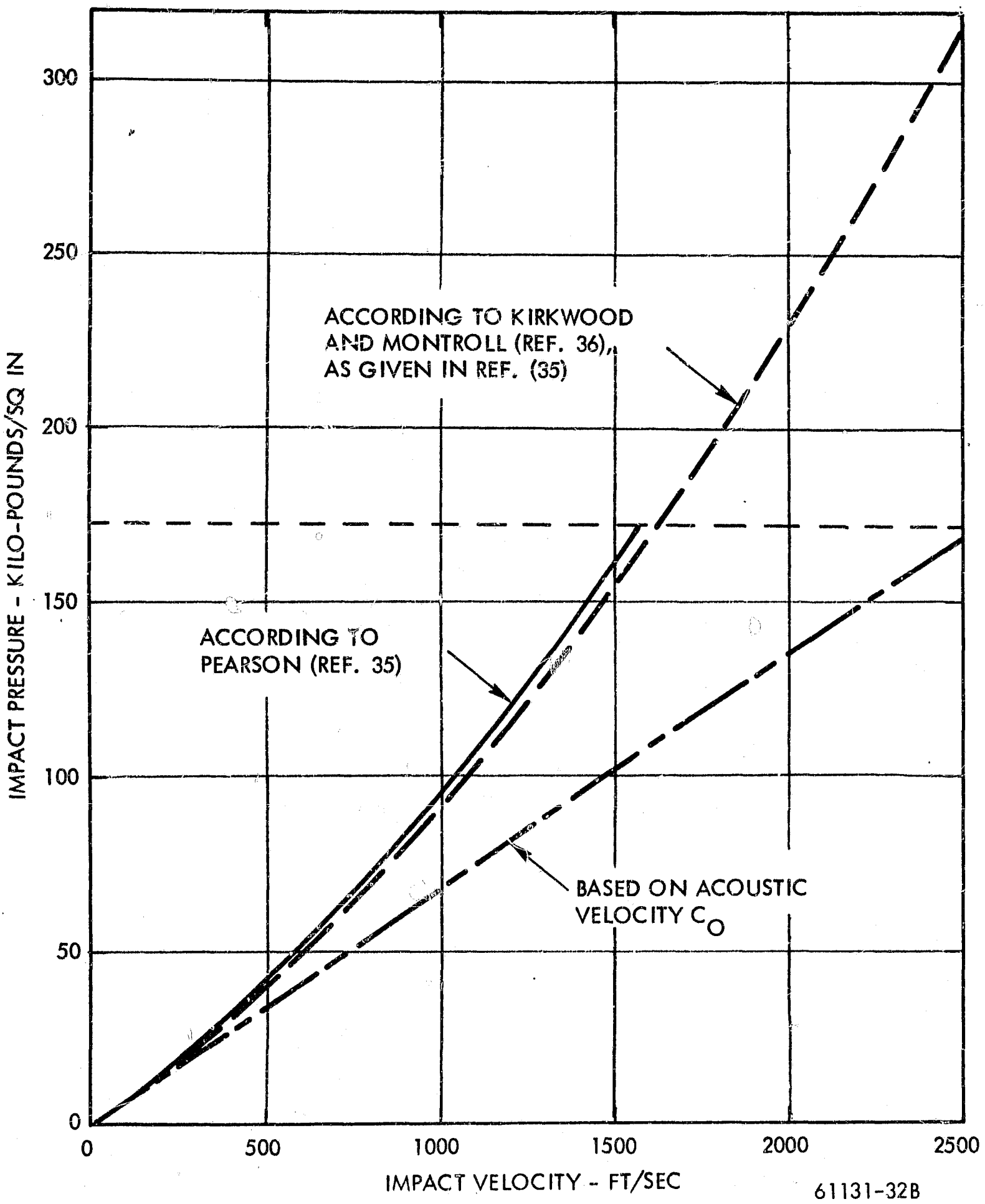

Figure 20. Impact Pressure Versus Velocity (Adapted from Reference 35)

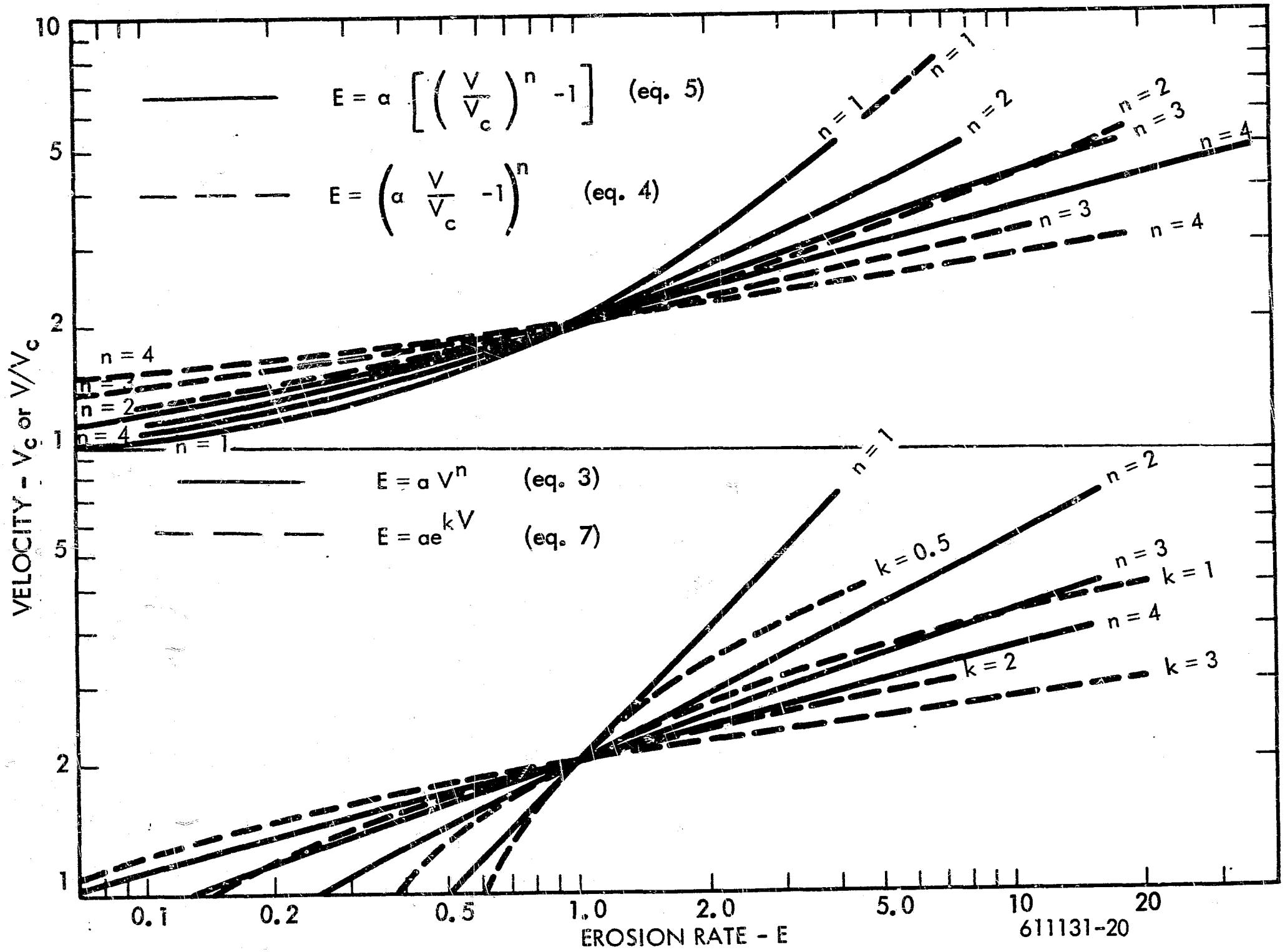

Figure 21. Families of Hypothetical Erosion Versus Velocity Curves, According to Equations (3) through (7)

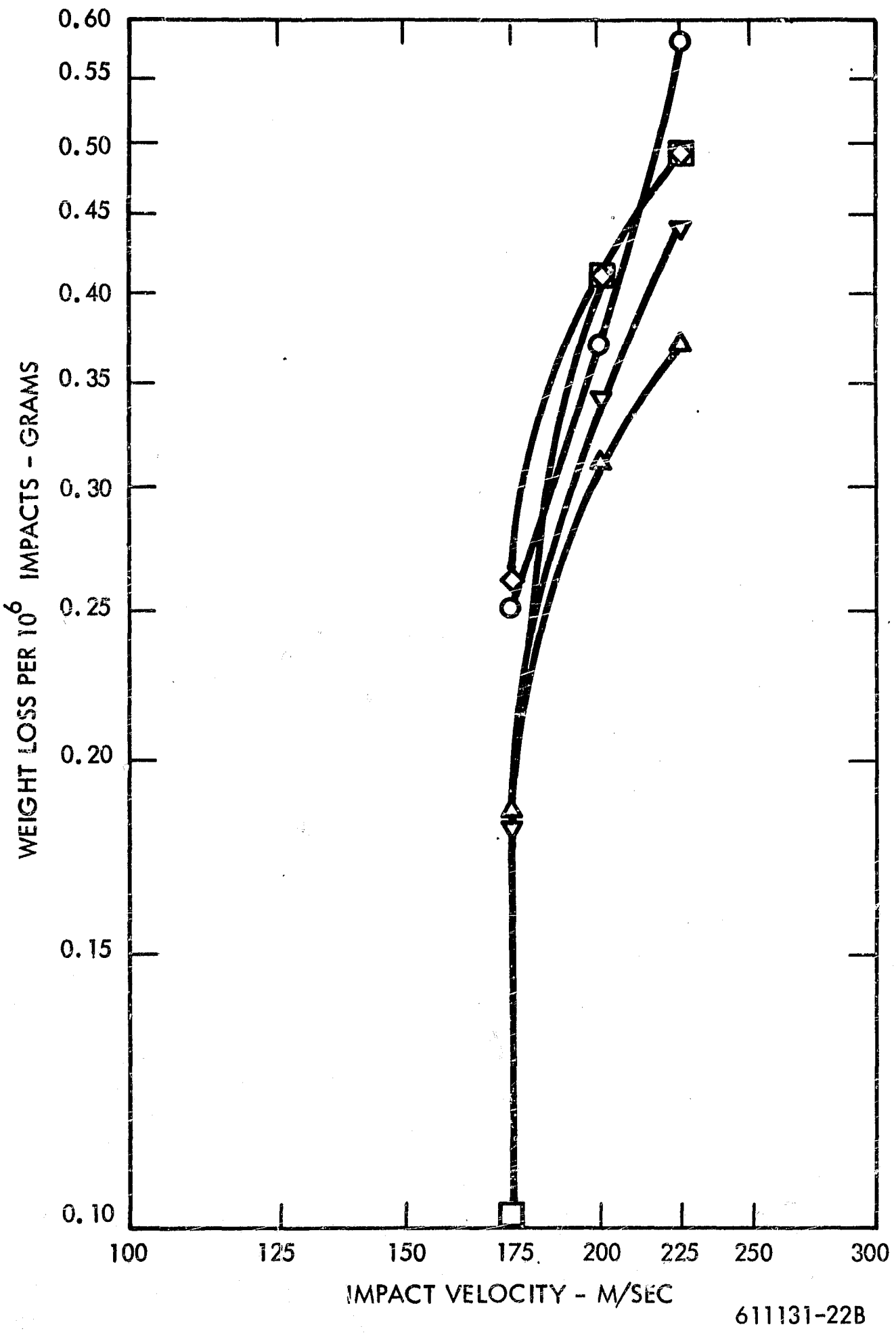

Figure 22. Erosion Versus Velocity Curves, Computed from Data in Reference 5

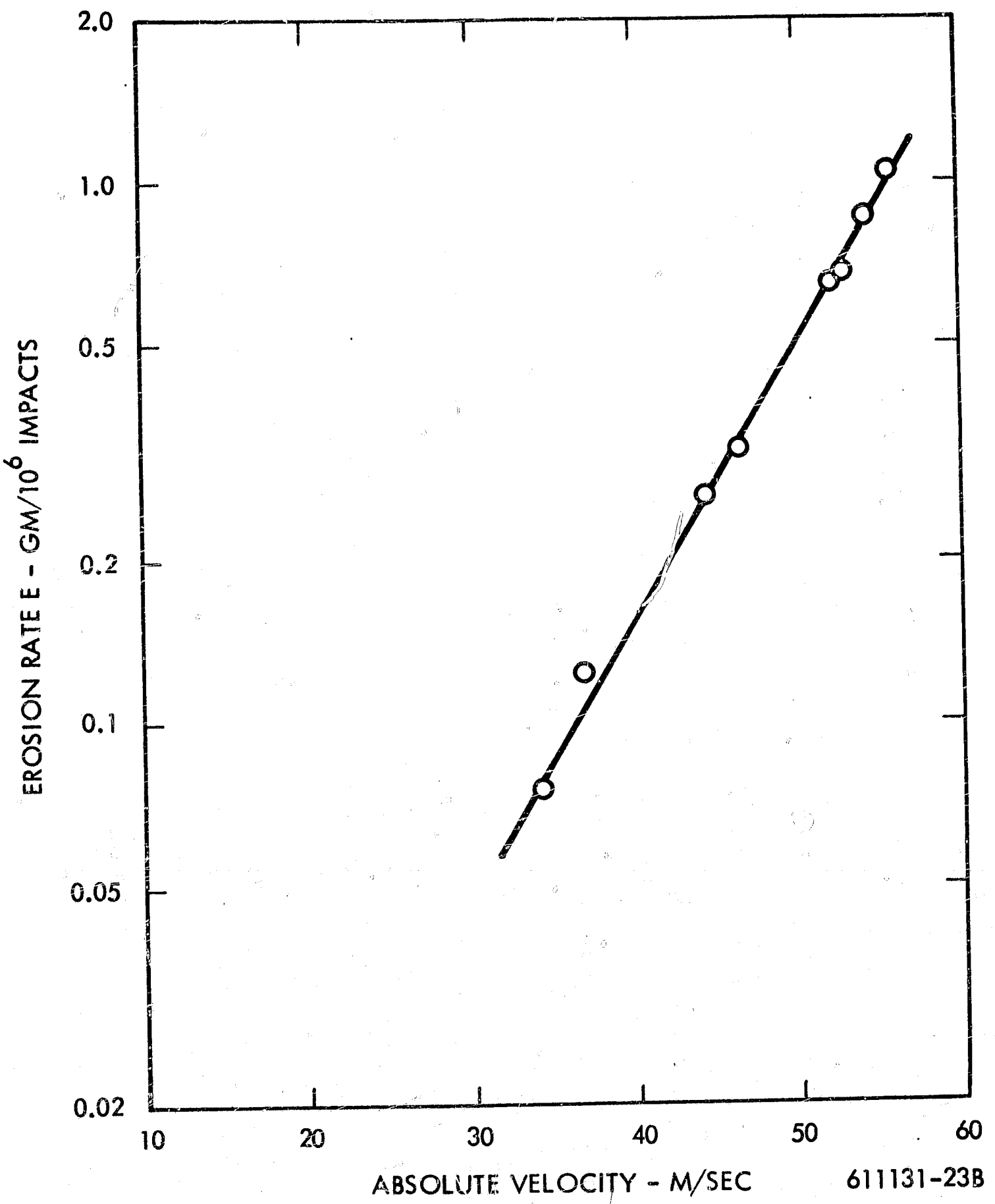

Figure 23. The Data of Figure 7b, Plotted on Semi-Log Paper

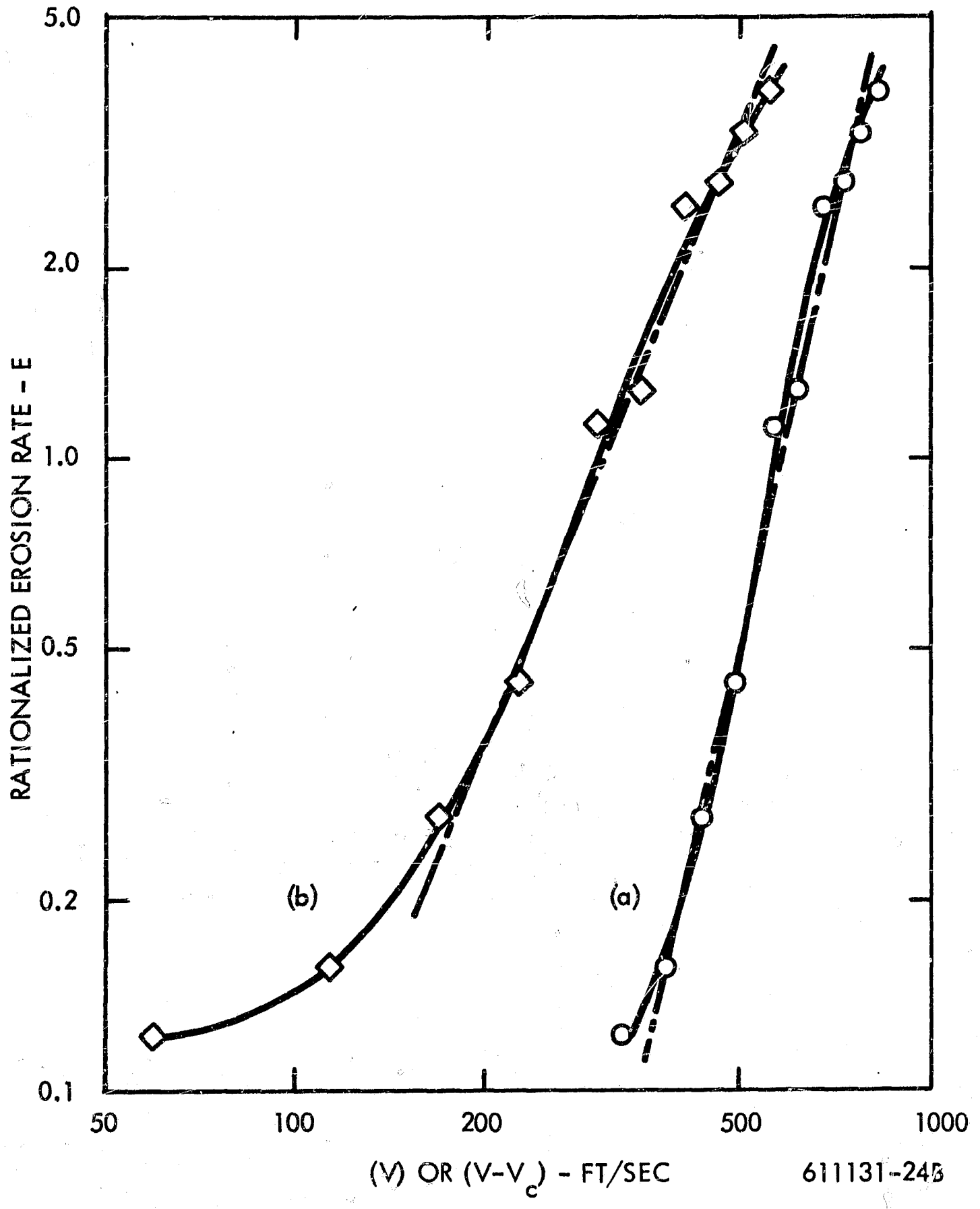

Figure 24. Data of Hobbs in Reference 37, Plotted both Versus V, (Curve "a"), and Versus (V-270), (Curve "b").

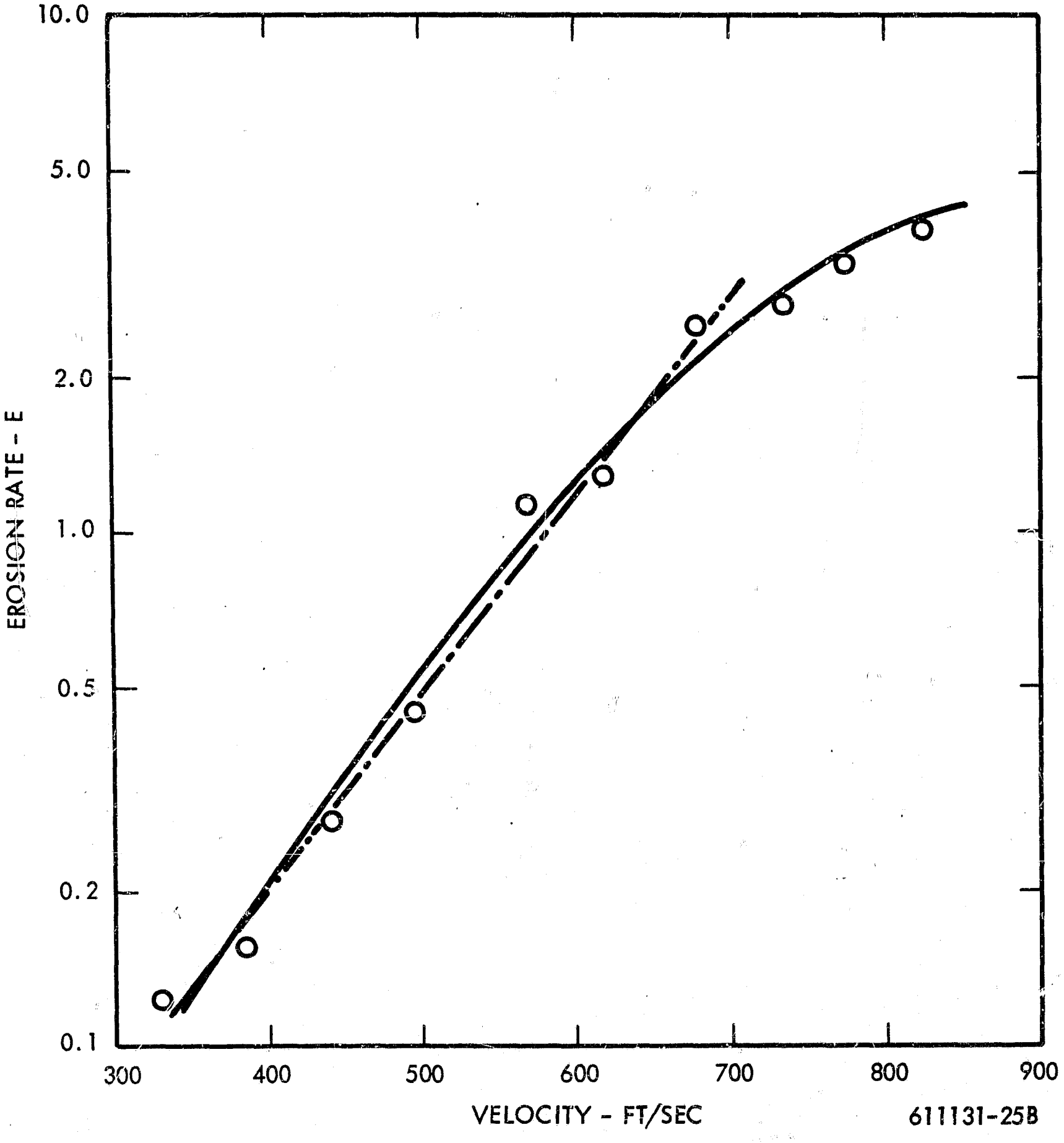

Figure 25. Data of Figure 24a, on Semi-Log Paper

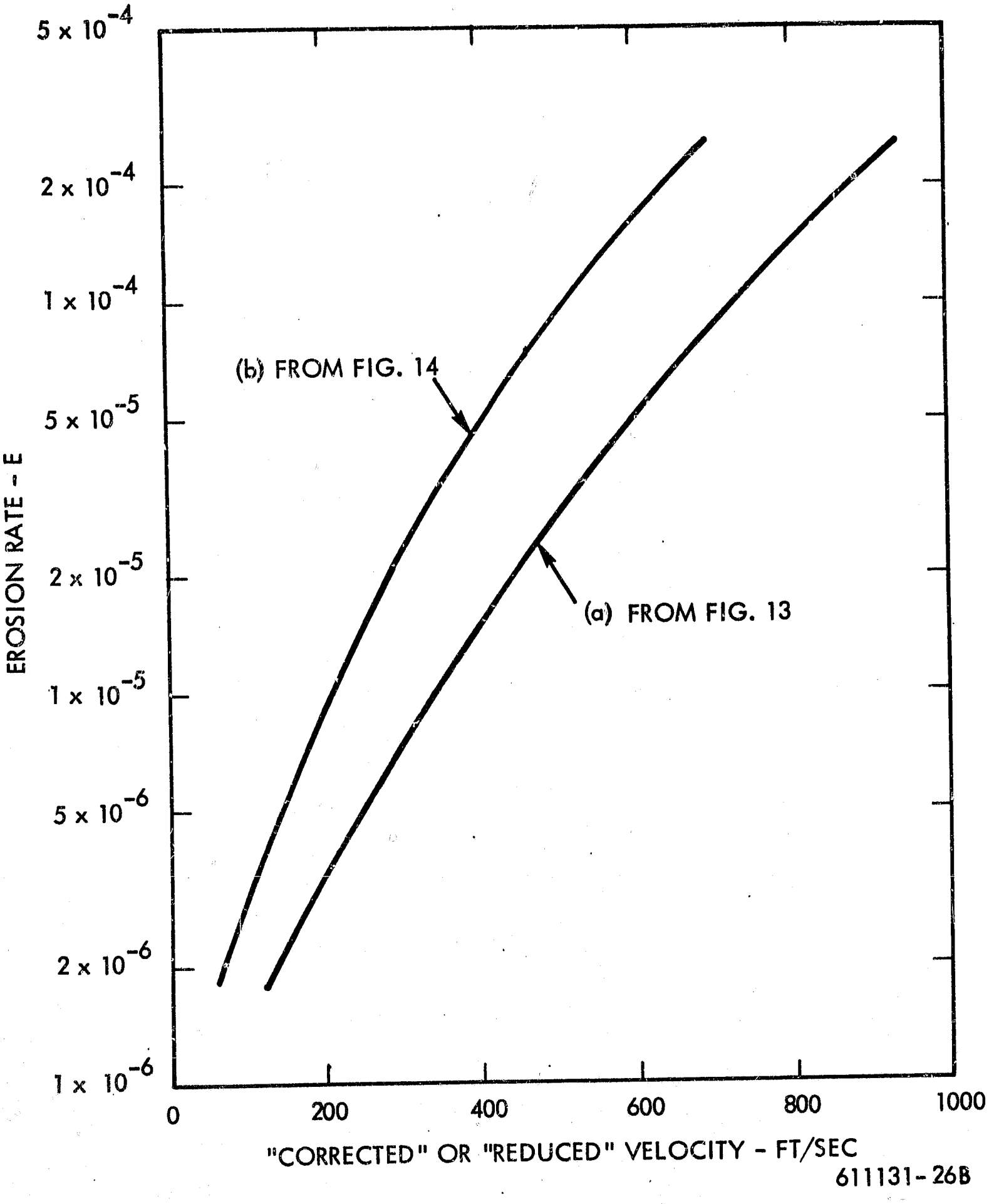

Figure 26. Curves Based on the Data Points of Figures 13 and 14. (Original Data from Reference 13)

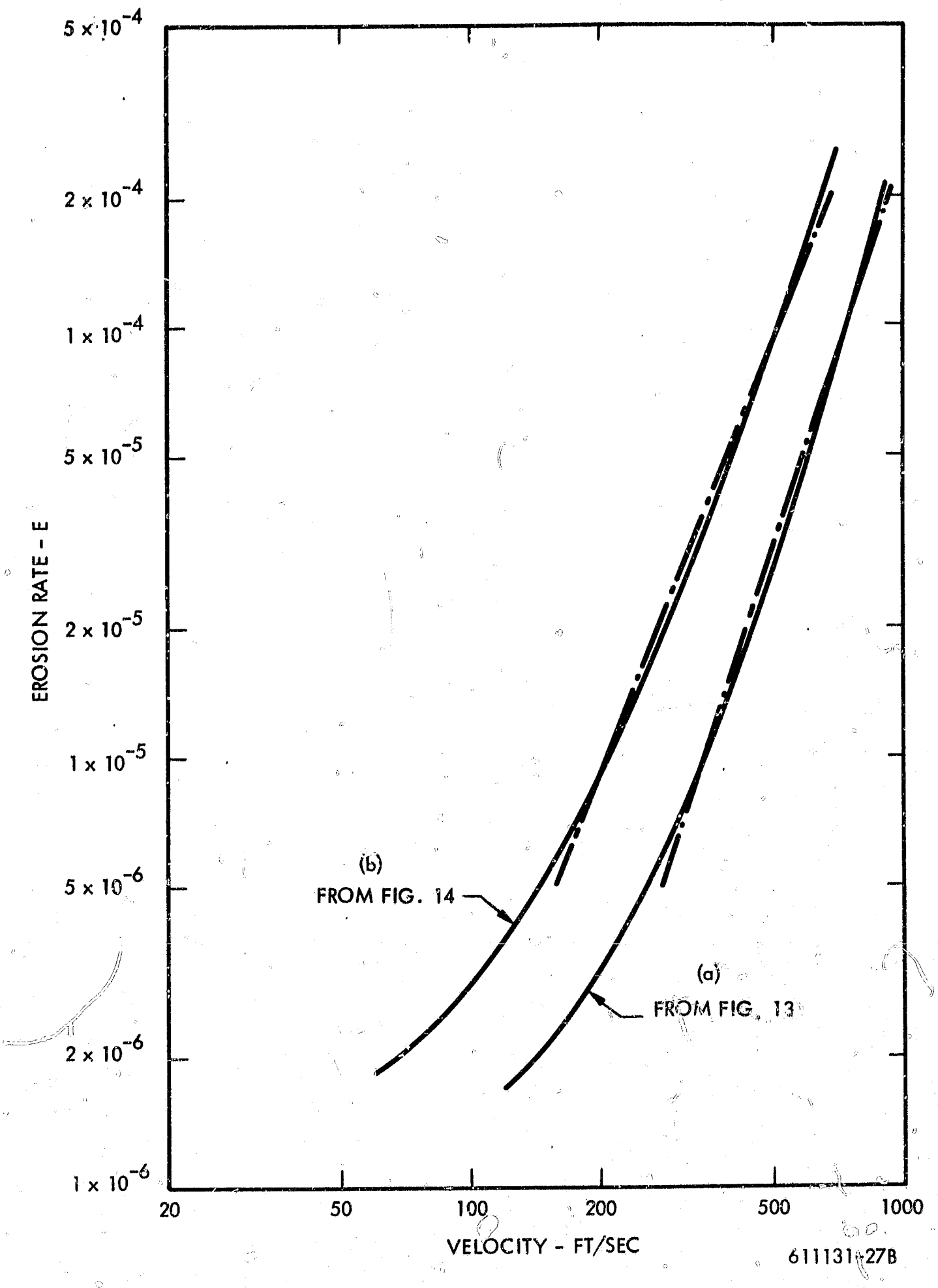

Figure 27. Curves of Figure 26 on Log-Log Plot

5.0 DEPENDENT PARAMETERS OTHER THAN RATE

5.1 The "Incubation Period"

All of the correlations discussed in the previous three sections have related to the slope of the "second stage" or "steady state region" of the erosion versus time curve, and little or no attention has been given to the "incubation period" or "first stage" of erosion, which may be defined as the duration to the intercept of the "steady state" or second-stage erosion line when that is extended to cross the zero-erosion axis. A proper understanding of the effect of velocity (and the other variables discussed) must eventually predict their effect on the incubation period as well as on the subsequent erosion rate, since the incubation period may under some conditions be a substantial portion of the effective life of the component being eroded. Figure 2 defined the incubation period as the term is used in this section and by the authors cited here.

Pearson (11 and 13) has plotted incubation periods for different velocities drop sizes, and impingement angles, and found more scatter in these data than in the corresponding erosion rate data. Figure 28 reproduces his data for different drop sizes in Reference 13, including the average curve he has drawn because "the amount of scatter . . . obscures the effect of drop diameter". It is nevertheless instructive to draw the best curves for each drop size separately, as is done in figure 29, from the data points in figure 28. From these one can see a trend for the curvature of the lines to increase with decreasing drop size; this one would expect if the critical velocity increases with decreasing drop size, since near the critical velocity W_o would tend to infinity. In particular, the 350 μ curve seems consistent with the prediction from table 3 (in Section 3) that the critical velocity for this drop size is 535 ft /sec.

The simplified fatigue analogy which led to equation 7 certainly also implies that the incubation period should be proportional, or analogous to, the number of cycles to obtain fatigue failure. Some evidence supporting this has been given by Ripken et al 1965 (38).

For one material, Ripken has measured the number of impacts corresponding to the incubation period as previously defined, and the resulting impact stress assumed to be given by $\frac{1}{2}\rho CV$, and superimposed these points on a standard S-N fatigue curve for the same material. His plot is reproduced as figure 30, and one may see that the agreement is encouraging despite the boldness of this direct comparison.

However, as pointed out earlier, the validity of the simple fatigue analogy is quite questionable. Part B of this report describes a statistical model of the erosion rate-time relationship, also based on an assumed fatigue mechanism for erosion damage. This model has as one of its consequences that the whole shape of the rate-time curve is highly dependent on the scatter associated with erosion fragment sizes and life-times, and thus neither the maximum erosion rate nor the length of the incubation period can be related to the conventional S-N diagram alone. It may yet prove more satisfactory to correlate erosion data on the basis of total duration to achieve a specified damage level, rather than somewhat artificially dividing the process into an incubation period followed by a so-called steady-state period.

5.2 Limit of "Steady-State" Erosion Stage

Also of interest in this connection is the damage level or other criterion at which the assumed "steady-state" or "second phase" of erosion ceases and the erosion rate diminishes. Hobbs [39] has suggested that this occurs at about the same rationalized erosion (i.e. MDP) value for all materials, but examination of erosion-time curves given by Pearson [11] do not seem to bear this out. Here, again, the analysis of Part B would predict that the truth is more complicated than that. Since in so many cases authors have not given the information necessary for transforming the weight loss data into rationalized form, it has not been thought worthwhile to attempt any correlations of this parameter at this time.

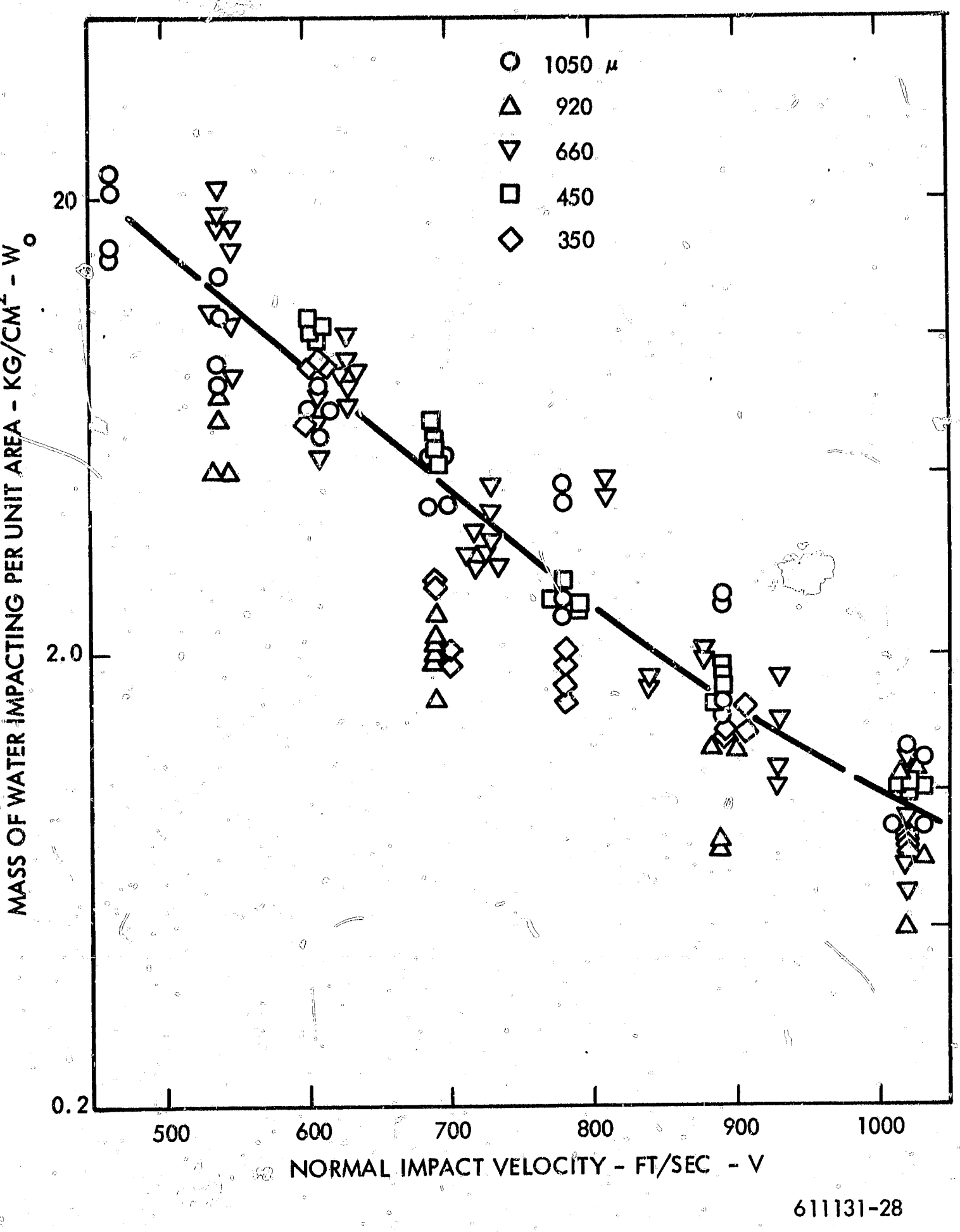

Figure 28. Rationalized Incubation Periods at Various Drop Diameters and Velocities (Copy of Figure 7 of Reference 13)

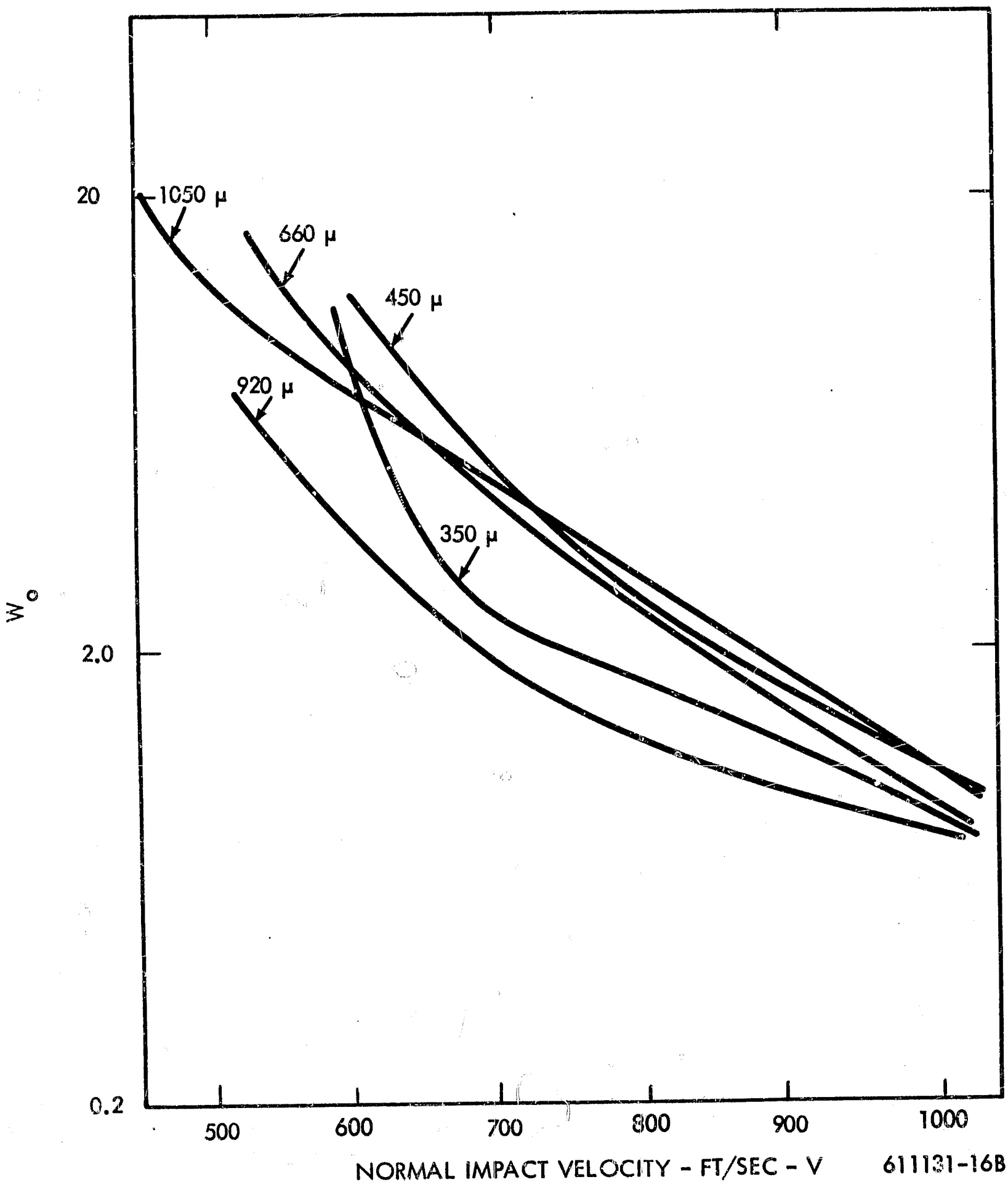

Figure 29. Individual Curves for Different Drop Sizes, Based on Data Points of Figure 28

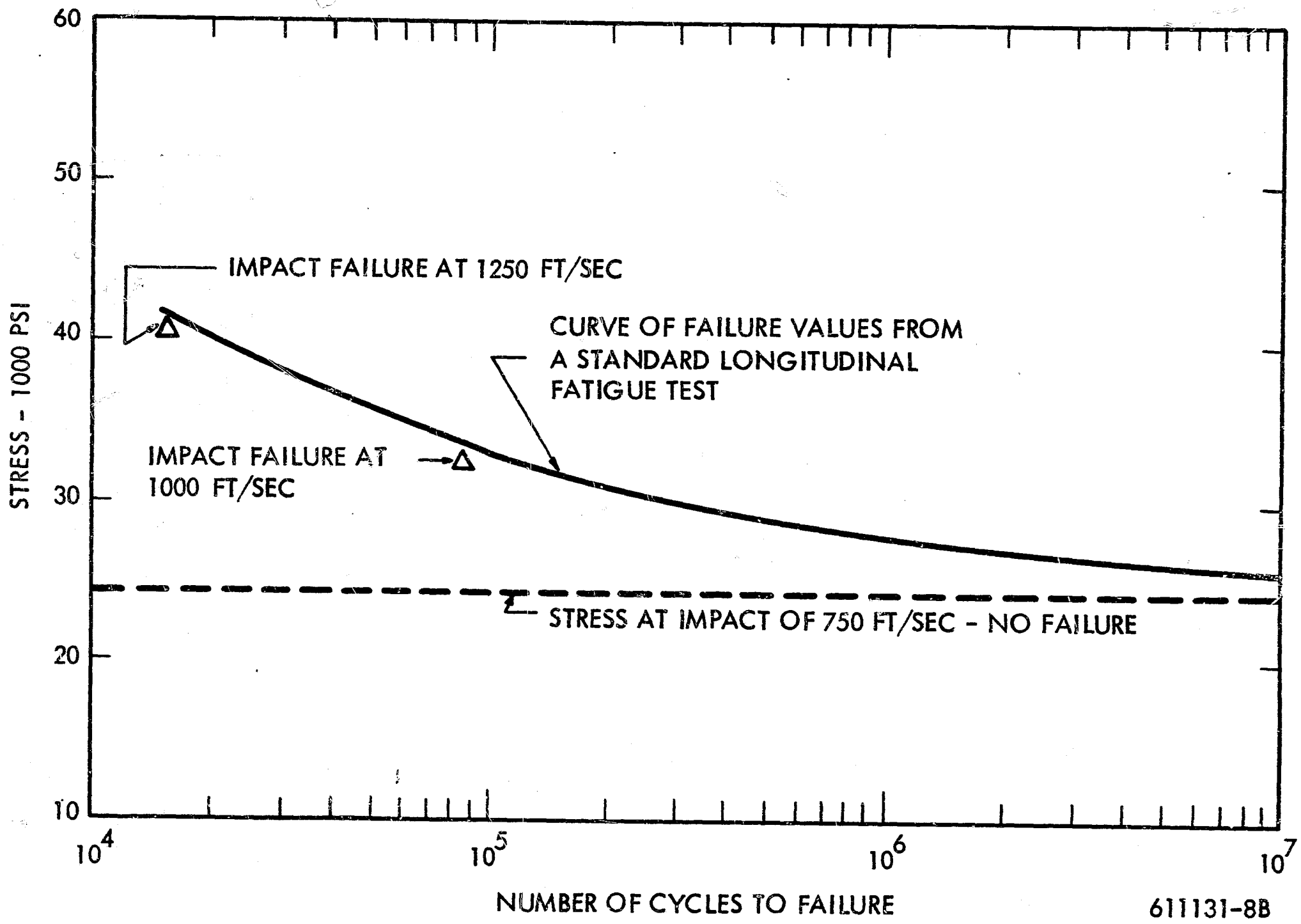

Figure 30. A Comparison of Impact Failure with Failure by a Standard Fatigue Method for 304 Stainless Steel (Ripken et al, Reference 38)

6.0 SUMMARY AND CONCLUSIONS FOR PART A

This part has described a study of the impingement erosion literature, with a view to deducing from it laws or empirical relationships which would describe the influence of the impingement conditions--in particular of the droplet size, impact velocity and direction--on the erosion-time history to be expected. An attempt has been made to define a rational approach toward this objective and to clarify some of the problems which are involved and the considerations which must be borne in mind. Possible analytic approaches have been introduced and discussed where appropriate.

There is a considerable body of data and theory relating to single-impact tests, notably the work of Engel (40 and 41), Jenkins (42 and 43), Bowden and his group (16 and 24), and DeCorso (25 and 44). These have not been made use of, at this time, to help develop the desired relationships, for several reasons: The damage measurement obtained in such tests is usually pit depth, or at best pit volume, neither of which is a true indication of material actually removed since a good deal of plastic deformation is taking place. Moreover, it would be dangerous to apply laws found from such tests to conditions in which fatigue-type erosion is predominant. It is the latter which holds our main interest, since in any practical turbine one certainly cannot afford to operate under conditions where single-impact damage is predominant. Eventually, one hopes for an understanding which would encompass the whole spectrum from fatigue-type erosion to hypervelocity impact. But for the time being we are restricting the damage correlation attempts to repeated-impact test data, while making use of single-impact research for the knowledge it has provided of the impact hydrodynamics.

The most comprehensive recent tests on the effect of engineering variables on erosion are those performed by Pearson (11 and 13) at the British Central Electricity Generating Board's Marchwood Laboratories, and many of the conclusions derived herein are based primarily on his data. Some of these data at least will shortly be in the open literature, Reference 10. One questionable point concerning his correlations is that they

are based on the maximum slope of the erosion-time curves, rather than on an average slope over some reasonably well defined damage range, as suggested in Section 1. In some cases, judging from sample erosion-time curves found in his reports, the maximum slope occurs over only a very short period and therefore may not be representative of the whole range of interest.

Other recent erosion research has been or will be presented at three symposia (45, 46, 47). Some of the papers have been cited in pre-print form (3, 7, 8, 9, 17, 20, 31 and 32), but it does not appear that any give more comprehensive data on the effect of engineering variables than the above-mentioned studies of Pearson. A possible exception is the work of the Dornier-System group (8, 9, 12 and 48) which also is more theoretically-oriented than Pearson's work, but whose primary emphasis is non-metallic materials.

The effects of impingement velocity, impingement angle and drop-size may be summarized as follows:

None of the data examined has given evidence of any basic "law" relating erosion rate to impact velocity. The data do not in general plot as a straight line either on log-log or semi-log coordinates. Any of a number of simple equations can be used to approximate individual sets of data over limited ranges. A popular equation of that type is:

$$\text{Erosion Rate} = k(V - V_c)^n$$

and in most cases so far the exponent n seems to lie in the range 2.3 - 2.6, when the erosion rate is rationalized, i.e. based on equal rates of water impinging.

The normal component of the impact velocity appears to be the significant one and should be used in such an equation. Pearson has suggested that the additional damage due to the tangential component, under oblique impact conditions, can be approximated by dividing the above expression by (cos θ), where θ is the inclination of the absolute velocity vector from the normal.

Erosion due to a given amount of impinging liquid becomes more severe when the size of the impinging drops increases. It is tentatively suggested, on the basis of the few quantitative data bearing on this, that "critical" or "threshold" combinations of drop size and velocity are given by

$$(V^2 D)_c = \text{constant}$$

Thus, if one critical condition is established, the value of V_c for other drop sizes can be deduced and used in equations such as the above-mentioned one.

A question of relevance at this point is how to take into account a mixture of different drop sizes and impingement velocities, as will very likely be the case under real impingement conditions such as experienced by a turbine blade. If erosion occurs by a fatigue mechanism, then this would be related to the problem of cumulative fatigue damage. The physical and statistical aspects of fatigue life under repeated stress cycles of varying amplitude have been discussed, for instance, by Freudenthal [49], who presents a number of different possible approaches to the problem. Several of them lead to the conclusion that "high stress amplitudes shorten the fatigue life out of all proportion to their number of application or their cycle ratio". This would seem to argue against the adoption of a simplified approach such as a superposition of the erosion rates due to various droplet size or velocity ranges computed independently. However, the scope of the present report precludes any alternative suggestion.

To predict the amount of erosion to be expected after a finite length of time, one requires not only the erosion rate, or slope of the erosion-time curve, but also its intercept as a measure of the so-called "incubation time". The data on incubation times is too sparse and exhibits too much scatter to allow any conclusions beyond the very broad and obvious one that as the impingement conditions (velocity and drop size) decline toward the threshold value, the incubation time increases.

The erosion rate-time model to be developed in Part B of this report implies that both the incubation time and the maximum erosion rate are strongly influenced by the statistical variations in the sizes and life-times of the erosion fragments formed, which in turn are influenced by the scatter in drop sizes and velocities as well as the scatter inherent in fatigue properties themselves. Consequently, it suggested that future correlations should be attempted on the basis of the time required to attain specified damage levels (i.e. MDP values), rather than on the rather arbitrarily-defined incubation and rate parameters.

The view that erosion is a form of fatigue leads directly to a number of corollaries:

1) There is little likelihood of finding one specific independently measurable material property which will predict erosion resistance, since none has been found to predict fatigue strength uniquely, and far more research has been done on fatigue than on erosion.
2) In fatigue, the relation between stress and endurance is determined by test for each material, and is not expressible in simple analytical form. Similarly, the relation between impact velocity and erosion very likely does not follow any universal law but must be established empirically, perhaps in graphical form, for each material.
3) In erosion, as in fatigue, the condition of the surface is likely to be of considerable importance.
4) Although erosion is the result of many failures, and some of the statistical scatter found in fatigue data may well average out in an erosion test, yet to obtain valid results (or results with calculable confidence limits) many more data points must be taken and many more replications must be run than has been customary to date. Related to this is the need, often emphasized in this report, to establish accurately the erosion versus exposure curve, and to carry out all tests to the same degree of cumulative erosion damage if one wants to draw any quantitative comparisons from them. The amount of testing required and the validity of results should be optimized by proper statistical design of the experiments: this has seldom been done in erosion testing.

Astronuclear Laboratory

A final plea or suggestion to those generating erosion test data is that with the results they should give all the pertinent information--material identification and preparation, physical and mechanical properties, surface preparation, size and shape of specimen, area exposed to erosion, amount of water impinging,and if possible the drop size or drop size distribution, impact velocity etc.--which are necessary for computing the "rationalized" erosion and duration parameters and making meaningful correlations between these and the impingement and material parameters.

PART B

THE VARIATION OF EROSION RATE WITH EXPOSURE TIME

F. J. Heymann

7.0 OBSERVED RATE-TIME PATTERNS

The recent literature dealing with the resistance of materials to impingement and cavitation erosion has become increasingly concerned with the fact that the rate of material loss is not uniform in time. While this, as a fact, had been noted for many years, some of its consequences have only lately been emphasized. Thus, as Thiruvengadam and Preiser [50] have pointed out, the comparison of test results can be very misleading if not based on corresponding phases of the rate-time curve, and therefore the rather common practice in the earlier literature, of testing all specimens for the same length of time, is subject to criticism. The authors of Reference 50 proposed that characteristic erosion-time curves could be described in terms of four zones: an "incubation zone" with no weight loss, an "accumulation zone" with loss rate increasing to a peak, an "attenuation zone" with decreasing loss rate, and finally a "steady state zone" with constant loss rate, figure 31. They do not attempt any detailed explanation for these zones, but suggest that the first three zones are influenced by the initial condition of the surface and that only the final zone is truly characteristic of the material itself and that it should be used for comparison or correlation purposes. This particular suggestion is disputed by Plesset and Devine [51], who showed photographically that in a magnetostrictive oscillator the "attenuation zone" is associated with a cavitation cloud of much reduced intensity, attributed to hydrodynamic damping effects due to the heavily roughened specimen surface. Moreover, the authors of Reference 51 stated that the "accumulation zone" and the "attenuation zone" are connected by a period of essentially uniform high loss rate persisting for some time, rather than by the narrow peak described by Reference 50,and that there is no real indication of any final steady-state zone. (See figure 32). Similar observations have been made by a number of

recent investigators. Thus both Hobbs [39], using a magnetostrictive oscillator cavitation test, and Pearson [10 and 11], using a drop impingement erosion rig, have called the region of maximum erosion rate the "steady-state" period, and have based their correlations of erosion with material properties and test conditions (such as oscillation amplitude or impingement velocity) on this maximum loss rate. Both have associated the declining loss-rate of final period with heavy surface damage, as did Reference 51, and feel that it is not a practicable measure of the erosion resistance. This, for practical reasons, has also been the approach adopted in Part A of this report.

All of the previously mentioned results exhibited what may be called the "conventional" pattern or some minor variation thereof. (For an actual example see figure 33.) However, there are erosion results which do not follow this pattern at all. Thus, Lichtman et al in [52] presented loss-time curves of which many exhibit no apparent incubation or acceleration stages, but rather begin with a maximum rate which declines thereafter. (See figure 34.) These results were obtained in a rotating disc cavitation device.

Exactly the same type of result has been obtained in the spray impingement erosion test facility at the Westinghouse Steam Divisions Development Laboratory. Erosion rates invariably seem to begin at a maximum value and then decrease-- rapidly at first, and then more gradually leading into or approaching a lower steady-state value. Figure 35 shows some "characteristic erosion rate curves", obtained by curve fitting through points obtained from several specimens for each material. One might suspect that incubation and acceleration stages lie in the region to the left of the curves as shown, and were simply missed because initial weight loss readings were generally not taken until after about two hours of exposure. In order to check this, the weight loss of one specimen-- a titanium alloy of fairly good erosion resistance -- was measured after five minutes of exposure and several more times during the first hour of testing. The result is shown in figure 36 and suggests that the erosion rate does in fact begin at a maximum value, or, if there is an incubation stage, it occurred within the first minute. The latter alternative is supported by the analytic model to be

described. In all of the titanium specimens which were tested the erosion rate has continued to decrease for at least 30 hours. It may, however, be worth noting that Thiruvengadam [29] has shown the rotating disc to be the most intensive cavitation damage device, and that the Westinghouse test facility produces impingement of probably rather small droplets at a high velocity, probably exceeding 2000 ft/sec. Thus, single-impact damage may be occurring in both cases, contributing to the de-emphasis or lack of an incubation period.

The object of this part of the report is to show that a simple statistical model of the erosion process, which regards erosion as a multiplicity of fatigue failures, can predict characteristic rate-time curves of most observed types, and to discuss some of the implications of this model in relation to the measurement and correlation problem.

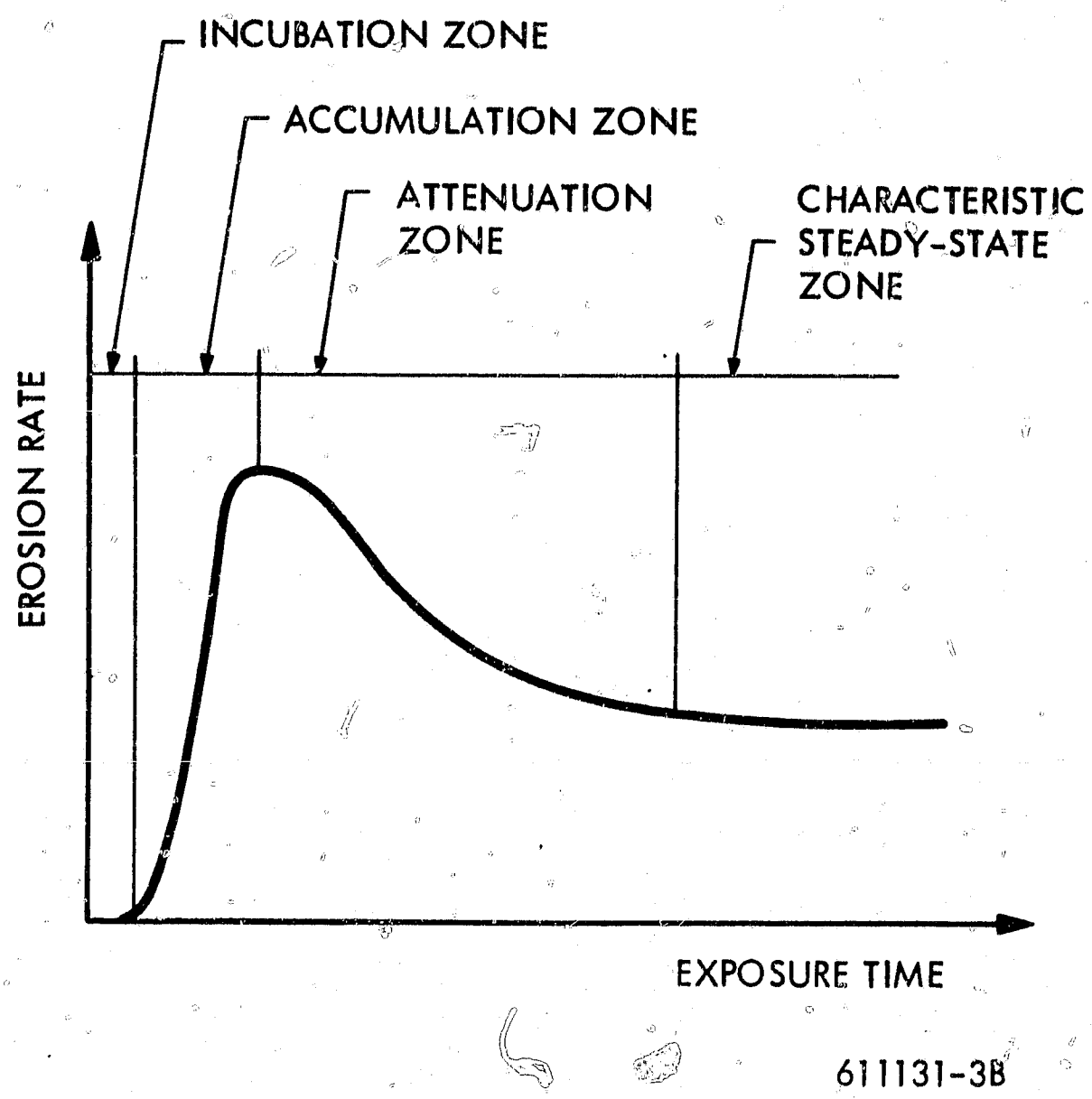

Figure 31. Characteristic Rate-Time Curve According to Thiruvengadam

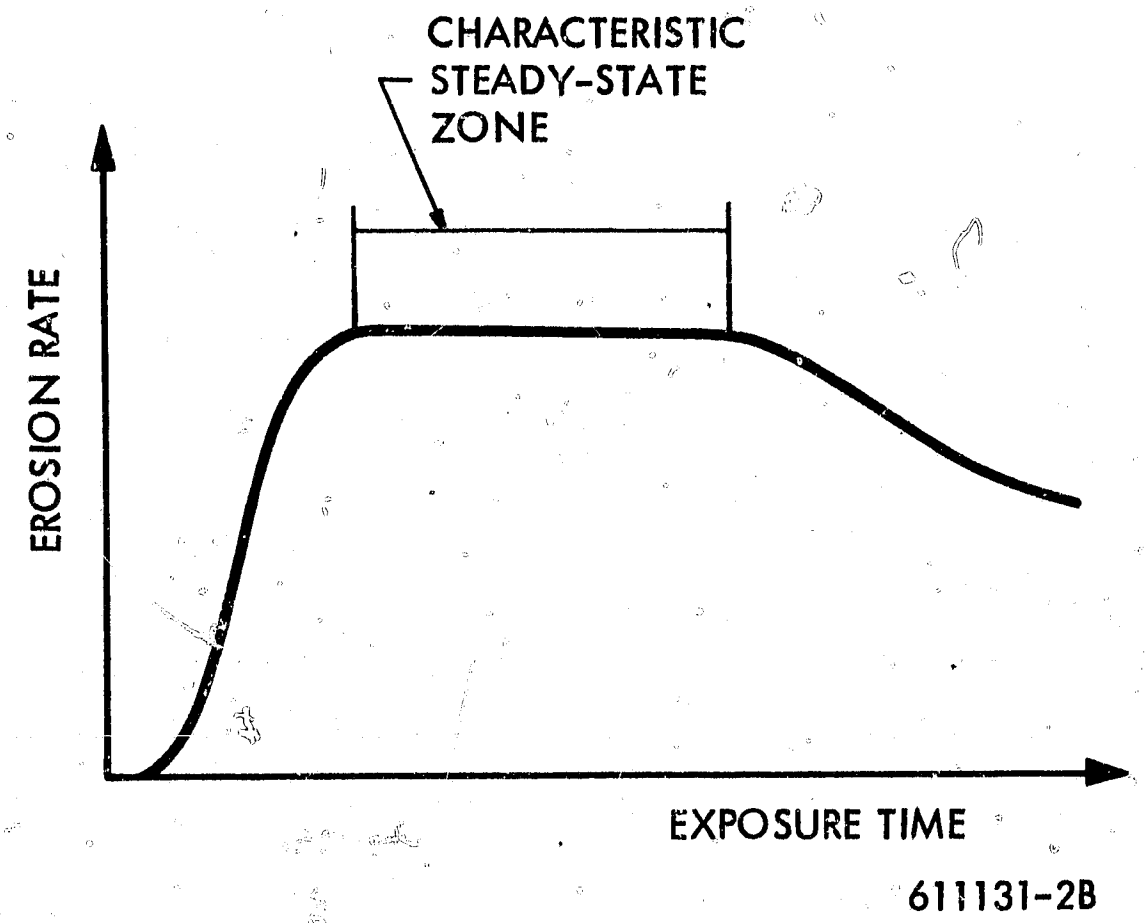

Figure 32. Characteristic Rate-Time Curve According to Plesset, Hobbs, and Pearson

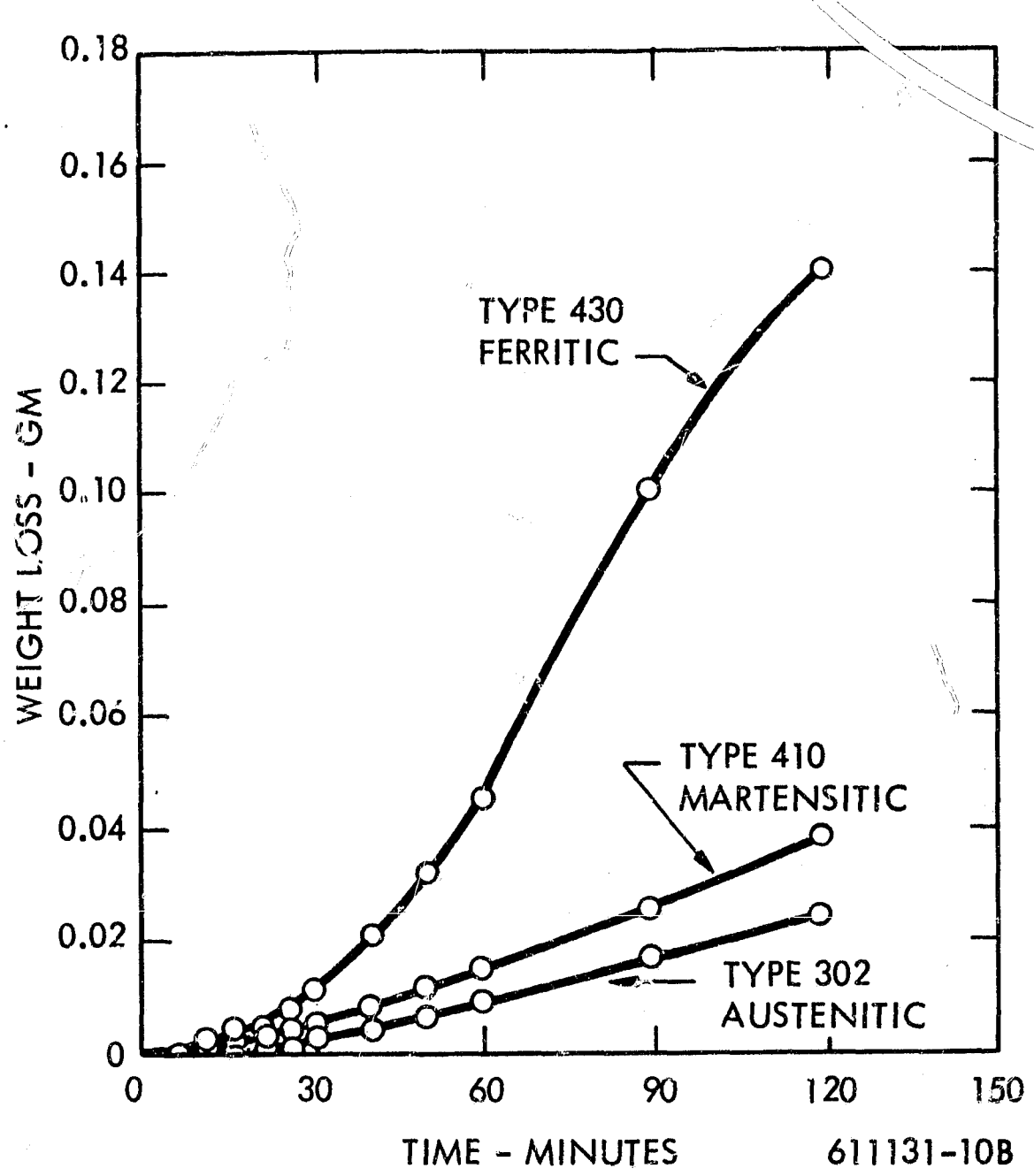

Figure 33. Typical Cumulative Erosion-Time Curves from Cavitation Tests, Adapted from Figure 7 of Reference 37. (Magnetostriction Device, in Distilled Water)

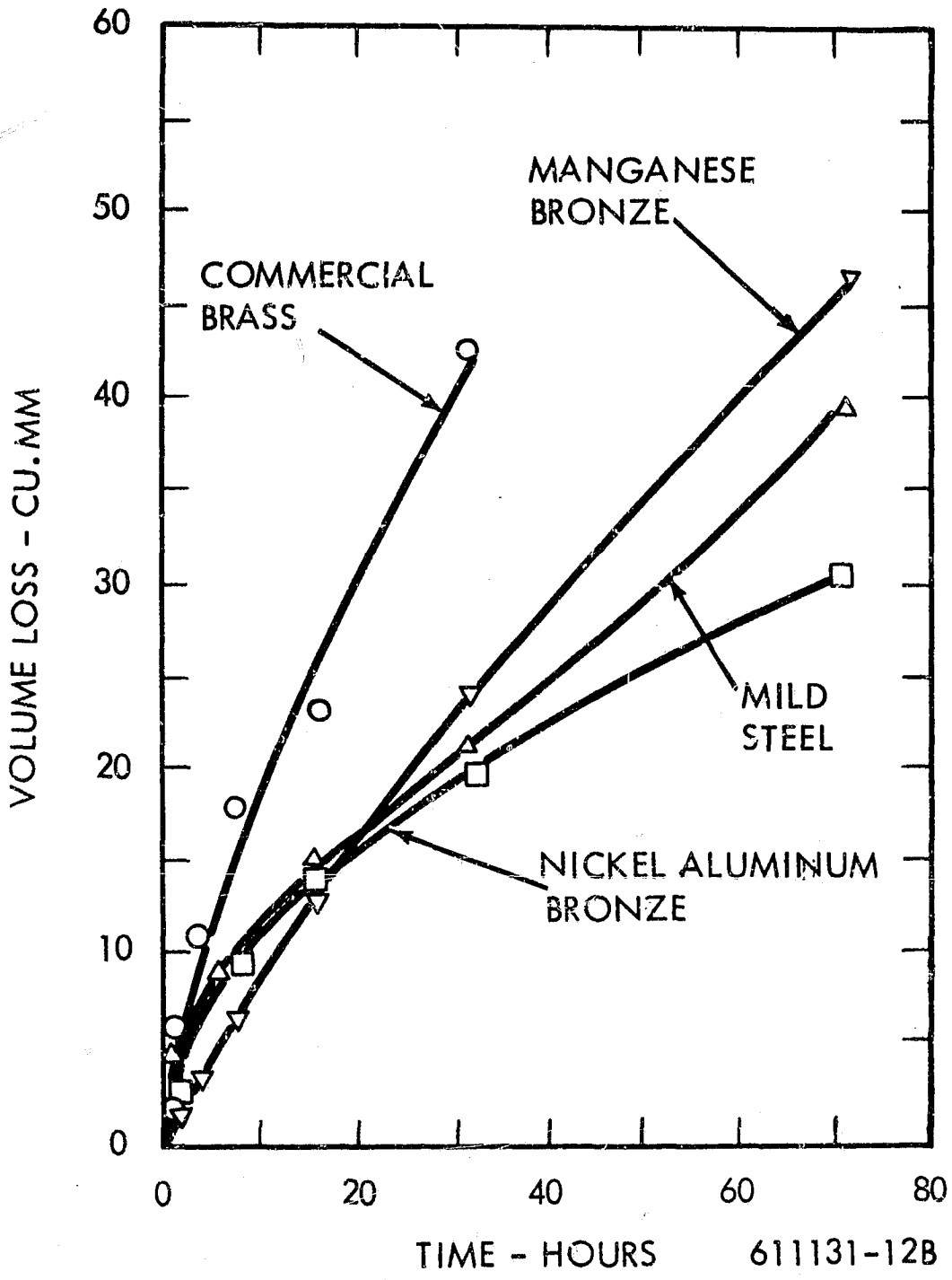

Figure 34. Cumulative Cavitation Erosion-Time Curves Which Begin at Maximum Rate, Adapted from Figure 24 of Reference 52. (Rotating Disc Device at 150 ft/sec.)

Astronuclear Laboratory

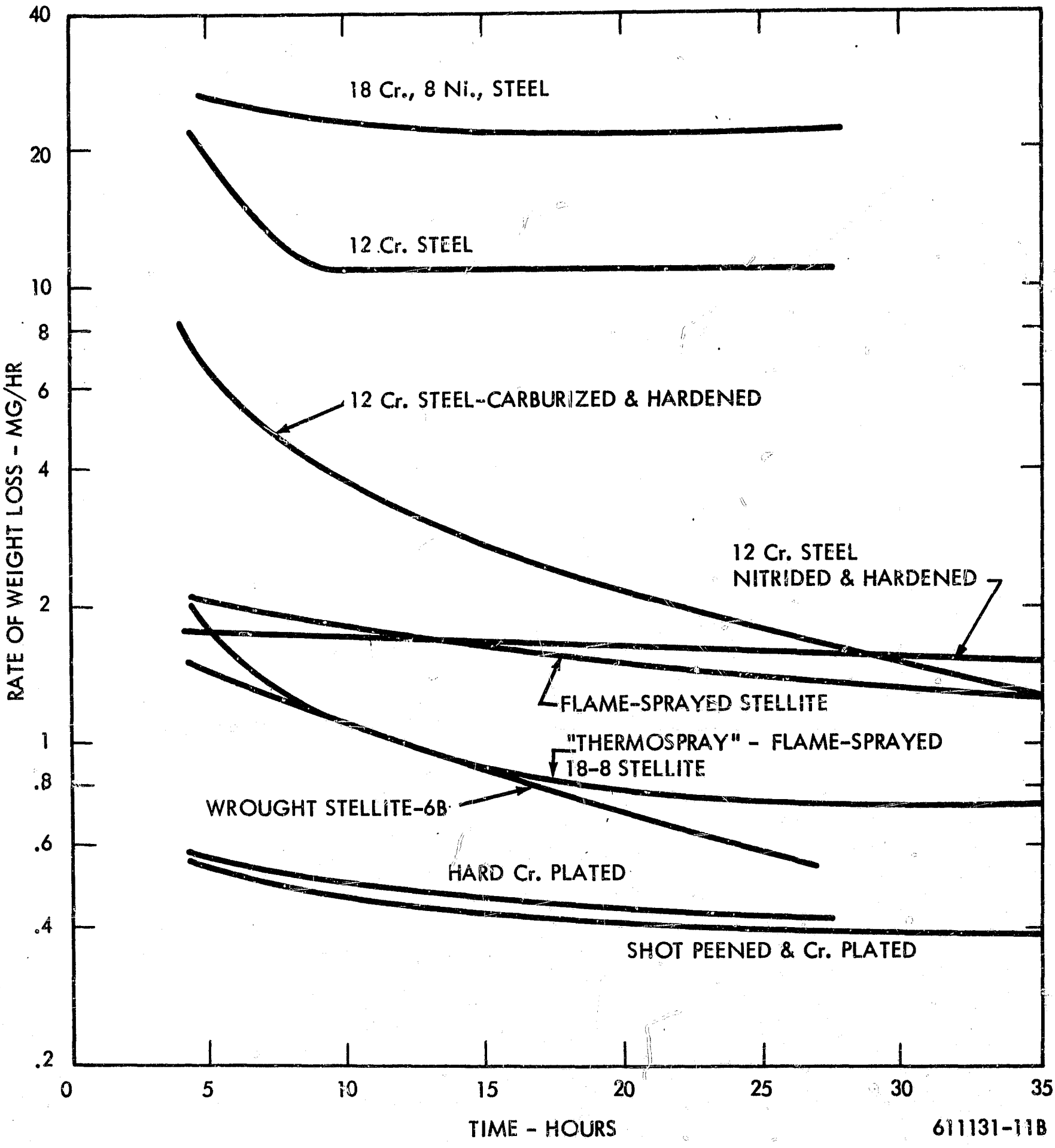

Figure 35. Typical Erosion Rate-Time Curves Obtained in Westinghouse Steam Division Spray Impingement Facility During 1956-1959

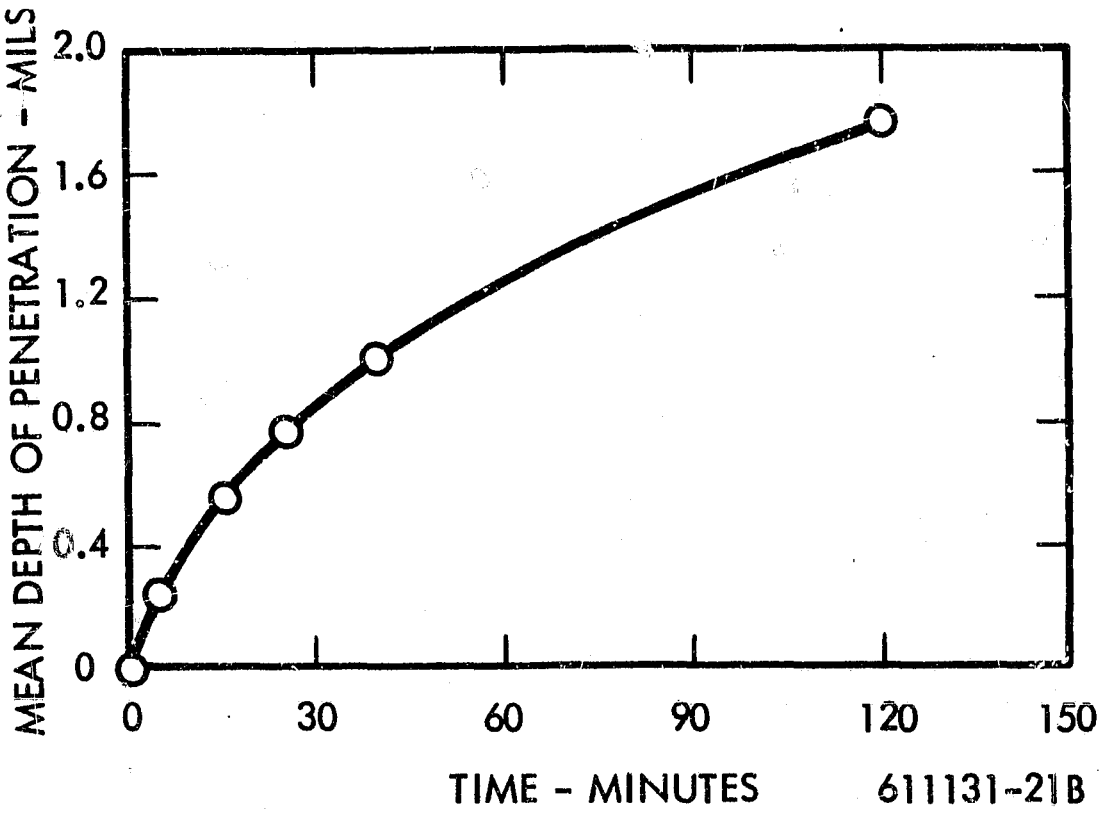

Figure 36. Early Loss Measurements for a Titanium (6 % Al, 4% V) Alloy Tested in the Westinghouse Steam Division Facility

8.0 EFFECT OF MATERIAL REMOVAL MECHANISMS ON RATE-TIME PATTERN

For the sake of argument, the spectrum of erosion mechanisms in a ductile material may be divided into several regimes as a function of impact intensity, or, in the case of droplet impingement, as a function of impact velocity if drop size is held constant. These regimes obviously merge one into the other; there are no sudden transitions between them.

For very low velocities below some "first threshold" value, no measurable damage or material loss will occur during any practical exposure time, or material loss is confined to isolated weak spots. Such threshold velocities, empirically deduced from test or operating experience or arbitrarily derived from the endurance limit of the material by some safety factor, have been used as design guides in some phases of steam turbine and condenser design. It is not fully established whether there actually is a velocity below which erosion will never occur: Honegger [5] doubted it; and Vater [26], who suggested that the dependence of erosion on velocity could be regarded and plotted analogously to the dependence of fatigue life on applied stress, regarded th erosion process as one somewhat similar to corrosion fatigue (in which there is no endurance limit). He therefore stated that the "threshold velocity" had to be defined as that velocity below which no measurable weight loss occurred after some specified number of impacts. In any case, one might say that in this first regime the erosion, if any, corresponds to that in the incubation stage of the conventional rate-time pattern: i.e. it will be low, possibly gradually increasing with some random fluctuations, and will be highly influenced by the initial surface conditions and by the possibility of simultaneous corrosion as shown by Wheeler [53].

As the velocity exceeds the first threshold, something akin to fatigue failure becomes the predominant failure mechanism. Metallurgical observations substantiating this, and descriptions of the probable sequence of events leading to failure and the formation of loose fragments, have been provided by many investigators including Vater [26], von Schwartz et al [54], Brunton [55], Thomas [17], and Marriott and Rowden [20].

Some investigators have found more plastic deformation in the surface than might be expected: thus Thomas [17] noted small plastic depressions in the surface during the early stages of exposure at velocities whose presumed impact pressures were less than the yield point of the material. Brandenberger and de Haller [4], on the basis of extensive radiographic studies concluded that fracture in erosion is neither like static fracture nor like fatigue fracture, but is accompanied by a degree of damage to the crystal structure which is intermediate between that associated with those failure modes. It must be remembered, though, that the stress-geometry condition -- at least when the surface is still relatively smooth -- is not of such a nature as to make "static" rupture easily possible: thus the general regime of predominant fatigue or repeated-impact rupture will extend well into the velocity range where each drop could be expected to produce noticeable plastic deformation. As the velocity increases, so, presumably, the regions of plastic deformation spread from the immediate vicinity of the fracture surface toward a general deformation of the eventually-produced erosion fragments. In this regime one may expect to find rate-time curves exhibiting the "conventional pattern", i.e. an incubation stage related to the fact that a certain number of impacts are required before fatigue failures occur, an acceleration stage, possibly a steady-state stage, an attenuation stage, and possibly a final steady-state stage though probably no generalizations should be made about the behavior when gross surface damage has set in. The possibility of relating these phases in the erosion rate-time curve more specifically to the fatigue properties of the material will be explored in the following sections of this report.

A second "threshold velocity" may be associated with that velocity at which the material loss due to single-impact damage process becomes significant. This is probably related to the "visible damage threshold" described by DeCorso and Kothmann [25 and 44], above which a single impact leaves a distinct crater in a smooth material surface. This regime eventually must merge into the regime of hypervelocity impact. The exact determination of the second threshold velocity from the point of view of material removal is difficult, because in single-impact experiments -- such as those performed by DeCorso [25],

and also by Brunton [55], Engel [40 and 41] and others -- the actual amount of material removed from the surface could not be reliably established, although crater depths or crater profiles were measured. From two curves given in Reference 56, one can deduce that for hypervelocity impact of 1/16 inch diameter aluminum spheres on an aluminum surface, the ratio of target volume loss to crater volume is approximately 0.15 at a velocity of 7 km/sec (23,000 ft/sec), reducing to about 0.09 at 4 km/sec (13,000 ft/sec). One may cautiously infer from this that at the velocities of interest, say 1000-4000 ft/sec, the corresponding ratio will be very much smaller yet. (This inference should be valid qualitatively although the actual material removal mechanism in the hypervelocity regime is a liquid-like flow of the target material accompanied with some "splashing out", whereas that in the regime of interest is related to the shear effect of radial outflow, as described earlier). Of course, this must be balanced by the fact that such loss occurs with each impinging drop whereas many repeated impacts over some finite area are required to generate one erosion fragment by the fatigue failure mechanism. For any quantitative estimate of the relative significance of the two mechanisms, more data are needed on each.

Qualitatively, one may say that as single-impact erosion becomes significant, the incubation period can no longer be a zero-weight loss period, but rather will begin by exhibiting an erosion rate corresponding to the single-impact erosion, this rate increasing in time as additional fatigue-type erosion sets in. Fatigue in this instance probably corresponds more to low-cycle fatigue due to strain cycling than to high-cycle fatigue due to stress-cycling. The geometry of the eroded surface will now be affected by the heavy plastic deformation due to each drop as well as the breaking away of larger erosion fragments due to fatigue fractures. Eventually, as single-impact erosion becomes the predominant mechanism, one would expect to find little or no evidence of any incubation period, and the surface geometry should rapidly approach a steady-state condition, so that one might expect relatively little change of erosion rate with time.

9.0 AN ANALYTIC MODEL OF THE EROSION RATE-TIME RELATIONSHIP

9.1 Qualitative Description of Proposed Model

As seen in the previous section, the "conventional" erosion-rate versus time pattern is that associated with a predominant fatigue mechanism for material removal. It is in this regime that most of the test data and the practical experience lie. As is well known, fatigue is intrinsically a statistical process exhibiting a considerable scatter, and this fact will be made use of in developing an analytical model for the erosion rate-time pattern applicable to this regime. The qualitative results have interesting implications with reference to the previously reviewed findings and to previously-attempted correlations between erosion and fatigue data. The approach to be described, though numerical in nature, can at this time predict no more than qualitative trends and should be considered as exploratory.

The mathematical and logical formulation of the model, both in a preliminary and in an elaborated form, is given in detail in Section 10. The basic reasoning of the model is as follows:

It is assumed that each small element of surface is subjected to an impact fatigue environment and that after a certain time (i.e., a certain number of impacts) it will be detached from the surface as an erosion fragment, due to sub-surface fatigue failure. Further, we assume that when many such surface elements are considered, the individual times required for their removal would be described by some statistical distribution function, much as the number of cycles to failure of a large number of fatigue specimens (stressed to the same level) can be described by a distribution function. When erosion fragments are removed and expose "fresh" surface to impingement attack, the time to remove elements of this new surface will likewise be described by a distribution function, and so on. The time-to-failure distribution function for these newly-exposed surfaces will probably not be the same as that for the original surface, since they will have been subjected to some sub-surface stress condition even before being exposed to direct impingement, and since the surface geometry will be different.

In the case of conventional fatigue specimens, the distribution occurs primarily as a result of the statistical nature of the fatigue process itself. In the case of erosion fragments, it must ultimately reflect the variations in the concentration and the severity of impacts (i.e., droplet velocities and sizes), variations in the local surface geometry and properties, and variations in the size of fragments formed. At present, however, one arbitrary distribution curve is assumed to represent all of these sources of scatter.

Qualitatively, it can be seen that if these distributions had very little scatter or dispersion, i.e., if the lifetimes of all surface elements were about equal, then the erosion rate would be zero until that lifetime was reached, at which instant a very high rate would be exhibited while all of the original surface flaked off, to be followed by another interval of zero rate until the second layer flaked off, etc.

If, however, these distributions have a significant dispersion, one can intuitively predict that this will result in a rate-time curve which up to a first peak looks somewhat like the distribution curve, but in which subsequent peaks and valleys are attenuated and a steady-state rate is approached. An "incubation period" will exist if the dispersion is not excessive. One might think of the variation in the surface element lifetimes as "dispersing" the periodicity associated with one layer being removed after another.

The preliminary mathematical formulation and computer program considered one distribution function applicable to the original surface, and one other applicable to each of the subsequently exposed "surfaces". Both were specified as normal distributions truncated and normalized over a finite time span. Thus the significant input parameters were the nominal mean lifetime (M_F) and standard deviation (σ_F) for the original surface, and the corresponding values (M_G and σ_G) for the "undersurfaces". Figure 37 shows some rate-time curves obtained by this program, with the distribution parameters as indicated. Note that the attaining of a steady-state rate is hastened both by increasing the dispersion of the functions, and by specifying a shorter mean lifetime for the undersurfaces as compared to the original surface.

Fluctuations such as shown in figure 37 have occasionally been observed, as illustrated by figure 38 which shows rate-time curves computed from experimental cumulative erosion curves presented by Kent [57]. Moreover, fluctuations which would appear quite prominent in rate-time curves are not nearly as evident if the same data are plotted as cumulative erosion versus time -- which, after all, is how the data are actually obtained. Therefore it seems quite conceivable that in many cases such fluctuations would barely have been noted and would have been "smoothed" out of the raw data, or might have been lost entirely through the data points being too far apart in time.

The fluctuations, however, are by no means an inevitable consequence of this model if non-symmetrical distribution functions are used, as will be seen in the results obtained from the elaborated formulation of the model, described below.

9.2 Description and Results of Elaborated Model

In the elaborated analysis we have chosen to use log-normal distribution functions, since -- as shown by References 58 and 59 -- these provide a reasonable representation of fatigue life data. For added flexibility one can adopt a "delayed" log-normal, i.e., one which would appear as a normal distribution if the frequency of failures were plotted versus log $(t-T_o)$, where T_o represents a "delay time" introduced to ensure that no failures occur prior to time $t = T_o$.

The distribution, when plotted on a $\log_{10}$ scale, is then described by its mean (m) and its standard deviation (σ). But one must use the distribution as transformed onto arithmetic or "real-time" scales. An important point to note is that while in a symmetrical distribution the mean, median, and mode values coincide, that is not true for a skew distribution such as the log-normal. The "real-time" value corresponding to m, which is denoted by $T_m = 10^m$, establishes the median value of the log-normal distribution -- i.e., that value of t at which half of the specimens (or surface elements) will have failed. This is the value generally used to establish a point of an engineering S-N curve. In the

"delayed" log- normal, the median value is given by $M = T_o + T_m$. The mode, or peak in the distribution curves, will occur at a time value less than M. The mean value, or arithmetic average of all life-times, will occur at a time value greater than M, or specifically at a time $E = T_o + T_m \times 10^{1.15\sigma^2}$. For purposes of discussion, we will characterize all distributions by their values of T_o, σ, and either M or E.

The elaborated model permits the specifying of a different distribution function for each "level" below the original surface, and of two different functions for the original surface: one for the "unaffected surface", in which erosion takes place by the initiation of new pits, and one for the "affected surface", which is that surrounding existing pits and in which erosion is presumed to take place by the lateral growth of these pits. The program computes the rate of erosion, the cumulative erosion, and the exposed area at each level, from which in turn, it can compute an average surface profile and surface roughness at selected time points.

The number of variations which could be investigated with this program is unlimited, and all that can be demonstrated here are some of the important effects. The most significant of these is the effect of the dispersion parameter σ. References 59 and 49 suggest that in conventional fatigue tests, σ, on a $\log_{10}$ scale, ranges approximately from 0.15 to 0.40, and for erosion fragment lifetimes even higher dispersions may be expected. Figure 39 shows computed erosion time curves for various values of σ from 0.15 to 0.80, with the median (M) held constant; Figure 40 shows a corresponding set of curves with the mean (E) held constant. In each case $T_o = 0$, and the same distribution is assumed for all surfaces and levels. Since in such cases the eventual steady-state erosion rate must be proportional to the reciprocal of the mean life-time, all curves in figure 40 approach the same steady-stage rate.

Two striking results appear from these curves: Firstly, the maximum erosion rates vary considerably. Secondly, almost all of the experimentally-found rate-time patterns can be at least qualitatively generated by proper choice of the dispersion parameter σ.

When σ is small, the curves exhibit damped fluctuations similar to those of figure 37. When σ is increased, the fluctuations die out and the steady-state rate is attained quite quickly. When σ is further increased, a single peak appears in the curve, and at very high values of σ this peak may occur so early that the time resolution is just not fine enough to show the acceleration stage of the rate-time curve, and the curve therefore appears to begin at its maximum value. The same is probably true for experimental data like that of figures 34 - 36. It does not seem unreasonable to suppose that erosion due to very small droplets, where each impact stresses only a minute portion of the surface area, would be characterized by a high dispersion in the fragment life-times.

In many of the curves of figures 39 and 40 the ratio of the erosion peak to the expected steady-state value is not as great as sometimes found in practice -- but it should be recognized that at time values greater than the median, the surface has suffered heavy erosion damage and one may therefore expect that geometric effects such as suggested by References 5, 11 and 51 may have set in by this time and have caused an additional diminution of the erosion rate and possibly suppression of further fluctuations. Certainly one would expect the results predicted by this analysis to be at least modified by the geometric effects. Thus, figures 39(d) and 40(b) may correspond to experimental results of the type of figures 31, and figures 39(b) and 40(a) to results of the type of figure 32. It is possible, however, that some appropriate combination of distribution functions for the different surfaces could result in an elongated "hump" such as in figure 32, which then again would not correspond to a steady-state value.

Figure 41 shows an example of slowing down the loss rate from the "unaffected" surface as compared to that of all other surfaces -- which are presumed to be more susceptible to erosion because of the irregular geometry. This case is identical to that of figure 39(d) except that for the unaffected surface the median lifetime has been increased to 3.0. Note that the shape of the rate curve has been made more similar to that typified by figure 31; the cumulative loss rate is also shown and is quite similar to typical curves such as figure 33.

Figure 42 shows "surface profile" curves, at various values of time "T", for some of the previous cases. The ordinates indicate the surface "level", with 0 representing the original surface. The abscissas represent the area not yet eroded away at each level. The difference in abscissa between adjacent levels represents the area "exposed" at the lower of the two levels. Note that in figure 42(a), a case of low dispersion value ($\sigma = 0.25$), the erosion is shallower and more evenly distributed than in the other two cases which represent high dispersion values ($\sigma = 0.8$). This suggests that the geometric effects which tend to reduce the erosion rate -- i.e., those due to high roughness -- are delayed in the former case, which may explain why the maximum erosion rate in such a case may persist for some time and give rise to rate curves typified by figure 32. Figure 43 shows the computed surface roughness, versus computed mean depth of penetration, for the same three cases, confirming the lower roughness associated with a lower dispersion value.

9.3 Discussion and Conclusions

Now to examine the implications of this model with respect to correlations of incubation times and erosion rates. Since the incubation time seems obviously related to the fatigue nature of erosion, several investigators have attempted correlations reflecting this. Thus Leith and Thompson [37] correlated the incubation times of several materials with the corrosion fatigue limit for 10^7 cycles of these materials. Mathieson and Hobbs[60] made a similar correlation with the conventional endurance limit, for several aluminum alloys. In both cases the results were reasonably consistent, but the approach is hardly logical since the incubation time in erosion surely should be related to a finite-life-time to failure, rather than to a stress value at which no failure occurs. Thus the success of these correlations surely depended on a second, implicit, correlation between the finite fatigue lives at the test stress, and the endurance limits, valid for the group of materials compared. Ripken et al [38] have used a more logical approach, and have correlated the number of impacts corresponding to the incubation time at a given impact velocity, with the number of cycles to failure in bending fatigue at an equivalent stress level. The stress level was assumed to be

given by the waterhammer pressure (ρ CV). The incubation period was defined by the intercept, on the time axis of the cumulative weight loss curve, of the straight line approximating the high erosion rate stage.

If the previously developed model is valid, this procedure is still not quite correct. The statistical model implies that the apparent incubation period depends not only on the mean lifetime of the erosion fragments but also on the scatter or dispersion in these lifetimes. The erosion-rate becomes non-zero when the first "element" fails, and continues to increase until approximately the mode or most probable value of the lifetime is reached on the top surface. But it is the median value -- which may occur later yet if the distribution is skewed -- which corresponds to the nominal lifetime at the appropriate stress as obtained from a conventional S-N fatigue curve. Whether either the median lifetime or the associated scatter in erosion fragments corresponds to that of full-scale bending or pull-type fatigue specimens is at present a moot question. However, the discrepancies in the correlations of Reference 38 are in the direction which the above argument would predict.

If one stipulates a steady-state erosion process, then the erosion rate would certainly be inversely proportional to the mean lifetime of erosion fragments (provided their size distribution remained constant). This is the basis from which one can draw the analogy between the (loss rate)$^{-1}$ versus impact velocity in erosion, and cycles to failure versus stress level in fatigue, as proposed by Reference 26. This appears to provide a rational basis for attempting to predict an erosion-speed relationship on the basis of known fatigue data for the material, although to my knowledge this attempt has not been made. But here, again, the statistical model suggests that the "obvious" approach is not quite correct. It implies that the maximum erosion rate -- which many investigators have linearized and used in correlations, for good and valid practical reasons -- does not necessarily represent a steady-state erosion process at all, but rather the "deluge" of erosion fragments from the top surface layer which takes place in the vicinity of the "most probable" fragment lifetime from the beginning of exposure.

Thus the maximum instantaneous erosion rate is, again, not merely a function of the average fatigue life of the surface elements but also of the scatter in lifetimes. Consequently, any external or internal effect which influences that scatter will influence the maximum erosion rate, even though it may not affect the eventual hypothetical steady-state rate.

Finally, what can this model contribute toward the resolution of the dispute referred to in Section 7. It implies, firstly, that Reference 50 is correct in claiming that the erosion rates during the stages encompassing the first peak in the rate-time curve are not characteristic merely of the material under test, since, as we have seen, the shape of this curve depends on the shape of distribution functions which, in turn, depend in part on characteristics of the test method such as the distribution of bubble or droplet sizes, etc. It implies, secondly, that while the erosion rate would, in the absence of other influences tend toward a steady-state value as postulated by Reference 50, this generally occurs only after most of the original surface has eroded away, by which time the surface damage will be so severe as to make the erosion conditions susceptible to geometry effects such as described by Reference 51. In short, the instantaneous erosion rate may never be characteristic of only the material, and for valid correlations it will become necessary to standardize the test method very carefully, or to use properly chosen cumulative erosion measurements, such as the time required to attain some specified value of the rationalized erosion (MDP) of practical significance.

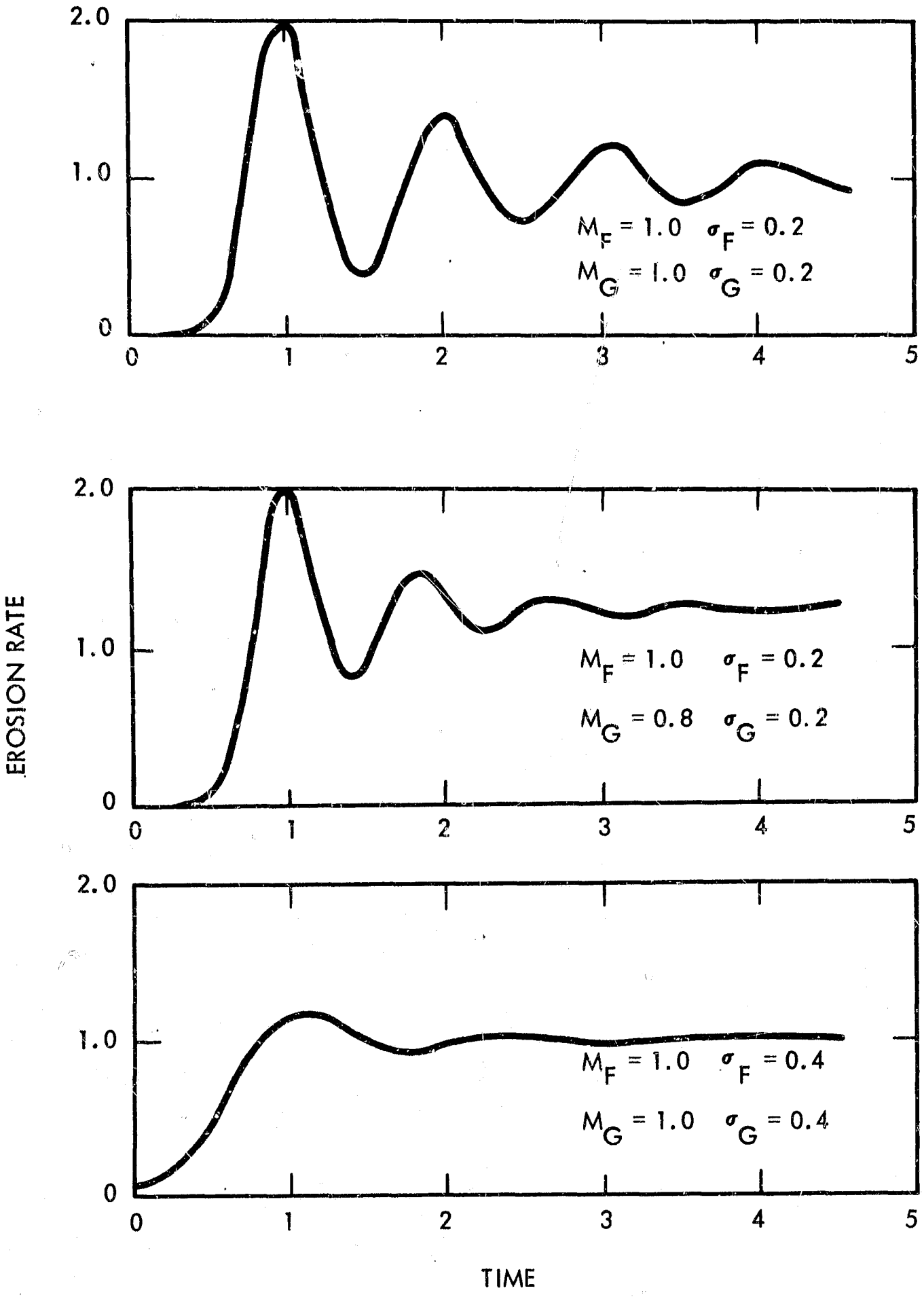

Figure 37. Typical Computed Erosion Rate-Time Curves from Preliminary Statistical Model, Using Normal Distribution Functions

Astronuclear Laboratory

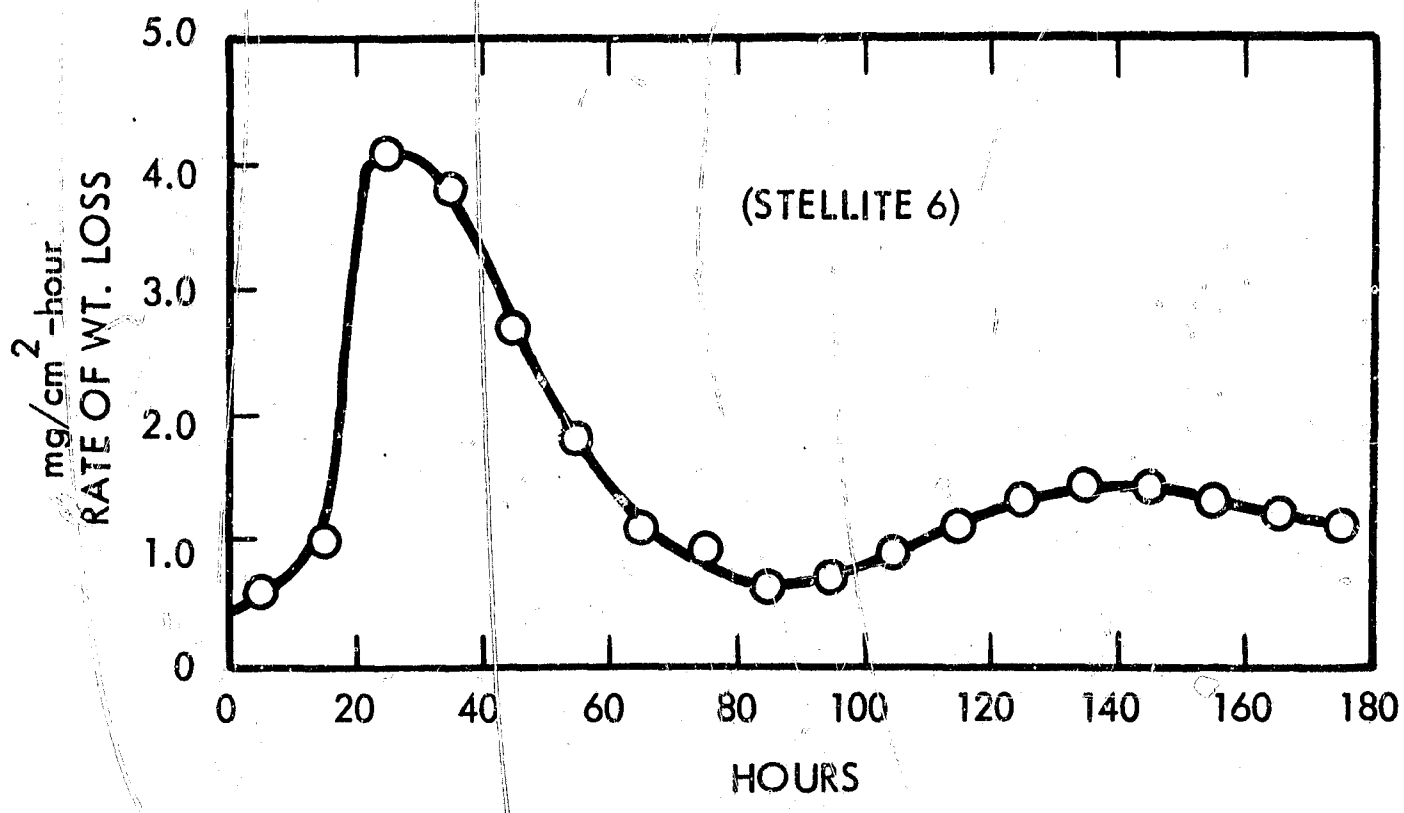

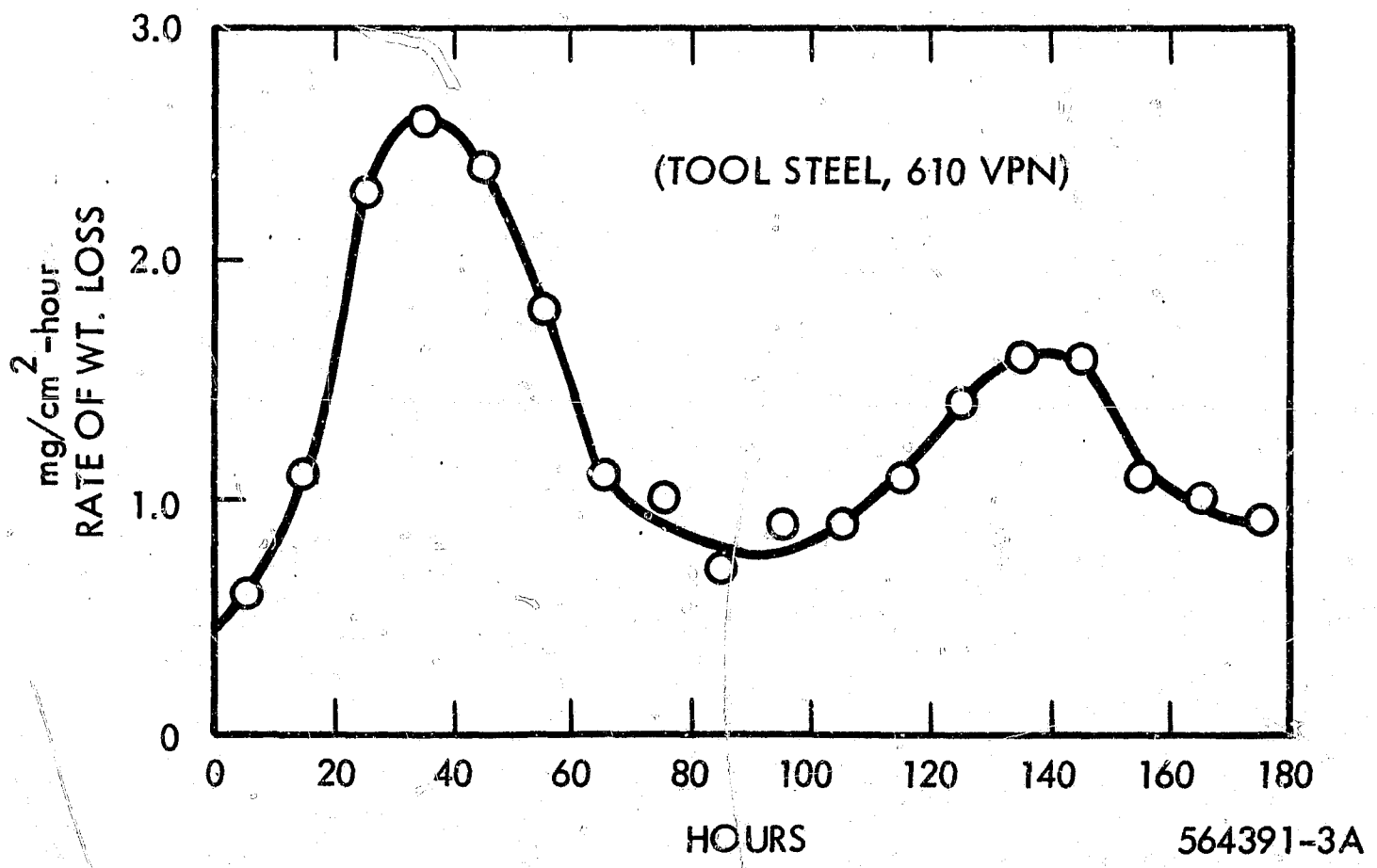

Figure 38. Experimental Erosion Rate-Time Curves, Computed from Cumulative Erosion Curves Given in Reference 33

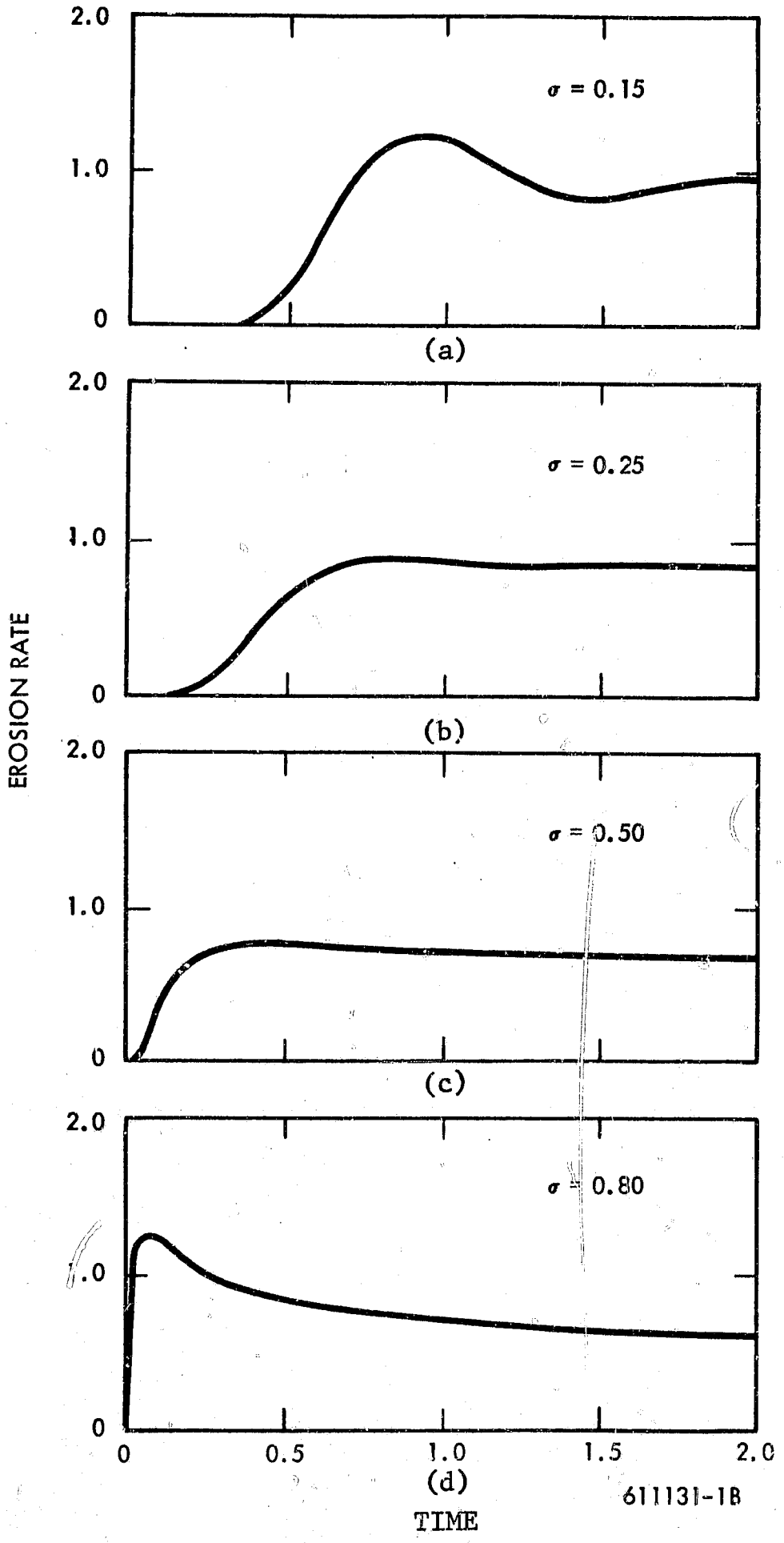

Figure 39. Computed Rate-Time Curves Based on Log-Normal Distributions, Showing Effect of Varying Dispersion, σ, with Median at Constant, M = 1.0

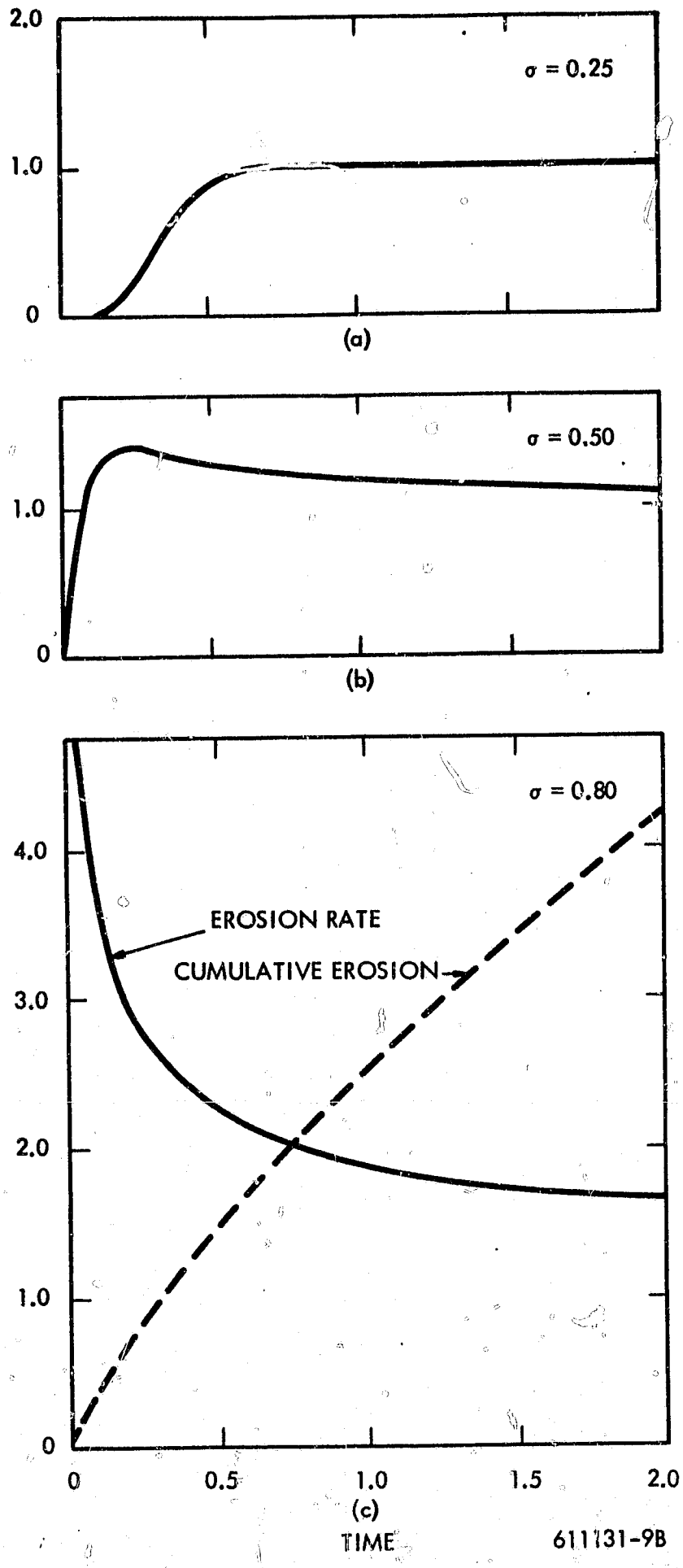

Figure 40. Computed Curves Based on Log-Normal Distributions, Showing Effect of Varying Dispersion, σ, with Mean at Constant, E = 1.0

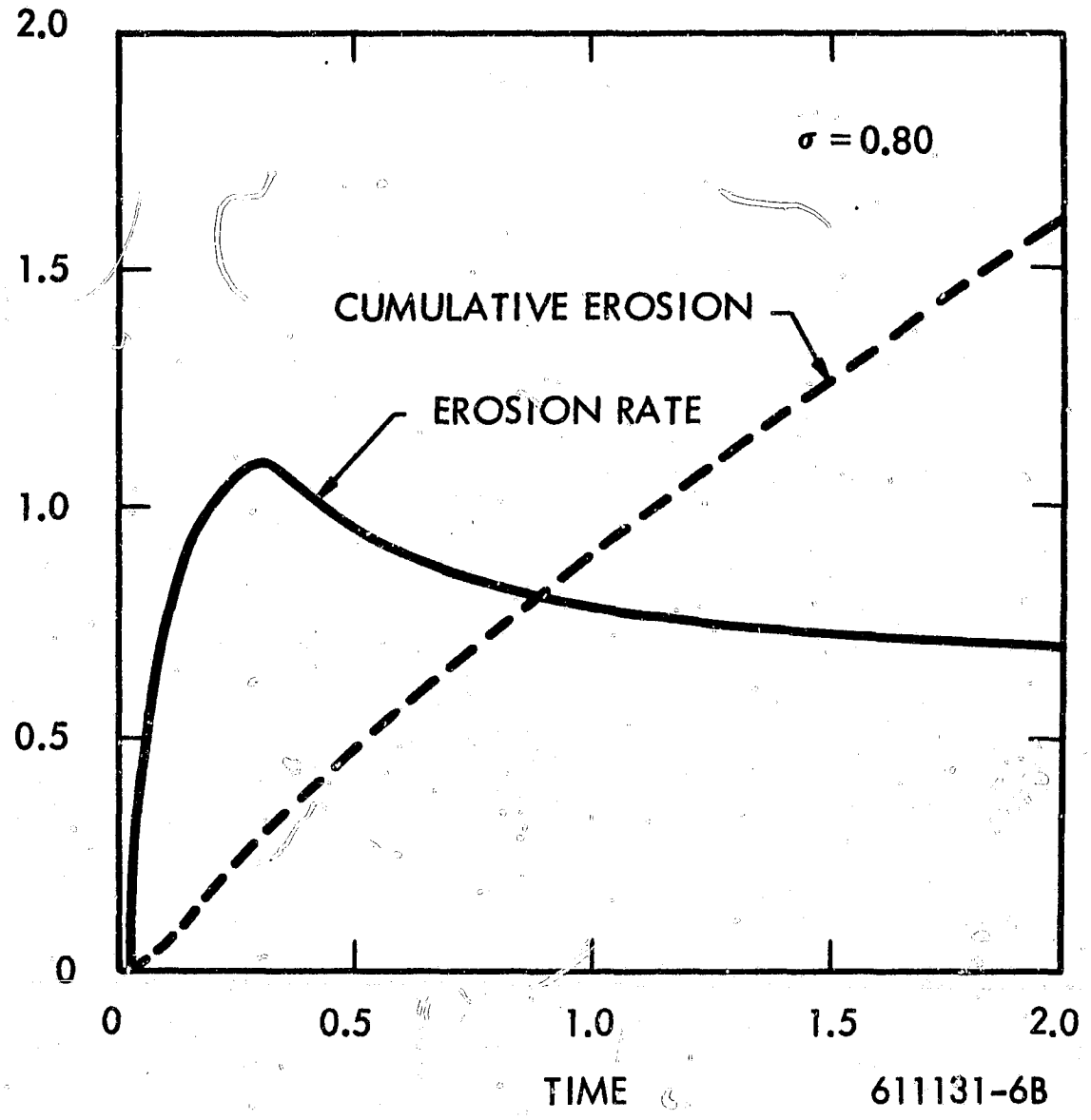

Figure 41. Effect of Higher Median Value for "Unaffected" Surface ($M_u = 3.0$) than for Other Surfaces (M = 1.0). (Compare with Figure 39d, but Note Difference in Vertical Scale.)

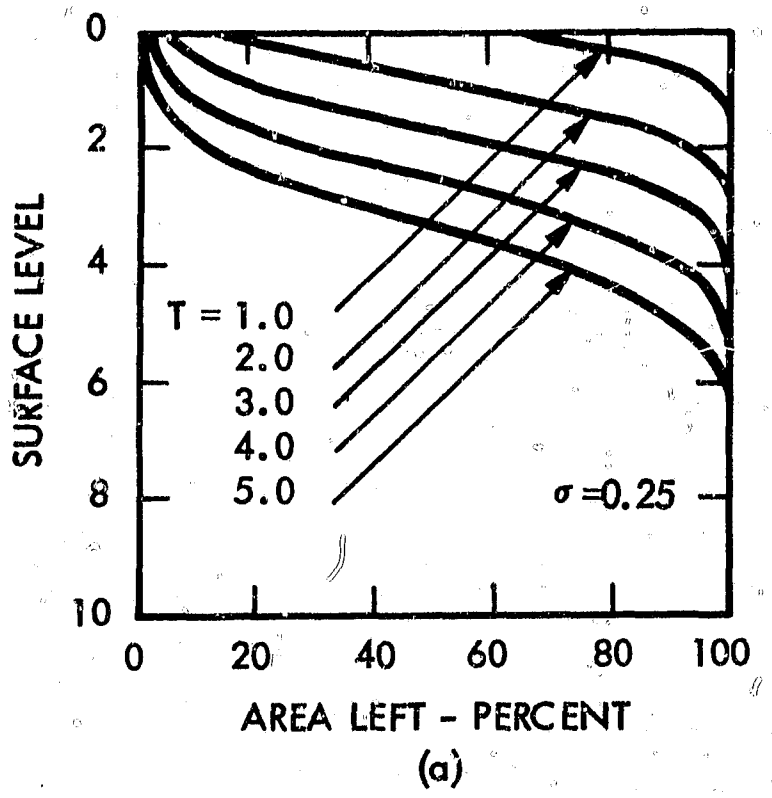

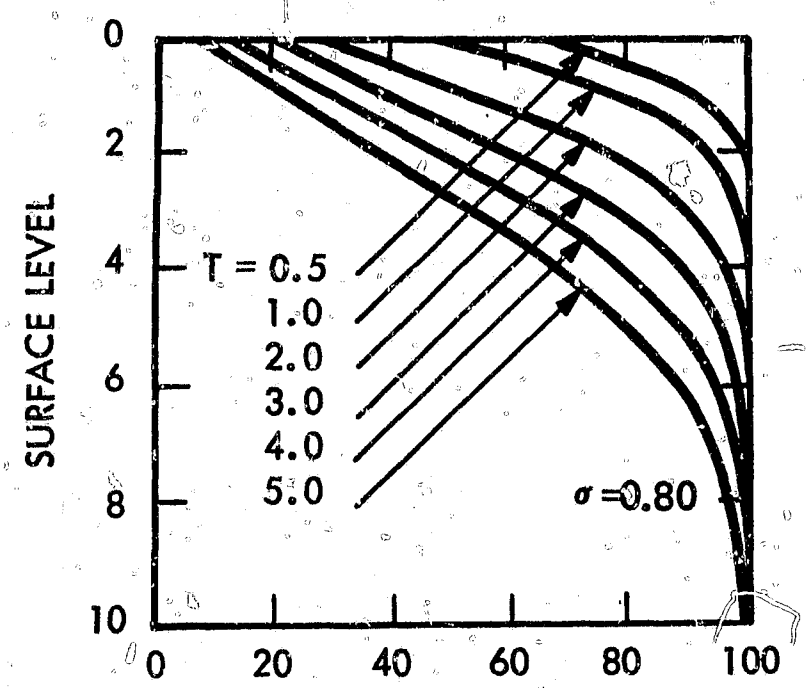

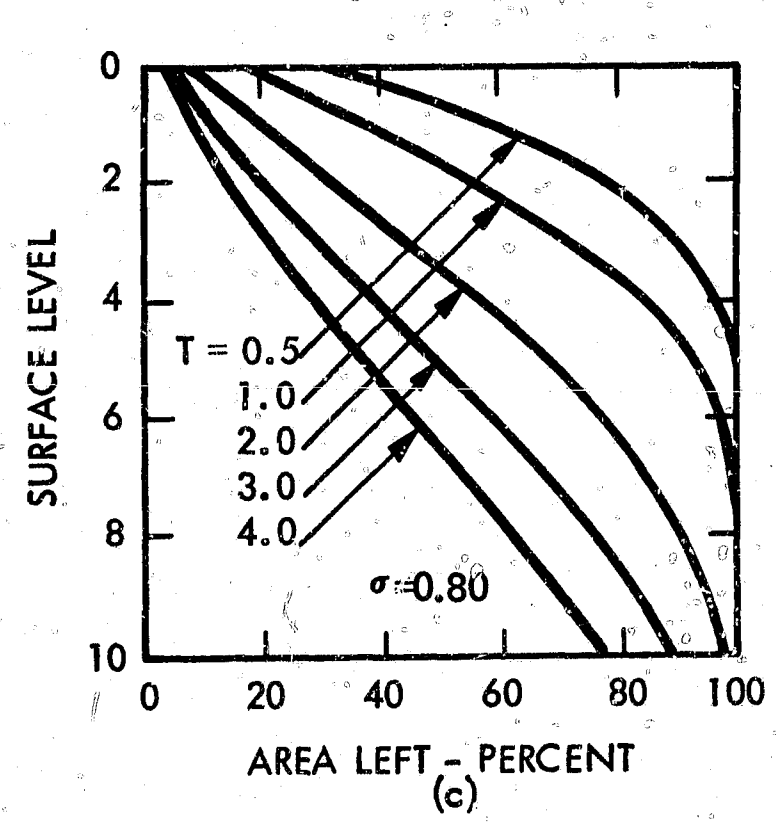

611131-36B

Figure 42. Examples of Computed "Surface Profile" Curves (Showing the Uneroded Area as a Function of Level Below the Original Surface, at Various Values of Time T: (a) - Corresponding to Figure 39b; (b) - Corresponding to Figure 41; (c) - Corresponding to Figure 40c)

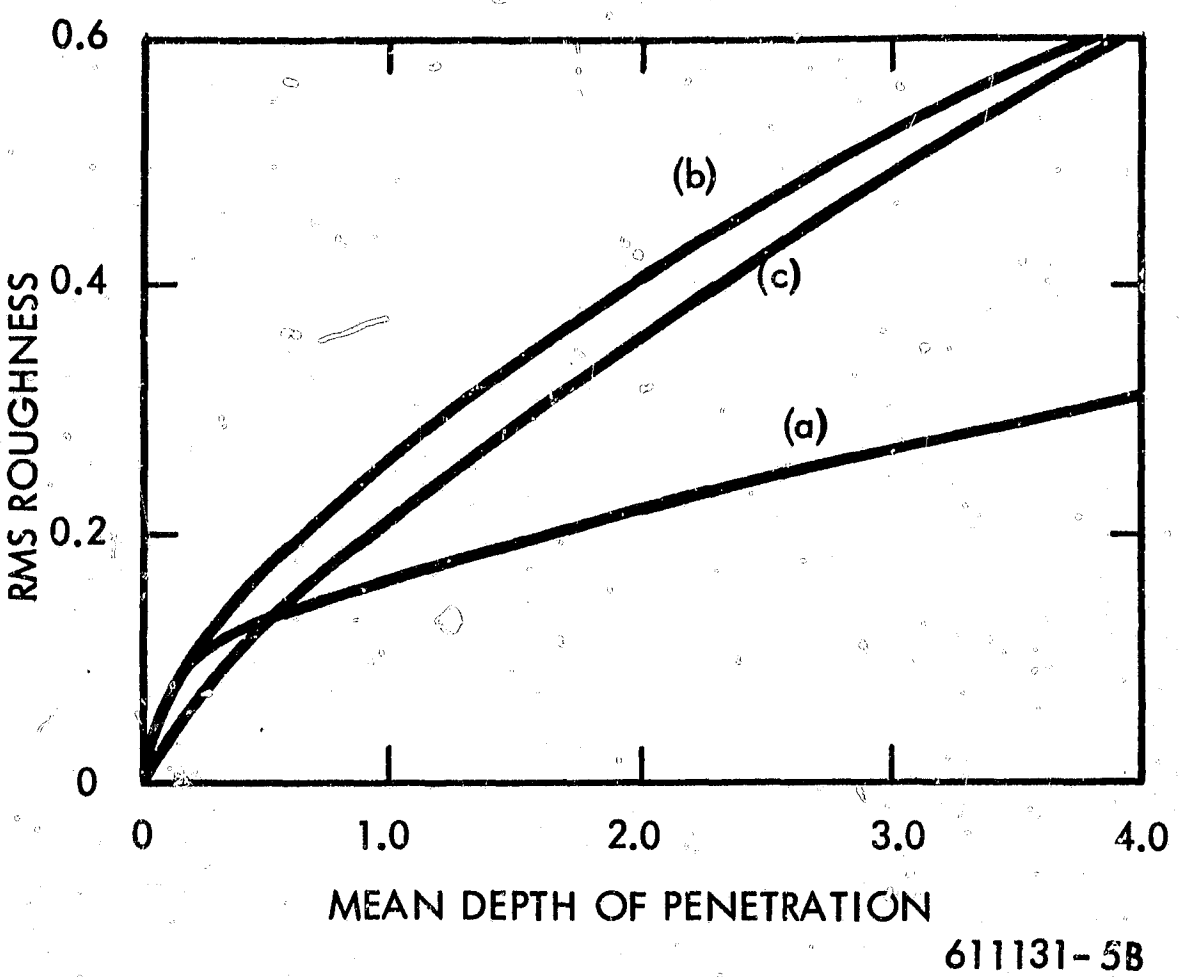

Figure 43. Computed rms Surface Roughness Versus Mean Depth of Penetration (Cumulative Erosion) for Figure 42. The letters (a), (b) and (c) Correspond to the Similarly-Designated Cases in Figure 42

10.0 MATHEMATICAL FORMULATION OF MODEL

10.1 First Simplified Formulation

Let any surface exposed to erosion be thought of consisting of elementary areas (or volumes, if their thickness is considered) whose life-times under the erosion attack can be described by a normalized distribution function f (t). Thus by definition

$$\int_{-\infty}^{\infty} f(t)\ dt = 1.0 \tag{21}$$

and the distribution function for a specific area A, exposed to erosion from time t = 0, is therefore

$$F_A(t) = A\ f(t) \tag{22}$$

Since a surface element is lost from the surface when its life-time is reached, equation 22 can equally well be regarded as a loss rate function for the area A.

Equation 22 may be further generalized by stating that the loss rate from an area A_1, first exposed to erosion at time $t = T_1$, is thereafter given by

$$F_1(t) = A_1\ f(t-T_1) \tag{23}$$

Let us now consider the original or "top" surface of a body exposed to erosion. One may take its area to be unity, and every portion of its area is simultaneously exposed to erosion at time t = 0. Thus f (t) adequately describes the loss rate from the top surface. As surface area is eroded, or lost, from the top surface, an equal area is created, or exposed, at the "second" level, located at distance h below the surface where h is assumed as the thickness of erosion fragments. For convenience the thickness h will also be assigned a numerical value of unity on some appropriate scale. In turn, the second level surface will be eroded to expose a third level surface, and so on. But in computing the actual loss rates from all of the "undersurfaces" one must recognize that the lifetimes of surface elements

must be measured from the time they were first exposed, and the total loss rate from all surface elements which were first exposed during a time increment dT at time T, depends on the total area which was first exposed during that time interval.

Let Y(t) be the total rate of erosion, from all levels, at time t. This is what one desires to compute. But Y(t) is, ipso facto, also equal to the rate at which new surface area is exposed, at all levels below the top surface, at time t. (Strictly speaking, it is proportional to it, but with h = 1.0 it is numerically equal.)

Thus the total surface area first exposed during increment dT at time T, is Y(T) dT, and the loss rate from this area at time t is, by equation 23.

$$F_T(t) = f(t-T)\ Y(T)\ dT \qquad (24)$$

The total loss rate at time t, from all undersurfaces, is composed of contributions from all undersurface areas first exposed during all time increments from T = 0 to T = t, or

$$\int_o^t f(t-T)\ Y(T)\ dT$$

The total loss rate or erosion rate or erosion rate, Y(t), is the sum of that from the top surface and that contributed by all undersurfaces, or

$$Y(t) = f(t) + \int_o^t f(t-T)\ Y(T)\ dT \qquad (25)$$

The fact that the contributions from the undersurfaces and from the top surface form two distinct terms in equation 25 makes it conveniently possible to assign a different distribution function for the top surfaces as compared to all undersurfaces. This is desirable if one wants to reflect the fact that the top surface has in many ways a different nature and history than the undersurfaces exposed as a result of erosion. Finally, then one can state

$$Y(t) = f(t) + \int_o^t g(t-T)\ Y(T)\ dT \qquad (26)$$

where f(t) = distribution function for top surface

g(t) = distribution function for undersurfaces

It is worth noting that equation 26 is a well-known integral equation having a convolution integral as its last term. A Laplace transformation yields

$$y(s) = f(s) + g(s)\ y(s)$$

By ordinary algebra

$$y(s) = f(s) \Big/ \left[1 - g(s)\right] \tag{27}$$

or

$$Y(t) = L^{-1} \left\{ f(s) \Big/ \left[1 - g(s)\right] \right\} \tag{28}$$

This solution may be useful if equation 26 has an easy Laplace transform and equation 27 has an easy inverse transform. Ordinarily, numerical methods are required.

For the initial explorations equation 26 was computer-programmed directly, using Normal distributions for functions f(t) and g(t), normalized over specified time spans rather than between the limits of plus and minus infinity as suggested by equation 21.

10.2 Formulation of Elaborated Model

In further explorations of this approach, it is desirable not only to keep track of the area exposed at each "level" as a function of time, so that an average surface profile or surface roughness can be computed, but it also may be desirable to assign different distribution functions for all levels. An analytical "continuity approach" to this becomes very cumbersome, and since the final evaluation is in any case a numerical one by computer, it becomes advantageous to develop the model as a step-wise process in time, and to have the computer program compute the processes occurring in each time interval, one after the other. In a sense, the computer program becomes a digitalized analog of the physical process.

The crux of the approach is that the program maintains, and up-dates for each time interval, the array $S_{L,\ J}$, in which each value represents the surface area presently existing at level L and dating back to time interval J during which it was first exposed as a result of loss from the next-higher level. Thus the total surface area presently existing at level L

would be given by $\sum_{J=1}^{N-1} S_{L,J}$, where N is the present time interval at which the evaluating is being done.

Let us now define a modified rate or quotient function q (t), which represents the loss rate as a proportion of the remaining area at time t. In terms of the previously used distribution function f(t), this is

$$q(t) = \frac{f(t)}{1.0 - \int_0^t f(t)\,dt} \tag{29}$$

For computation purposes the continuous function q (t) is replaced by a loss quotient Q_I representing the finite amount of loss during the I^{th} time interval after the surface has first been exposed. This can be represented by

$$Q_I = q(I\,\Delta t)\quad \Delta t$$

where Δt is the length of a time interval. The program computes and stores all values of $Q_{L,I}$, where the additional subscript L refers to the level; thus a different distribution function f(t) can be specified for each level.

The total erosion from all levels during time interval N, Y_N, will then be composed of all contributions of the type

$$R_{L,J} = S_{L,J}\quad Q_{L,N-J} \tag{30}$$

where $R_{L,J}$ represents the loss rate from that area at level L which was first created during time interval J. The total erosion rate is therefore approximated by

$$Y_N = \left[\sum_{L=L}^{M} h_L \sum_{J=1}^{N-1} R_{L,J}\right] \Big/ \Delta t \tag{31}$$

where h_L = thickness of erosion fragments lost from L^{th} level

M = total number of levels considered

Using the $R_{L,J}$ values computed from the $S_{L,J}$ array which was valid for the beginning of the N^{th} time interval, one can readily compute the new values of $S_{L,J}$ which are valid for the end of the N^{th} interval, i.e., for the beginning of the (N + 1)th interval:

$$\left[S_{L,J}\right]_{N+1} = \left[S_{L,J}\right]_{N} - \left[R_{L,J}\right]_{N} \tag{32a}$$

for all values of $J < N$, and

$$\left[S_{L,N}\right]_{N+1} = \left[\sum_{J=1}^{N-1} R_{L-1,J}\right]_{N} \tag{32b}$$

for $J = N$.

The manner in which the cumulative erosion, surface "profile" and surface roughness can be computed from the above-mentioned quantities is straightforward.

The log-Normal frequency distribution function as programmed is of the form

$$f(t) = \frac{1}{\sigma(t-T_o)\sqrt{2\pi}} \exp\left\{\frac{-\left[\log_e (t-T_o) - m\right]^2}{2\sigma^2}\right\} \tag{33}$$

This function has the following properties:

The mean, or expected value, is

$$E = T_o + e^{m+(1/2)\sigma^2} \tag{34}$$

The median value is

$$M = T_o + e^{m} \tag{35}$$

The mode, or most probable value, is

$$P = T_o + e^{m-\sigma^2} \tag{36}$$

The input may be prescribed in terms of T_o, m and σ directly; the latter two may also be prescribed in terms of the equivalent logarithms to base 10, or in terms of the equivalent real-time quantities $T_m = e^m$ and $R = e^\sigma$.

10.3 Discrete Pit Formation and "Affected" Surface

In order to model the probable progress of erosion damage more faithfully, a further elaboration has been introduced for the top surface only. This is based on the observation that erosion tends to proceed by the formation and growth of discrete pits -- which may extend to a considerable depth while adjacent "top surface" is still intact -- rather than by a randomly-distributed depth.

To approach this condition, the top surface is considered as consisting of two "kinds" of surface: "affected areas" and "unaffected areas". Affected areas are defined as those areas of the top surface immediately surrounding existing erosion pits, whose resistance to erosion may be assumed to be influenced by this fact. Therefore, one distribution function, $f_a(t)$, is provided for the affected area, and another, $f_{u(t)}$ for the unaffected area which is the remainder of the still existing top surface. (In general one would suppose that f_a is such as to result in more rapid erosion than f_u, but the program does not make this a requirement). The actual amount of area considered as affected is computed as follows: Let w be a characteristic dimension of erosion fragments, which must be prescribed in the program input. Then the affected area A_a associated with a pit of surface area A_p is defined as the area of an annulus of width w surrounding a circle of area A_p. In other words, all of the potential erosion fragments bounding upon an existing pit are considered "affected area". To carry this calculation through it is of course necessary to know the number and size distribution of all pits. This is done as follows: During any time interval N, the loss from the existing "unaffected" surface, based on the f_u distribution function, is divided into an integral number of values A_o (where A_o is the area of a circle of diameter w). Thus a known number of new pits -- all of area A_o -- are said to be "initiated". For the subsequent time interval, the new pits are assigned their annulus of affected area. Further enlargement

of each of this generation of pits takes place by erosion from the affected area surrounding it, requiring the "transformation" of additional surrounding area to maintain the previously specified relationship between affected area and pit area. Thus the number and present size of each generation of pits, and extent of affected area surrounding them, can be established and updated.

The rate of loss from the affected areas is based on the f_a distribution function, but not in a simple manner. Let us for the moment talk in terms of the continuous functions, though the actual calculations are of course carried through in terms of step-wise loss quotients as explained previously. Consider now an area which existed as unaffected area until time T_T, at which time it becomes "transformed" into affected area. Up until T_T the loss from this area was governed by f_U; henceforth it is to be governed by f_a. Upon reflection it can be seen that our purpose would not be served in any realistic way by simply saying that at $t = T_T$ the loss rate jumps from $f_U(T_T)$ to $f_a(T_T)$ and henceforth is given by $f_a(t)$. (In an extreme case, $f_a(t)$ may represent such rapid erosion that T_T is well beyond the mean or mode value and $f_a(T_T)$ is already sensibly zero. Thus no further erosion, rather than more rapid erosion, would result from this switch.) A wholly rigorous approach would have to be based on cumulative fatigue damage theory, but a device which is adequate for our purpose is to require that the f_a distribution function be entered at an "effective time" T_E, such that the cumulative loss due to f_a at T_E is equal to the cumulative loss due to f_U at T_T, or

$$\int_0^{T_E} f_a(T)dT = \int_0^{T_T} f_U(T)dT \qquad (37)$$

If T_E is defined by equation 37, then the loss rate from the area under consideration, at any time t subsequent to $t = T_T$, is given by $f_a(t - T_T + T_E)$. This device will at least ensure that if a given area is "transformed" at any time T_T whatever, then 100% of it -- no more and no less -- will have been lost at time $t = \infty$; which is the minumum logical requirement of any realistic approach. For some types of distribution functions, it is possible to express

T_E in terms of T_T and the function constants. Thus, for the simple case of (normalized) exponential functions, where

$$f_u(t) = p_u e^{-p_u t} \quad \text{and} \quad f_a(t) = p_a e^{-p_a t}$$

it is easy to show that

$$T_E = T_T \left(p_a / p_u \right)$$

An analytic expression can also be obtained for the log-normal distribution, but in many other cases, including the normal distribution, T_E would have to be computed by trial-and-error procedures from the relationship of equation 37.

A consequence of this approach is that not only must the total affected area associated with each "generation" of pits be known, but so must each "generation" of affected area, since the rate of loss from any portion of the affected area depends on when it had been "transformed" from the unaffected to affected status. The number of pertinent computations required during the N^{th} time interval is therefore N^2, and the number of memory locations required for the affected area array is M^2, where M is the maximum number of time intervals to be computed. This is a compelling argument for making M reasonably small (100 in our program), which makes for a rather coarser time "grid" than one would otherwise desire.

The details of the computation method would require too much space to present here, but are generally analogous to the method described for the undersurfaces by equations 30 through 32. It should be emphasized merely that the concept of erosion by discrete particles of specified size is applied only to the initiation of new pits in the unaffected surface, and that the loss rates from the second and lower layers do not concern themselves with whether the second layer surface was exposed as a result of loss from unaffected or affected surface. This distinction is only made for the loss rates from the top surface itself.

The program in its present form has provision for using either log-normal distributions (to represent fatigue damage), or exponential distributions (to represent single-impact damage).

Astronuclear Laboratory

PART C

CHEMICAL DISSOLUTION BY LIQUID METALS

F. R. Arcella

11.0 MODEL OF TURBINE BLADE DISSOLUTION IN LIQUID METALS

11.1 Background

The chemical dissolution of various materials into alkali and heavy liquid metals has been extensively investigated. Results, particularly with alkali metal systems, have been scattered. This scatter occurs because many difficulties arise when working with alkali liquid metals. Dissolution rates, besides varying with the standard parameters of temperature, material, flow rates, and temperature gradients, are also strongly influenced by alkali metal purity (small ppm concentrations of oxygen, carbon, or nitrogen contribute to increased corrosion), by dissimilar metal couples within the system, hot trap and getter efficiency, etc. Also, as experimental techniques and controls improve, the comparison of recent experimental results with earlier data further contributes to the problem.

Most liquid metal corrosion data, either from refluxing capsules, natural convection loops, or pumped loops, has been of a qualitative nature. General surface dissolution, grain boundary penetration, and general mass transfer have been noted. However, the vast number of variables involved in most systems has not permitted the mathematical approaches expressed by Epstein in Reference 61 or Gill in Reference 63 to be extended to these more complex systems. Thus, experience with materials and systems has been relied upon to designate the materials and their properties most compatible to the system in which they are to be incorporated.

Within the last few years improved experimental techniques and equipment have permitted investigators to reduce some of the variables (especially oxygen contamination) to less influential levels. The quantitative data being generated today can, with due consideration of its source and system, be extrapolated to other similar systems for rough, predictive comparisons.

In this section the chemical dissolution of a turbine blade material into the thin stream of condensed potassium that flows radially outward along the blade is considered. Epstein's static dissolution equation in Reference 61 was solved with dynamic dissolution parameters from

Gill in Reference 63. The resulting approximation of 2.3 mils/10,000 hours compares with actual test data (chemical dissolution) of 1.5 in Reference 67 and 1.0[60] mils/10,000 hours.

These figures indicate the relative range of dissolution attack by direct chemical action that could be expected in a system of low oxygen concentrations. Unless flow rates across turbine blades are substantially higher than those considered here, it would seem unlikely that direct chemical dissolution will result in any serious damage by alkali-metals to turbine rotor blades.

It is known that chemical dissolution of a material will occur preferentially on the least densely packed crystal surfaces and at grain boundaries. Such preferred dissolution may have a weakening effect on the material which, when coupled with the impact stresses of droplets, may result in an acceleration of the impact erosion process.

11.2 Turbine Blade Dissolution in Liquid Metal

For a flow of liquid metal across a turbine blade, as in figure 44, consideration can be given to the removal of blade material through the ordinary dissolution of a solid into a liquid.

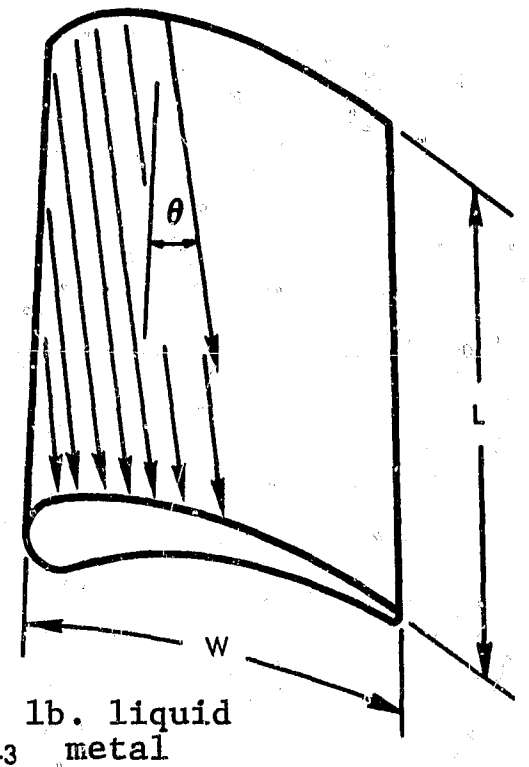

Figure 44. Radial Liquid Flow Along Turbine Blade (with a Shallow Angle (θ) with the Radial Direction)

For a flow given as the pounds of liquid metal impacting along the blade per foot of blade length per second, the following additional considerations are made:*

1) All flow is assumed radial and to contact the surface of the blade over a band two centimeters deep from the leading edge.
2) Time of actual contact between liquid and blade will be required, since dissolution will follow an Arrhenius relation with time.
3) Assumption of a proper Arrhenius solution-rate constant must be found through correlations with the literature.
4) The time of contact between liquid metal in flow and the blade is assumed to be as though all flow originated at the hub instead of being of distributed origin as is the actual case. (Obviously overstating the residence time.)
5) Dimensionless parameters and velocity boundary layer effects are neglected as such, and the theoretical form of the equation used implies a reaction-rate limited, constant temperature process. However, the empirical constants used in this development were selected from data taken at flow velocities of the order expected on turbine blades.
6) Although the liquid metal flowing over the blade would ordinarily contain some concentration of blade material (dissolved), it is assumed that the flow considered begins as pure liquid metal. (Obviously overstating potential dissolution capacity.)

According to Epstein in Reference 61, the dissolution of a metal into a liquid can be described as

$$n(t) = n_o \left[1 - \exp \left(- k \frac{A}{V} t\right)\right] \qquad (38)$$

*The rates of liquid metal flow, velocities of flow, film thickness and width used here are all assumed quantities and do not represent actual calculations or data from liquid metal turbines. They do represent some insight into the probable magnitudes of the assumed quantities based on steam turbine calculations.

where

$n(t)$	is the concentration of dissolving solute as a function of time
n_o	is the equilibrium saturation solubility of solute in the solvent
A	is the area of contact between solid and liquid
V	is the volume of liquid in contact with the solid
t	is the time of contact
k	is the solution-rate constant

The parameter k varies with temperature, flow rate (mixing), materials, surface, etc. and at best must be determined for each system under consideration. Although few k values are recorded in literature, the values and systems in the table below will indicate the range of k. A choice of $k = 5 \times 10^{-6}$ cm/sec was made for this calculation. The basis for this choice was influenced by the materials and system of Reference 63.

TABLE 1

SOLUTION-RATE CONSTANTS

System	Temperature	k (cm/sec)	Reference
Cu → Pb (liq.)	510°C	6.07×10^{-4}	62
Cu → Bi (liq.)	510°C	1.91×10^{-3}	62
304 s/s → Li (liq.)	510°C	1.54×10^{-6}	63
304 s/s → Li (liq.)	612°C	7.50×10^{-6}	63

Since it is assumed the liquid metal flows at an average width of flow from the leading edge of 2 cm, the area of contact per foot of length would thus be approximately 2 cm x 30.4 cm = 60.8 cm^2.

Since the centrifugal acceleration force on the liquid on a rotor blade surface is quite high, the radial flow of liquid along the leading edge of the blade may be assumed to be less than 1 mil thick. The radial flow velocity V is chosen = 2 ft/sec. Thus the duration time per unit of flow in a 1 ft path is 0.5 sec.

In 0.5 sec the volume V of liquid metal flowing across the 1 ft length of surface is

$$V = 0.4 \times 10^{-3} \ \frac{\text{lb liquid metal}}{\text{ft (path) sec}} \times \frac{454 \text{ gms}}{\text{lb}} \times 0.5 \text{ sec} \times \frac{\text{cc}}{0.9 \text{gms(liquid metal)}} = 0.106 \text{ cc}$$

n_o, the saturation solubility, of various materials in liquid potassium is given in table 2.

TABLE 2

SATURATION SOLUBILITIES IN LIQUID POTASSIUM (K)

System	Temperature	n_o (ppm)	Reference
Fe → K	1000°C	500*	64
Ta → K	1250°C	6	64
Ta → K	500°C	3	65
Fe → K	1000°C	100*	66
Mo → K	1000°C	20	66

Thus in equation 38

$$n(t) = n_o \left(1 - \exp\left[-k \ \frac{A}{V} \ t\right)\right]$$

$$n(t) = 300 \text{ ppm}^* \left[1 - \exp\left(-5 \times 10^{-6} \text{ cm/sec} \ \frac{60.8 \text{ cm}^2}{0.106 \text{ cc}} \ (.5) \text{ sec}\right)\right]$$

$$= 300 \text{ ppm} \left[1 - e^{-.00144}\right]$$

$$= 300 \text{ ppm} \left[1.44 \times 10^{-3}\right]$$

$$= 0.431 \text{ ppm}$$

---

* 300 ppm saturation solubility chosen as the average of n_o for Fe → K from table 2.

Each mass unit of liquid metal that flows over 1 ft length of turbine blade (radially) picks up 0.431 ppm of blade material (here assumed to be ironlike in makeup, physical properties, etc.) through the process of dissolution. Each foot of blade material has a liquid metal flow rate of 0.4×10^{-3} lb/sec. For 10,000 hours operation, the amount of blade lost would be

$$= 0.4\,(10^{-3})\ \frac{\text{lb (liquid metal)}}{\text{sec}} \times (0.431)\ 10^{-6}\ \frac{\text{lb (blade)}}{\text{lb liquid metal}} \times 10^{4}\ \text{hr} \times \frac{3.6\,(10^{3})\ \text{sec}}{\text{hr}}$$

$$= 6.2 \times 10^{-3}\ \text{lb blade lost/10,000 hours/ft blade length}$$

For an area of 60.8 cm^2 and a blade density of 8 gms/cc, the thickness loss would be

$$= \frac{6.2 \times 10^{-3}\ \text{lb}}{8\ \text{gms/cc}} \times \frac{454\ \text{gms}}{\text{lb}} \times \frac{1}{60.8\ \text{cm}^2} \times \frac{1\ \text{inch}}{2.54\ \text{cm}}$$

$$= 2.28\ \text{mils/10,000 hours}$$

ORNL [67] reporting on attack by flowing NaK (2-10 ft/sec) in the SNAP-8 system, found that maximum attack occurred in a system (with less than 30 ppm oxygen) on Hastelloy N at the outlet end of the SNAP-8 reactor. Extrapolation of this data indicates that corrosion at this point will be less than 1.5 mils in 10,000 hours at 1300 °F.

These figures indicate the relative range of dissolution attack by direct chemical action that could be expected in a system of low oxygen concentrations. Unless flow rates across turbine blades are substantially higher than those considered here, we do not think it likely that direct chemical dissolution will result in any serious damage by alkali-metals to turbine rotor blades.

ORNL [68 and 69] has also been investigating the compatibility of potential turbine materials (D-43, TZM, FS-85, T-111, and Cb-1 Zr) in potassium, boiling and condensing loops. One Cb-1 Zr forced-circulation loop with Cb-1 Zr nozzle and turbine-blade specimens was operated for 300 hours with a maximum temperature of 1100 °C

(minimum 355°C). Maximum attack was one mil at the impingement area of the second stage blade. No evidence of attack or deposits was found in the boiler, condenser or subcooler. Tests on 316 s/s, Haynes-25 and TZM again revealed the maximum erosion damage at the middle nozzle-blade position (three blade positions in the test) with the lowest vapor quality (82 percent). These tests revealed little damage beyond formation of a smooth, shallow depression at the second-stage blade impingement area.

It is known that chemical dissolution of a material into a liquid metal will occur preferentially on the least densely packed crystal surfaces and at grain boundaries. Such preferred dissolution may have a weakening effect on the material which, when coupled with the impact stresses of droplets, may result in an acceleration of the impact erosion process.

ACKNOWLEDGEMENTS (PARTS A AND B)

Thanks are due to Messrs. E. A. Eaton and D. Pearson of the British Central Electricity Generating Board for personal discussions and making available a group of CEGB Marchwood Engineering Laboratories reports which have been of paramount value to this study.

Acknowledgements are also due to R. I. Shrager and L. B. Godio, who collaborated on the mathematical formulations and computer programs involved in Part B of this report.

Thanks should also go to L. G. Hays of the C.I.T. Jet Propulsion Laboratory for his help in the role of Technical Program Manager on behalf of NASA.

REFERENCES

1. "Second Quarterly Progress Report; October 1, 1965 through January 15, 1966; Basic Investigation of Turbine Erosion Phenomena; Contract NAS 7-390", WANL-PR (DD)-077, Westinghouse Astronuclear Laboratory, February 1966.

2. "Progress Report on Contract NAS 7-390", WANL-PR(DD)-001, Westinghouse Astronuclear Laboratory, July 1965.

3. Heymann, F. J., "On the Time Dependence of the Rate of Erosion due to Liquid Impact or Cavitation", Westinghouse Steam Division Report E-1448, June 1966. (Also Paper No. 136, ASTM Annual Meeting, Atlantic City, June 1966.)

4. Brandenberger, E. and P. DeHaller, "Untersuchungen über Tropfenschlagerosion." Schweitzer Archiv-Annales Suisses, Vol. 10; n. 11, pp. 331 - 341, November 1944; and n. 12, pp. 379-386, December 1944.

5. Honegger, E., "Tests on Erosion Caused by Jets." The Brown Boveri Review, Vol. 14, n. 4, pp. 95-104, April 1927.

6. Fyall, A. A., R. B. King and R. N. C. Strain, "Rain Erosion Aspects of Aircraft and Guided Missiles." J. Roy Aero. Soc., Vol. 66, pp. 447-453, July 1962.

7. King, R. B., "Rain Erosion Testing at Supersonic Speeds using Rocket-propelled Vehicles." Paper presented at Rain Erosion Conference, Meersburg, Germany, May 1965.

8. Langbein, G., "The Dependence of Rain Erosion on the Velocity and the Angle of Incidence of Drops." Paper presented at Rain Erosion Conference, Meersburg, Germany, May 1965.

9. Hoff, G., G. Langbein and H. Rieger, "Investigations of Material Destruction due to Liquid Impact." Paper to be presented at ASTM Symposium on Erosion by Impingement and Cavitation, Atlantic City, June 1966.

10. Baker, D. W. C., K. H. Jolliffe and D. Pearson: "The Resistance of Materials to Impact Erosion Damage." Paper No. 13 at Discussion on the Deformation of Solids by the Impact of Liquids, The Royal Society, London, May 27, 1965. To be published in Phil. Trans. Roy. Soc., 1966.

11. Pearson, D., "Some Factors Influencing the Erosion of a Stainless Steel." Central Electricity Generating Borad (of Gt. Britain), Report RD/M/N 100, June 1964.

12. Busch, H. and G. Hoff, "Rain Erosion in High-speed Flight." Interavia, Vol. 20, pp. 675-676, May 1965.

13. Pearson, D., "The Effect of Drop Size on the Erosion of a Stainless Steel." Central Electricity Generating Board (of Gt. Britain) Report RD/M/N 128, December 1964.

14. Vater, M., "Prüfung und Verhalten metallischer Werkstoffe gegen Tropfenschlag und Kavitation." Korrosion and Metallschutz, Vol. 20, n. 6, pp. 171-179, June 1944.

15. Engel, Olive G., "Waterdrop Collisions with Solid Surfaces." J. Research NBS, Vol. 54, n. 5, pp. 281-298, May 1965.

16. Bowden, F. P., and J. E. Field, "The Brittle Fracture of Solids by Liquid Impact, by Solid Impact, and by Shock," Proc. Roy. Soc. A, Vol. 282, pp. 331-352, 1964.

17. Thomas, G. P., "Multiple Impact Experiments and Initial Stages of Deformation," Discussion on the Deformation of Solids by the Impact of Liquids, The Royal Society, London, 1955. (To be published, Phil. Trans. Roy, Soc., 1966).

18. Thiruvengadam, A., "A Unified Theory of Cavitation Damage." ASME Trans. (J. Basic Engrg), Vol. 85D, pp. 365-376, September 1963.

19. Peterson, R. E., "Application of Stress Concentration Factors in Design." Experimental Stress Analysis (Proc. SESA), Vol. 1, n. 1, pp. 118-127, 1943.

20. Marriott, J. B., and G. Rowden, "The Deformation of Steam Turbine Blade Materials by Liquid Impact," Discussion on the Deformation of Solids by the Impact of Liquids, The Royal Society, London, 1965. (To be published, Phil. Trans. Roy. Soc., 1966).

21. Weibull, W., "Basic Aspects of Fatigue." IUTAM Colloquium on Fatigue (Stockholm, 1955), Springer-Verlag, Berlin, pp. 289-298, 1956.

22. Backer, W. R., E. R. Marshall, and M. C. Shaw, "The Size Effect in Metal Cutting", Trans. ASME, Vol. 74, pp. 61-72, 1952.

23. Finnie, I., "The Mechanism of Erosion of Ductile Materials", Proc. 3rd National Congress Applied Mechanics, pp. 527-532, 1958.

24. Bowden, F. P., and J. H. Brunton, "The Deformation of Solids by Liquid Impact at Supersonic Speeds." Proc. Roy. Soc. A, Vol.263, pp. 433-450, October 1961.

25. DeCorso, S. M., and R. E. Kothmann, "Erosion by Liquid Impact," Symposium on Erosion and Cavitation, ASTM STP-307, Am. Soc. Testing Mats., pp. 32-45, 1962.

26. Vater, M., "Das Verhalten metallischer Werkstoffe bei Beanspruchung durch Flüssigkeitsschlag." Z. VDI, Vol. 81, n. 45, pp. 1305-1311, November 6, 1937.

27. Weibull, W., "Fatigue Testing and Analysis of Results", Oxford, Pergamon Press, 1961 (Published for and on behalf of AGARD).

28. Roark, R. J., "Formulas for Stress and Strain", New York, McGraw-Hill, 4th Edition, 1965.

29. Thiruvengadam, A., "A Comparative Evaluation of Cavitation Damage Test Devices." ASME Symposium on Cavitation Facilities and Techniques, 1964, pp. 157-164. (Also Hydronautics, Inc. Tech. Rept. No. 233-2, November 1963.)

30. Thiruvengadam, A., and S. Waring, "Mechanical Properties of Metals and their Cavitation Damage Resistance." Hydronautics, Inc. Tech. Rept. No. 233-5, Contract Nonr-3755(00)FBM, June 1964.

31. Thiruvengadam, A., "The Concept of Erosion Strength." Hydronautics, Inc. Technical Report 233-9, December 1965. (Also to be presented at ASTM Symposium on Erosion, Atlantic City, June 1966.)

32. Shalnev, K. K., J. J. Varga and G. Sebestyen, "Verification of Energy Parameter for Cavitation Damage", Paper to be presented at ASTM Symposium on Erosion by Impingement and Cavitation, Atlantic City, June 1966.

33. McAdam, J. D., Jr., "Endurance Properties of Steel: Their Relation to Other Physical Properties and to Chemical Composition." ASTM Proc., Vol. 23, pp. 56-105, 1923.

34. Halford, G. R., "The Energy Required for Fatigue." Journal of Materials, Vol. 1, no. 1, pp. 3-18, March 1966.

35. Pearson, D., "Pressure Rise Due to Water Hammer at High Impact Velocities." Central Electricity Generating Board (of Great Britain) Report RD/M/N82, April 1964.

36. Kirkwood, J. G., and E. W. Montroll, "Progress Report on the Pressure Wave Produced by an Underwater Explosion - II", OSRD No. 676, 1942.

37. Leith, W. C., and A. L. Thompson, "Some Corrosion Effects in Accelerated Cavitation Damage", ASME Trans., (J. Basic Engrg.), Vol. 82D, pp. 795-807, 1960.

38. Ripken, J. F., et al, "A New Facility for Evaluation of Materials Subject to Erosion and Cavitation Damage." Univ. of Minn., St. Anthony Falls Hydro. Lab., Project Report No. 77, Contract Nonr 710(56), March 1965.

39. Hobbs, J. M., private communication. (See also L. Hays, "Turbine Research in Great Britain." Informal trip report in connection with NAS 7-390 and NAS 7-391. Jet Propulsion Laboratory, November 11, 1965.)

40. Engel, O. G., "Pits in Metals Caused by Collision with Liquid Drops and Soft Metal Spheres." J. Research NBS, Vol. 62, n. 6, pp. 229-246, June 1959.

41. Engel, O. G., "Pits in Metals Caused by Collision with Liquid Drops and Rigid Steel Spheres." Journal of Research, National Bureau of Standards, Vol. 64A, pp. 61-72, 1960.

42. Jenkins, D. C., J. D. Booker, and J. W. Sweed, "An Experimental Method for the Study of the Impact Between a Liquid Drop and a Surface Moving at High Speed." Ministry of Supply (Gt. Britain), R & M 3203; Obtainable from NASA as N62-10146.

43. Jenkins, D. C., and J. D. Booker, "The Impingement of Water Drops on a Surface Moving at High Speed", in "Aerodynamic Capture of Particles", Pergamon Press, pp. 97-103, 1960.

44. DeCorso, S. M., "Erosion Tests of Steam Turbine Blade Materials." Proc. ASTM, Vol. 64, pp. 782-796, 1964.

45. International Conference on Rain Erosion Problems. Held in Meersburg/Bodensee, Germany, May 1965. Proceedings in English to be published by the Royal Aircraft Establishment, edited by A. A. Fyall.

46. Discussion on the Deformation of Solids by the Impact of Liquids, held at the Royal Society, London, England, May 27, 1965. To be published in Phil. Trans. Roy. Soc., 1966.

47. Symposium on Erosion by Cavitation and Impingement. (To be held during ASTM Annual Meeting), Atlantic City, N. J., June 1966. Proceedings will probably be published in 1967 as a "Special Technical Publication" by ASTM.

48. Busch, H., G. Hoff, and G. Langbein, "General View on Rain Erosion Tests in Germany," Discussion on the Deformation of Solids by the Impact of Liquids, The Royal Society, London, 1965. (To be published, Phil. Trans., Roy. Soc., 1966).

49. Freudenthal, A. M., "Physical and Statistical Aspects of Cumulative Damage," IUTAM Colloquium on Fatigue (Stockholm, 1955), Springer-Verlag, Berlin, pp. 53-62, 1956.

50. Thiruvengadam, A., and H. S. Preiser, "On Testing Materials for Cavitation Damage Resistance," Technical Report 233-3, Hydronautics, Inc., December 1963.

51. Plesset, M. S., and R. E. Devine, "Effect of Exposure Time on Cavitation Damage," Paper No. 65-WA/FE-23, Am. Soc. Mechanical Engrs., 1965.

52. Lichtman, J. Z., D. H. Kallas, C. K. Chatten and E. P. Cochran, Jr., "Study of Corrosion and Cavitation-Erosion Damage," Transactions, Am. Soc. Mechanical Engrs., Vol. 80, pp. 1325-1341, 1958.

53. Wheeler, W. H., "Mechanism of Cavitation Erosion," Cavitation in Hydrodynamics, (National Physical Laboratory Symposium, Teddington, England, 1955), Philosophical Library, New York, 1957.

54. von Schwarz, M., W. Mantel and H. Steiner, "Tropfenschlaguntersuchungen zur Feststellung des Kavitationswiderstandes (hohlsog), "Zeitschrift fur Metallkunde, Vol. 33, pp. 236-244, 1941.

55. Brunton, J. H., "Deformation of Solids by Impact of Liquids at High Speeds," Symposium on Erosion and Cavitation, ASTM STP-307, Am. Soc. Testing Mats., pp. 83-89, 1962.

56. Eichelberger, R. J., "Hypervelocity Impact," Behavior of Materials Under Dynamic Loading, Am. Soc. Mechanical Engrs., pp. 155-187, 1965.

57. Kent, R. P., "Some Aspects of Metallurgical Research and Development Applied to Large Steam Turbines," Parsons Journal, Vol. 10, pp. 285-295, Christmas 1964.

58. Roeloffs, R., and F. Garofalo, "A Review of Methods Employed in the Statistical Analysis of Fatigue Data," Proceedings, Am. Soc. Testing Mats., Vol. 56, pp. 1081-1090, 1956.

59. Epremiam, E., and R. F. Mehl, "The Statistical Behavior of Fatigue Properties and the Influence of Metallurgical Factors," Symposium on Fatigue with Emphasis on Statistical Approach, ASTM STP-137, Am. Soc. Testing Mats., pp. 25-27, 1953.

60. Mathieson, R., and J. M. Hobbs, "Cavitation Erosion: Comparative Tests," Engineering, Vol. 188, pp. 136-137, January 22, 1960.

61. Epstein, L. F.,"Static and Dynamic Corrosion and Mass Transfer in Liquid Metal Systems," Chem. Engr. Prog. Symp. Series, Vol. 53, No. 20, p. 67 (1957).

62. Ward, A. G., and J. W. Taylor,"Solution-Rate Studies with Liquid Metals: Solution of Copper in Liquid Lead and Bismuth," Journal of Inst. of Metals, Vol. 85, p. 145 (1956-57).

63. Gill, W. N., et al,"Mass Transfer in Liquid-Lithium Systems," A.I.Ch.E. Journal, Vol. 6, No. 1, p. 139 (1960).

64. Teitel, R. J. and W. S. Ginell,"Determination of the Solubility of Several Transition Metals in Molten Potassium," Trans. Amer. Nucl. Soc., p. 393, November 1965.

65. Grand, J. A., et al,"The Solubility of Tantalum and Cobalt in Sodium by Activation Analysis," J. Phys. Chem., v. 63 (1959).

66. McKisson, R. L. and R. L. Eichelberger, Solubility and Diffusion Studies of Ultra Pure Transition Elements in Ultra Pure Alkali Metals (Al), Seventh Quarterly Report, NASA-CR-54097 or Al-65-93. (Contract NAS 3-4163.) June 2, 1965.

67. ORNL-3898, SNAP-8 Corrosion Program, Summary Report, December 1965.

68. DeVan, J. H., et al,"Compatibility of Refractory Metals with Boiling Alkali Metals" (ORNL), Trans. Amer. Nucl. Soc., p. 390, November 1965.

69. Cunningham, C. W., et al,"Screening Tests of Turbine Nozzle and Blade Materials," Trans. Amer. Nucl. Soc., p. 401, November 1965.

70. Brunton, J. H., Lecture given at Westinghouse Research Laboratories, September 29, 1960.